JAERI-M
88-213

EVALUATION REPORT ON SCTF CORE-III TEST S3-06

(EFFECT OF RADIAL POWER DISTRIBUTION ON THERMAL HYDRAULIC CHARACTERISTICS OF PWR WITH COMBINED INJECTION TYPE ECCS)

October 1988

Takamichi IWAMURA, Tadashi IGUCHI, Hajime AKIMOTO
Tsutomu OKUBO, Akira OHNUKI, Akihiko MINATO*
Isao SAKAKI,**Hiromichi ADACHI and Yoshio MURAO

日本原子力研究所
Japan Atomic Energy Research Institute

JAERI-Mレポートは，日本原子力研究所が不定期に公刊している研究報告書です。
入手の問合わせは，日本原子力研究所技術情報部情報資料課（〒319-11茨城県那珂郡東海村）あて，お申しこしください。なお，このほかに財団法人原子力弘済会資料センター（〒319-11 茨城県那珂郡東海村日本原子力研究所内）で複写による実費頒布をおこなっております。

JAERI-M reports are issued irregularly.
Inquiries about availability of the reports should be addressed to Information Division Department of Technical Information, Japan Atomic Energy Research Institute, Tokai-mura, Naka-gun, Ibaraki-ken 319-11, Japan.

編集兼発行　日本原子力研究所
印　　刷　いばらき印刷㈱

JAERI-M 88-213

Evaluation Report on SCTF Core-III Test S3-06 (Effect of Radial Power Distribution on Thermal-Hydraulic Characteristics of PWR with Combined Injection Type ECCS)

Takamichi IWAMURA, Tadashi IGUCHI, Hajime AKIMOTO, Tsutomu OKUBO
Akira OHNUKI, Akihiko MINATO*, Isao SAKAKI**, Hiromichi ADACHI
and Yoshio MURAO

Department of Reactor Safety Research
Tokai Research Establishment
Japan Atomic Energy Research Institute
Tokai-mura, Naka-gun, Ibaraki-ken

(Received September 28, 1988)

In order to investigate the effect of radial power distribution on the thermal-hydraulic characteristics during the reflood phase of a PWR-LOCA with a combined injection type ECCS, a core cooling separate effect test S3-06 and a combined injection test S3-16-Phase 2 were performed using the Slab Core Test Facility (SCTF) Core-III. The radial power distributions in these two tests simulated a reference distribution for a PWR with a combined injection type ECCS and a steep distribution for a PWR with a cold leg injection type ECCS, respectively.

Under the radial power distribution of a PWR with a combined injection type ECCS, the radial power distribution had little effect on the thermal-hydraulic behavior in the two-phase up-flow region due to the approximately flat power distribution in this region (power ratio = 1.04 ∿ 1.08). The overall fluid behavior in the pressure vessel was also little affected by the radial power distribution.

On the other hand, under the steep radial power distribution (peak power ratio = 1.36), the degree of heat transfer enhancement in high

---

The work was performed under contract with the Atomic Energy Bureau of Science and Technology Agency of Japan.

* Hitachi, Ltd.

** NAIG, Co. Ltd.

power bundles in the two-phase up-flow region was dominated by the bundlewise radial power ratio as in the case of a PWR with a cold leg injection type ECCS.

Keywords: LOCA, ECCS, Combined Injection, German PWR, Two-Phase Flow, Fall Back, Two-Dimensional Effect, Heat Transfer, Reflood, SCTF

ＳＣＴＦ第３次炉心試験Ｓ３－０６評価報告書（複合注入型ＥＣＣＳ付PWRにおける熱水力学的特性に及ぼす半径方向出力分布の影響）

日本原子力研究所東海研究所原子炉安全工学部
岩村　公道・井口　　正・秋本　肇
大久保　努・大貫　　晃・湊　明彦*
榊　　勲**・安達　公道・村尾　良夫

（1988年9月28日受理）

複合注入型ECCS付ＰＷＲのＬＯＣＡ時再冠水過程における熱水力学的特性に及ぼす半径方向出力分布の影響を調べるため，平板炉心試験装置（SCTF）第３次炉心を用いて，炉心冷却個別効果試験Ｓ３－06及び複合注入試験Ｓ３－16－Ｐhase２を実施した。両試験の半径方向出力分布は，それぞれ，複合注入型ECCS付ＰＷＲ参照炉心の出力分布及びコールドレグ注入型ECCS付ＰＷＲの急峻出力分布を模擬した。複合注入型ECCS付ＰＷＲ出力分布条件下では，二相上昇域内での出力比が1.04～1.08と，比較的平坦なため，出力分布の差に基づく落水域での熱水力学的挙動の差が，二相上昇域における熱水力学的挙動に及ぼす影響は極めて小さかった。また，圧力容器内の流体挙動にも出力分布の有意な影響は認められなかった。一方，急峻出力分布条件下（最大出力比＝1.36）においては，二相上昇域内の高出力バンドルにおける熱伝達促進の程度は，半径方向出力比に依存し，コールドレグ注入型ECCS付ＰＷＲの場合と同様な取り扱いが可能なことがわかった。

本報告書は，電源開発促進特別会計法に基づき，科学技術庁からの受託によって行った研究の成果である。

東海研究所　：〒319－11　茨城県那珂郡東海村白方字白根２－４

＊　日立製作所（株）

＊＊　日本原子力事業（株）

Contents

目　　次

List of Tables

List of Figures

1. INTRODUCTION

The Slab Core Test Facility (SCTF) test program is a part of the large scale reflood test program performed under contract with Atomic Energy Bureau of Science and Technology Agency of Japan together with the Cylindrical Core Test Facility (CCTF) test program. The SCTF test program is one of the research activities based on the trilateral agreement among Japan Atomic Energy Research Institute (JAERI), the United States Nuclear Regulatory Commission (USNRC) and the Federal Minister for Research and Technology (BMFT) of the Federal Republic of Germany (FRG).

The SCTF Core-I and Core-II test series have been performed mainly to investigate the two-dimensional thermal-hydraulic behavior in the core during the reflood phase of a loss-of-coolant accident (LOCA) of a Westinghous-type (US/J-type) pressurezed water reactor (PWR). On the other hand, one of the major objectives of the SCTF Core-III test series is to investigate the effectiveness of the combined-injection-type emergency core cooling system (ECCS)for a German-Type PWR (GPWR)[1]. In addition, simulation tests for a US/J-type PWR are also planned with the SCTF Core-III[2].

Under the combined injection mode, ECC water is simultaneously injected into the hot leg and the cold leg. Therefore, the core is expected to be cooled before the beginning of the bottom-up reflooding due to the fall back water from the upper plenum into the core. In a full size core, the water fall back is considered to occur nonuniformly because of the nonuniform distributions of water level and temperature in the upper plenum. Resultantly, a two-dimensional core cooling behavior may be induced.

In order to investigate the two-dimensional core cooling behavior peculiar to the combined injection mode for a GPWR, eight core cooling separate effect tests have been performed with the SCTF Core-III. Major test conditions for these tests are listed in Table 1.1. The results of the core cooling base case test (S3-SH1) were reported in reference (3). The radial power distribution was set to be flat in the core cooling separate effect test series except in Test S3-06. On the other hand, the radial power distribution in Test S3-06 simulated an actual power distribution in a combined injection type GPWR. Therefore, the effect of the radial power distribution on the core cooling behavior was investigated by comparing Test S3-06 with Test S3-SH1.

Since the peak radial power ratio of 1.08 in Test S3-06 was too small to find a significant effect of radial power distribution, an informal com-

bined injection test S3-16-Phase 2 was performed under more steep radial power distribution. By comparing this test with a gravity feed test S3-16, which was performed under the same steep power distribution, the effect of ECC injection mode on the two-dimensional core cooling behavior was also investigated.

Presented in Appendix A is a brief description of the SCTF Core-III. Some selected data obtained in Test S3-06 are presented in Appendix B.

2. Test Description

2.1 Test Facility

A schematic diagram of SCTF is shown in Fig. 2.1. The primary coolant loops consist of a hot leg equivalent to four actual hot legs, a steam/water separator corresponding to four actual steam generators, an intact cold leg equivalent to three intact cold legs, a broken cold leg on the pressure vessel side, and a broken cold leg on the steam/water separator side. These two broken cold legs are connected to each other by a pressure equalizing pipe.

The flow area scaling ratio is 1/21 of a 1,100 MWe class Westinghouse-type PWR, whereas the height of each component is preserved.

The ECC water injection ports for the SCTF-III core cooling test series were selected from the four top injection nozzles and the eight side injection nozzles located above the upper core support plate (UCSP). The top and the side injection nozzles were used to simulate the hot leg injection of a GPWR combined injection mode.

Figure 2.2 shows a vertical cross section of the pressure vessel. The pressure vessel includes a simulated core, an upper plenum with internals, a lower plenum, a core baffle and a downcomer. The configurations of the upper plenum structure and the end box simulate those of a 1,300 MWe class GPWR as practically as possible.

The simulated core consists of 8 bundles arranged in a row with full radial width. Bundle 1 corresponds to the center bundle and Bundle 8 to the peripheral bundle of a PWR. Each bundle consists of 236 heated rods and 20 non-heated rods arranged in a 16 × 16 array. The outer diameter and the heated length of the heated rod are 10.7 mm and 3,613 mm, respectively. The arrangement pitch of the rods is 14.3 mm.

The core and the upper plenum are enveloped by honeycomb thermal insulators with wall plates to minimize the wall thermal effects.

The design of SCTF Core-III is described more in detail in Appendix A.

2.2 Test Conditions

The SCTF tests discussed in this report are Test S3-06 and Test S3-16-Phase 2. Test S3-06 is the sixth formal test in the SCTF Core-III series. Test S3-16-Phase 2 is an informal combined injection test performed just

after Test S3-16 which is a gravity feed test under a steep radial power distribution[4]. Major test conditions for these two tests are tabulated in Tables 2.1 and 2.2, respectively.

(1) Test S3-06

As shown in Fig. 2.3, the radial power ratios of Test S3-06 are; 1.04 (Bundle 1), 1.08 (Bundles 2 and 3), 1.04 (Bundles 4, 5 and 6), 0.97 (Bundle 7) and 0.71 (Bundle 8), based on the radial power distribution of a reference GPWR. On the other hand, the radial power distribution of the base case test S3-SH1 was flat so as to avoid the effect of radial power distribution on the two-dimensional core cooling behavior.

The other test conditions for Test S3-06 were set to be equal to those for Test S3-SH1. These test conditions were determined based on the CCTF combined-injection test results (C2-19) and the TRAC-PF1/MOD1 calculation results under GPWR evaluation model (EM) conditions. The ECC injection ports used in these two tests were the four upper head injection nozzles and the two side flow injection nozzles above Bundles 7 & 8, simulating the water flow from the hot leg into the upper plenum. Since the main purpose of the core cooling separate effect test series is to investigate the core cooling characteristics before and after the beginning of the bottom-up reflood, no ECC water was injected into the cold leg and the initial water inventory in the lower plenum was set to be zero. The top injection flow rate was 2.5 kg/s with a water temperature of 308 K for each of the four top injection nozzles. The total side injection flow rate was 30 kg/s with a water temperature of 343 K. Total ECC flow rate of 40 kg/s was determined from the TRAC GPWR EM calculation results. The water temperature of the side injection was based on the fluid temperature just above the UCSP at the hot leg side in CCTF Test C2-19.

(2) Test S3-16-Phase 2

The radial power distribution of Test S3-16-Phase 2 is also shown in Fig. 2.3. The maximum radial power ratio is 1.36 in Bundle 4.

The other test conditions for Test S3-16-Phase 2 were determined based on the TRAC-PF1/MOD1 calculation results under GPWR evaluation model (EM) conditions. The ECC water was injected simultaneously into the upper plenum and the lower plenum simulating the combined injection mode.

2.3 Test Procedure

(1) Test S3-06

Figure 2.4 shows the test sequence of Test S3-06.

The core heating was initiated at time "zero" under the specified non-uniform radial power distribution with the total power of 7.5 MW. When four cladding temperatures exceeded 943 K (670 °C), ECC injection into the upper plenum was initiated. At the same time, the core power decay started, simulating the reactor time from 25 s after shutdown. The decay curve was based on the (1.03 x ANS standard + Actinides). The top injection through the four top injection nozzles and the side injection above Bundles 7 & 8 were terminated at 300 s after the initiation of injection. The whole core was expected to be quenched before the termination of the top injection.

After the termination of the top injection, the side flow injection rate was reduced to 10 kg/s and the temperature was raised to 406 K and then the cold leg injection started at 450 s as illustrated in Fig. 2.4. This phase of the test aimed to investigate the effect of ECC water injection condition on the flow direction in the core. However, the test results of this phase are not involved in the present report.

(2) Test S3-16-Phase 2

Figure 2.5 shows the test sequence of Test S3-16-Phase 2.

Test S3-16-Phase 2 was performed sequentially after Test S3-16. After the quench of the whole core in Test S3-16, the core heating power was shut down followed by the drain of water in the core. Then the core heating was restarted. When four cladding temperatures exceeded 1083 K (810 °C), ECC injection into the upper plenum and the lower plenum was initiated. The ECC water was injected into the upper plenum through the side injection nozzles above Bundles 7 and 8. The core power decay started with the initiation of ECC injection. The decay curve was based on the (1.03 × ANS standard + Actinides).

3. TEST RESULTS AND DISCUSSIONS

3.1 Comparison between Test S3-06 and Test S3-SH1

3.1.1 Measured Boundary Conditions

Figures 3.1 and 3.2 show the comparisons of top and side injection flow rates into the upper plenum through the top injection nozzles and the side injection nozzles, respectively. The side injection started at 103 s and the top injection at 107 s for Test S3-06. The injection time of the side flow injection for Test S3-06 was 9 s earlier than that for Test S3-SH1, because the maximum core heating power in Test S3-06 was 1.08 times as large as that in Test S3-06, while the maximum rod temperature for the ECC injection actuation was the same for these two tests. The injection rates were 2.5 kg/s per each of four top injection nozzles and 30 kg/s for the side injection as specified.

Figures 3.3 and 3.4 show the comparisons of temperatures of the top and side injection water, respectively. The side injection water temperatures agreed with each other for these two tests after the initiation of injection, while the top injection water temperature was slightly higher in Test S3-06 than in Test S3-SH1.

Figure 3.5 shows the transient of heating power for each bundle for these two tests. The radial power distribution was non-uniform in Test S3-06 while completely flat in Test S3-SH1 as specified.

Compared in Fig. 3.6 are the pressures at the core center and the top of the containment tank-II. The pressure transients after the initiation of ECC injection well agreed between these two tests. The initial decrease of pressure was caused by the condensation of steam by the injected subcooled water. After the bottom of core recovery (BOCREC), the pressures increased due to the increasing of the steam generation rate in the core.

The chronology of major events for Test S3-06 is listed in Table 3.1

3.1.2 Overall Fluid Behavior in Pressure Vessel

(1) Fluid Behavior in Upper Plenum and around UCSP

As shown in Fig. 3.7, no significant difference is observed in the collapsed liquid levels in the upper plenum between Tests S3-06 and S3-SH1. That is, the collapsed liquid levels in the upper plenum are less than

0.05 m before the BOCREC and then increase rapidly. After the BOCREC, the collapsed liquid levels are higher at the hot leg side. The low liquid level before the BOCREC indicates that most of the injected water fell down to the core during this period.

Figure 3.8 shows the comparison of fluid temperatures in the upper plenum at 0.25 m from the UCSP. Before the BOCREC, subcooled water is observed except above Bundle 1 for these two tests. After the BOCREC, subcooled water is clearly seen above Bundle 7. The significant spikes of the fluid temperature above Bundle 7 indicate intermittent steam flow in the subcooled water.

Compared in Fig. 3.9 are the fluid temperatures in the UCSP holes. The fluid temperatures above Bundles 7 and 8 show significant subcooling of about 50 K after the initiation of ECC water injection. Subcooled water is also observed above Bundles 4, 5 and 6 especially before the BOCREC. On the other hand, the fluid temperatures above Bundles 1, 2 and 3 are approximately saturated after the injection start. The trends of fluid temperatures in the upper plenum and the UCSP holes are quite similar to each other for these two tests.

(2) Fluid Behavior around End Box Tie Plate

Figures 3.10, 3.11 and 3.12 show the comparisons of differential pressures across the end box tie plate, steam and water mass flow rates measured with drag bodies at the tie plate and fluid temperature just below the tie plate, respectively. As noticed in these figures, no significant difference is observed in the fluid behaviors around the tie plate between Tests S3-06 and S3-SH1.

As shown in Fig. 3.10, the differential pressures above Bundles 1 through 6 are approximately zero or slightly positive before the BOCREC. Thereafter, these differential pressures exceed the static water head in the measurement span (0.69×10^{-3} MPa), indicating a large amount of two-phase up-flow rate in Bundles 1 through 6. On the other hand, the large negative differential pressures above Bundles 7 and 8 before and after the BOCREC indicate a strong downward flow in these bundles. Therefore, it is concluded that the fluid behavior in the core is separated into two regions; a water down-flow region (Bundles 7 and 8) and a two-phase up-flow region (Bundles 1 through 6). In Bundle 6, however, these two regions are mixed because the negative differential pressure is observed at the later

period. The differential pressures above Bundles 5 through 8 become very small after about 200 s. This is corresponding to the fact that the core was approximately filled with single-phase water at this time (Fig. 3.13).

As shown in Fig. 3.11, steam up-flow is observed in Bundle 4 after the ECC injection start, while no steam flow is recognized in Bundle 8. In Bundle 4, the water flow rate is negligibly small before the BOCREC and then the water up-flow rate gradually increases. In Bundle 8, the maximum fall back flow rate is about 25 kg/s.

As shown in Fig. 3.12, just below the end box tie plate, subcooled water is observed in Bundles 8 during the ECC water injection period and also in Bundle 6 before the BOCREC and at the later period. The spikes observed in the fluid temperature in Bundle 6 indicate the intermittent fall back of subcooled water into the core in this bundle. In Bundles 2 and 4, the fluid temperatures are approximately saturated except the overshoot just after the initiation of ECC water injection.

(3) Collapsed Liquid Levels in Downcomer, Lower Plenum and Core

The collapsed liquid levels measured with DP cells in the downcomer, the lower plenum and the core are compared in Fig. 3.13. These liquid levels show very good agreement between Test S3-06 and S3-SH1, indicating that the overall fluid behavior in the pressure vessel is not affected by the difference of radial power distributions in these two tests.

The collapsed liquid level in the core is very small before the BOCREC. After the BOCREC, the differential pressure increases rapidly and reaches 3.7 m water head. That is, the core is filled with single-phase water at the later period. The water accumulation rate in the lower plenum including the bottom of downcomer is estimated to be approximately 34 kg/s after the injection start. Therefore, about 85% of the injected water penetrated the core into the lower plenum before the BOCREC.

3.1.3 Two-Dimensional Hydraulic Behavior in Core

(1) Void Fraction and Fluid Density Distributions

The vertical differential pressures measured in Bundles 2, 4 and 8 at six separate elevations were converted directly to void fractions by neglecting the effects of frictional and accelerational pressure drops.

The results are compared in Fig. 3.14 for Tests S3-06 and S3-SH1. Just after the initiation of the ECC water injection, a water accumulation is observed in Bundle 8 especially at the upper elevations for these two tests. After the BOCREC, the void fractions decrease rapidly for all bundles. The void fractions in Bundle 8 are the lowest among these bundles for most of the test period, while the void fraction in Bundles 2 and 4 are approximately the same.

Figure 3.15 shows the comparisons of fluid densities measured with the γ-densitometers at the gaps between Bundles 1 & 2, 5 & 6 and 7 & 8 at elevation of 3.235 m. Before the BOCREC, a considerable amount of water is observed at the gaps between Bundles 5 & 6 and Bundles 7 & 8. At the gap between Bundles 7 & 8, the fluid density increases rapidly after the BOCREC and the gap is nearly filled with single-phase water at the later period. On the other hand, the fluid density is relatively small at the gap between Bundle 1 & 2. No significant difference in the void fractions and fluid densities is observed for these two tests.

(2) Horizontal Differential Pressures

Figure 3.16 shows the comparisons of horizontal differential pressures at elevations of 3.235, 1.905, 1.365 and 0.7 m. The positive differential pressure means that the pressure is higher at the Bundle 1 side and the cross flow direction is from the Bundle 1 side to the Bundle 8 side. It is shown in these figures that the radial power distribution has little effect on the horizontal differential pressures.

At 3.235 m, the cross flow from Bundle 4 to Bundle 8 is observed before the quench of the whole core. This is considered to be caused by the depressurization in the down-flow region due to the condensation of steam by the subcooled fall back water. On the other hand, the horizontal differential pressure at 1.36 and 0.7 m becomes negative at about 30 s and 12 s after the BOCREC, respectively. The cross flow direction at 1.905 m is reversed from positive to negative at about 25 s before the quench at this elevation in the two-phase up-flow region. These behaviors indicate that the fall back water in Bundles 7 and 8 flows into the other bundles below and just above the bottom-up quench front.

(3) Fluid Temperature

Figure 3.17 shows the fluid temperatures at elevation 2.545 m in Bundles 4 and 8. In Bundle 4, superheated steam is observed before 53 s (5 ~ 10 s after the BOCREC) in these two tests. After that time, the fluid temperature indicates a saturated temperature. On the other hand, from 35 s to 75 s, the fluid temperature in Bundle 8 in Test S3-06 is lower than that in Test S3-SH1. This is explained by the fact that the heating power of Bundle 8 in Test S3-06 was much lower than the bundle averaged power, while the radial power distribution was flat in Test S3-SH1.

3.1.4 Two-Dimensional Heat Transfer Behavior in Core

(1) Heater Rod Temperatures and Quench Front Propagation

Figure 3.18 shows the comparisons of heater rod temperatures for all bundle at elevations of 3.19, 1.905 and 1.38 m for Tests S3-06 and S3-SH1. The quench front propagation behaviors in Bundles 1, 3, 5, 6, 7 and 8 are compared in Fig. 3.19.

From these figures, following trends are commonly observed in these two tests; The heater rods in Bundles 7 and 8 are significantly cooled just after the initiation of the ECC injection especially at the upper elevations. On the other hand, the heater rod temperatures in Bundles 1 and 3 continue to rise almost adiabatically until the BOCREC. The heater rods in Bundles 2, 4, 5 and 6 are slightly cooled before the BOCREC at all elevations. The heater rods at the top and bottom parts of Bundles 7 and 8 are quenched prior to the BOCREC by the subcooled water falling back from the upper plenum. The bottom-up quench front propagation is approximately uniform over Bundles 1 through 6.

In Bundles 1 though 6, no significant difference is observed in the temperature transients and the quench propagation behaviors between these two tests. This is consistent with the fact that the difference in the radial power ratios between these two tests is quite small in these bundles as shown in Fig. 2.3. On the other hand, in Bundles 7 and 8, the rod temperatures are lower and the quench times are earlier in Test S3-06 because the heating power in these bundles is lower in this test especially in Bundle 8 as shown in Fig. 2.3.

Based on the above-mentioned thermal behaviors, it is concluded that

the rod temperatures in the two-phase up-flow region are not affected by the lower temperature and earlier quenching in the water down-flow region. The effect of the lower power ratio in Bundles 7 and 8 is limited only in these bundles.

(2) Heat Transfer Coefficient

Figure 3.20 shows the comparisons of heat transfer coefficients in Bundles 2, 4, 6 and 8 at elevation of 1.905 m. As in the case of the rod temperature behavior, no significant difference in the heat transfer behavior is observed between these two tests except the earlier quenching in Bundle 8 in Test S3-06 due to the lower power ratio.

Before the BOCREC, the heat transfer coefficients at 1.905 m in Bundles 6 and 8 are more than 100 W/m^2K, indicating the significant core cooling effect by the subcooled fall back water. After the BOCREC, the heat transfer coefficients in the two-phase up-flow region well agree with each other for these two tests. That is, the heat transfer behavior after the BOCREC is uniform and the effect of radial power distribution is not recognized in the two-phase up-flow region.

3.1.5 Fall Back Flow Rate, Maximum Steam Generation Rate and Mass Flow Rate in Hot Leg

(1) Fall Back Flow Rate

The fall back flow rate through the UCSP holes is calculated with the following mass balance equation;

Fall back flow rate = Total upper plenum injection rate
- Carryover mass flow rate into hot leg
- Water accumulation rate in upper plenum

The effect of condensation in the upper plenum is not considered in this calculation. The calculated results are shown in Fig. 3.21 together with the total injection rate into the upper plenum. It is indicated that most of the injected water fell down into the core before the quench of the whole core except from 60 to 100 s after the injection start.

(2) Maximum Steam Generation Rate

Figure 3.22 shows the comparison of estimated steam generation rates in the core. These steam generation rates were calculated from a heat balance method[5]. In this calculation, the total heat transfered from the heater rods is assumed to be absorbed in the fluid and the effect of condensation due to the subcooled water is not considered. In the present core cooling tests, however, some part of the generated steam is considered to be condensed by the subcooled fall back water mainly in the water downflow region (Bundles 7 and 8). Therefore, the estimated steam generation rates in the whole core in Fig. 3.22 indicate the maximum values.

The estimated maximum steam generation rate in Test S3-06 tends to be slightly lower than that in Test S3-SH1 before the quench of the whole core. This is explained as follows; Since the rod temperature setting value for the initiation of ECC water injection was the same for these two tests, the injection started earlier in Test S3-06 due to the non-uniform radial power distribution under the same total heating power as discussed in Section 3.1. Therefore, the total core stored energy at the injection initiation time is slightly smaller in Test S3-06, resulting in the slightly smaller heat release rate during the quenching period.

(3) Mass Flow Rate in Hot Leg

Total mass flow rates in the hot leg measured with a hot leg spool piece are compared in Fig. 3.23. As shown in this figure, no significant difference is observed between Tests S3-06 and S3-SH1. The mass flow rate before the BOCREC is very small due to the condensation of steam in the pressure vessel. After the BOCREC, the mass flow rate increases rapidly up to about 14 kg/s which is higher than the maximum steam generation rate of about 8 kg/s (Fig. 3.22), indicating that more than 6 kg/s of water was carried over into the hot leg. The mass flow rate becomes negative after 90 s due to the flow reversal from the steam/water separator to the upper plenum.

3.2 Comparison between Test S3-16-Phase 2 and Test S3-16

Figure 3.24 shows the heat transfer coefficients in Bundle 4 (power ratio = 1.36) and Bundle 1 (0.81) for Tests S3-16-Phase 2 and S3-16 with

respect to the distance from the bottom quench front. It is noted that the average of heat transfer coefficients is much higher in Test S3-16-Phase 2 than in Test S3-16. This is due to the fact that the effective flooding velocity in the combined injection mode was several times higher than that in the gravity feed mode[3]. In spite of the large difference in the average heat transfer coefficients between these two tests, the difference in the heat transfer coefficients between Bundles 4 and 1 is in the same order for these two tests.

The differences in the heat transfer coefficients between high and low power bundles for each of these two tests were averaged over the distance from the bottom quench front and plotted against the corresponding difference in the radial power ratios in Fig. 3.25. Since the thermal-hydraulic behavior under the combined injection mode such as Test S3-16-Phase 2 was separated into two regions; a water down-flow region (Bundles 7 and 8)and a two-phase up-flow region (Bundles 1 through 6), the heat transfer coefficients in the two-phase up-flow region were used for the comparison.

As shown in Fig. 3.25, the differences in the heat transfer coefficients are mostly overlapped with each other between these two tests within the range of the standard deviations. Therefore, it is suggested that the degree of heat transfer enhancement due to the radial power distribution in the two-phase up-flow region in Test S3-16-Phase 2 is dominated by the radial power ratio itself. That is, the ECC injection mode, combined injection or cold leg injection, has little effect on the two-dimensional core cooling behavior in the bottom-up quenching region.

4. CONCLUSION

(1) Thermal-Hydraulic characteristics in the core was separated into two regions; a water down-flow region (Bundles 7 and 8) and a two-phase up-flow region (Bundles 1 through 6), under various radial power distribution conditions for a PWR with a combined injection type ECCS.

(2) Under the radial power distribution of a PWR with a combined injection type ECCS, the radial power distribution had little effect on the thermal-hydraulic behavior in the two-phase up-flow region due to the relatively flat power distribution in this region (power ratio = 1.04 ~ 1.08). The overall fluid behavior in the pressure vessel was not affected by the radial power distribution.

(3) Under the steep radial power distribution (peak power ratio = 1.36), the degree of heat transfer enhancement in high power bundles in the two-phase up-flow region was dominated by the bundlewise radial power ratio and less dependent on the flooding velocity as in the case of a PWR with a cold leg injection type ECCS.

ACKNOWLEDGMENT

The authors would like to express their appreciation to Mr. W. Pointner, a regident engineer from Federal Republic of Germany, for his useful discussions.

REFERENCES

(1) Y. Murao, et. al., Reflooding phenomena of German PWR Estimated from CCTF and SCTF Test Results, 15th Water Reactor Safety Information Meeting, Gaithersburg, Oct. 26-29 (1987).

(2) T. Iguchi, et. al., SCTF III Test Plan and Recent SCTF III Test Result, 14th Water Reactor Safety Information Meeting, Gaithersburg, Oct. 27-31 (1986).

(3) T. Iwamura, et. al., Evaluation Report on SCTF Core-III Test S3-SH1 (Overall Thermal-Hydraulic Characteristics under Combined Injection Mode for a German-Type PWR), JAERI-M 83-125 (1988).

(4) T. Iwamura, et. al., Evaluation Report on SCTF Core-III Tests S3-14, S3-15 and S3-16 (Effect of Radial Power Profile Shape on Two-Dimensional Thermal-Hydraulic Behavior in Core), JAERI-M 88-060 (1988).

(5) T. Iwamura et. al., Two-dimensional Thermal-Hydraulic Behavior in Core in SCTF Core-II Cold Leg Injection Tests (Radial Power Profile Test Results), JAERI-M 85-106 (1985).

ACKNOWLEDGMENT

The authors would like to express their appreciation to Mr. W. Pointner, a regident engineer from Federal Republic of Germany, for his useful discussions.

REFERENCES

(1) Y. Murao, et. al., Reflooding phenomena of German PWR Estimated from CCTF and SCTF Test Results, 15th Water Reactor Safety Information Meeting, Gaithersburg, Oct. 26-29 (1987).

(2) T. Iguchi, et. al., SCTF III Test Plan and Recent SCTF III Test Result, 14th Water Reactor Safety Information Meeting, Gaithersburg, Oct. 27-31 (1986).

(3) T. Iwamura, et. al., Evaluation Report on SCTF Core-III Test S3-SH1 (Overall Thermal-Hydraulic Characteristics under Combined Injection Mode for a German-Type PWR), JAERI-M 83-125 (1988).

(4) T. Iwamura, et. al., Evaluation Report on SCTF Core-III Tests S3-14, S3-15 and S3-16 (Effect of Radial Power Profile Shape on Two-Dimensional Thermal-Hydraulic Behavior in Core), JAERI-M 88-060 (1988).

(5) T. Iwamura et. al., Two-dimensional Thermal-Hydraulic Behavior in Core in SCTF Core-II Cold Leg Injection Tests (Radial Power Profile Test Results), JAERI-M 85-106 (1985).

Table 1.1 Summary of test conditions for GPWR core cooling test series in SCTF Core-III

Run No.	702	703	705	706	710	711	712	716
	S3-AC2	S3-SH1	S3-01	S3-02	S3-06	S3-07	S3-08	S3-12
	BE simulation	Base case	High LP level	High sub.	Power profile	ECC location	ECC location changing	High pressure High temperature
Pressure (MPa)								
Containment tank	0.3	0.3	0.3	0.3	0.3	0.3	0.3	0.4
Power								
Initial power (MW)	6.8	7.5	7.5	7.5	7.5	7.5	7.5	7.5
Power decay curve	ANS×1.0+Act.	ANS×1.03+Act.	ANS×1.03+Act.	ANS×1.03+Act.	ANS×1.03+Act.	ANS×1.03+Act.	ANS×1.03+Act.	ANS×1.03+Act.
After scram (s)	40	25	25	25	25	25	25	25
Power profile	Flat	Flat	Flat	Flat	Uneven*1	Flat	Flat	Flat
Clad temperature (°C)								
Peak at ECC start	510	670	670	670	670	670	670	750
ECC location	UP*2	UP	UP	UP	UP	UP	UP	UP
Flow rate (kg/s)	50	40	40	40	40	40	40	40
Temperature (°C)	70	35/70	35/70	35	35/70	35/70	35/70	35
Initial water level								
Lower plenum (m)	0	0	1.4	0	0	0	0	0

*1 1.04 : 1.08 : 1.08 : 1.04 : 1.04 : 1.04 : 0.97 : 0.71
*2 Upper plenum

Table 2.1 Test condition for Test S3-06

System pressure	0.3 MPa
Initial total power	7.5 MW
Decay curve	1.03 × ANS + Actinides from 25 s after shutdown
Radial power distribution	non-uniform (Fig. 2.3)
Initial peak caldding temperature	943 K
ECC water injection mode	Upper plenum injection
Total injection rate	40 kg/s (constant)
Upper head injection	
Flow rate	2.5 kg/s × 4 nozzles
Water temperature	308 K
Injection period	300 s
UCSP injection	
Flow rate	30 kg/s
Injection location	above Bundles 7 & 8
Water temperature	343 K
Injection period	300 s

Table 2.2 Test conditions for Test S3-16-Phase 2

System pressure	0.2 MPa
Initial total power	7.12 MW
Decay curve	1.03 × ANS + Actinides from 25 s after shutdown
Radial power distribution	non-uniform (Fig. 2.3)
Initial peak caldding temperature	1083 K
ECC water injection mode	Upper plenum and lower plenum injection
Upper plenum injection	
Location	UCSP injection nozzles above Bundles 7 & 8
Maximum flow rate	39.1 kg/s
Water temperature	343 K
Injection period	240 s
Lower plenum injection	
Location	Lower plenum
Maximum flow rate	72.3 kg/s
Water temperature	308 K
Injection period	240 s

Table 3.1 Chronology of major events for Test S3-06

	Time after core power "ON"	Time after ECC injection initiation
Core power "ON"	0 s	-103
Core power decay initiation	103	0
Side injection initiation	103	0
Top injection initiation	107	4
BOCREC	150.5	47.5
Maximum pressure at the top of containment tank-II (0.318 MPa)	170	67
Maximum pressure at the center of core (0.335 MPa)	174	71
Maximum core temperature (1101 K)	155.5	52.5
Whole core quenched	281.5	178.5
End of top injection	402	299
End of side injection (7 & 8 Bundles)	404	301

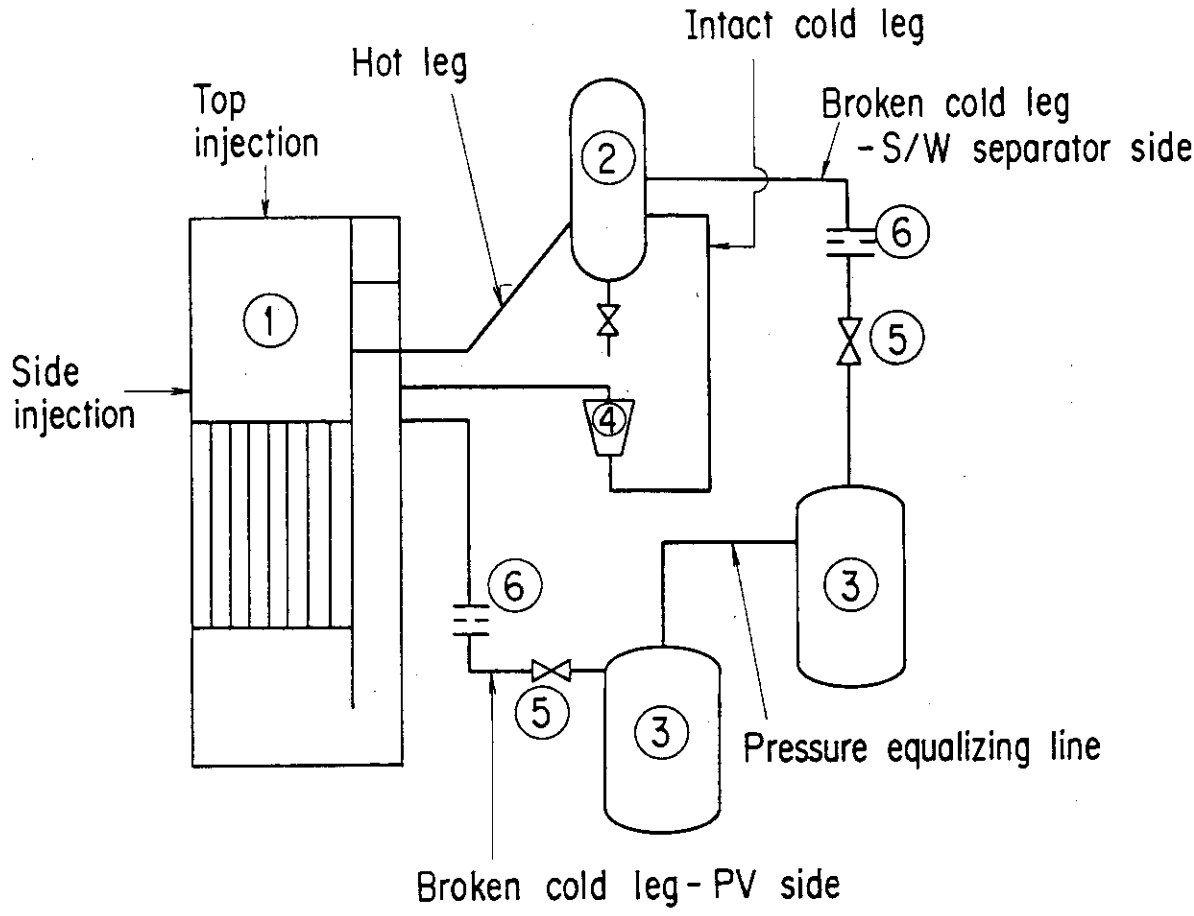

① Pressure vesel
② Steam / water separator
③ Containment tanks
④ Pump simulator
⑤ Break valves
⑥ Flow resistance simulators

Fig. 2.1 Schematic diagram of SCTF

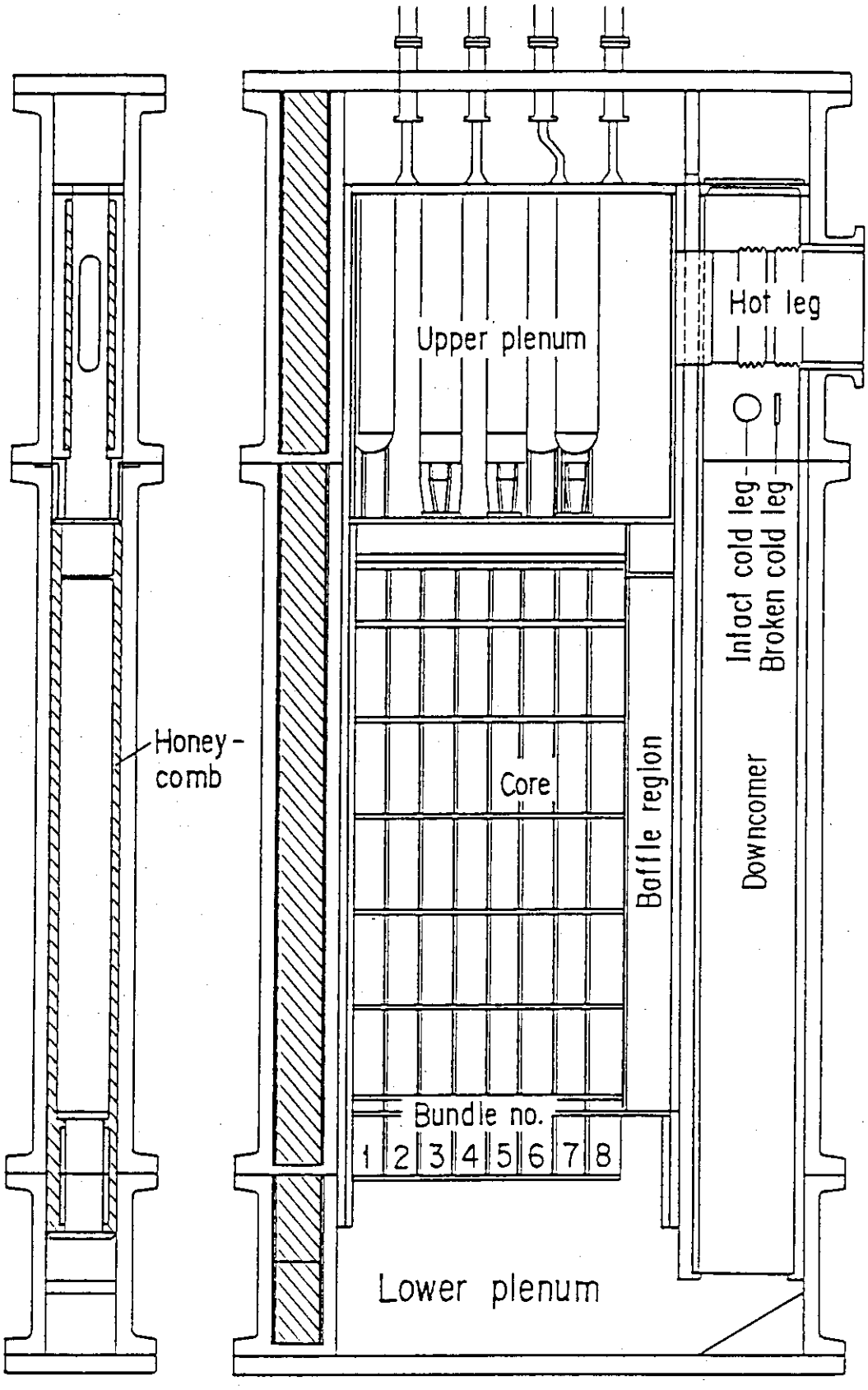

Fig. 2.2 Pressure vessel of SCTF Core-III

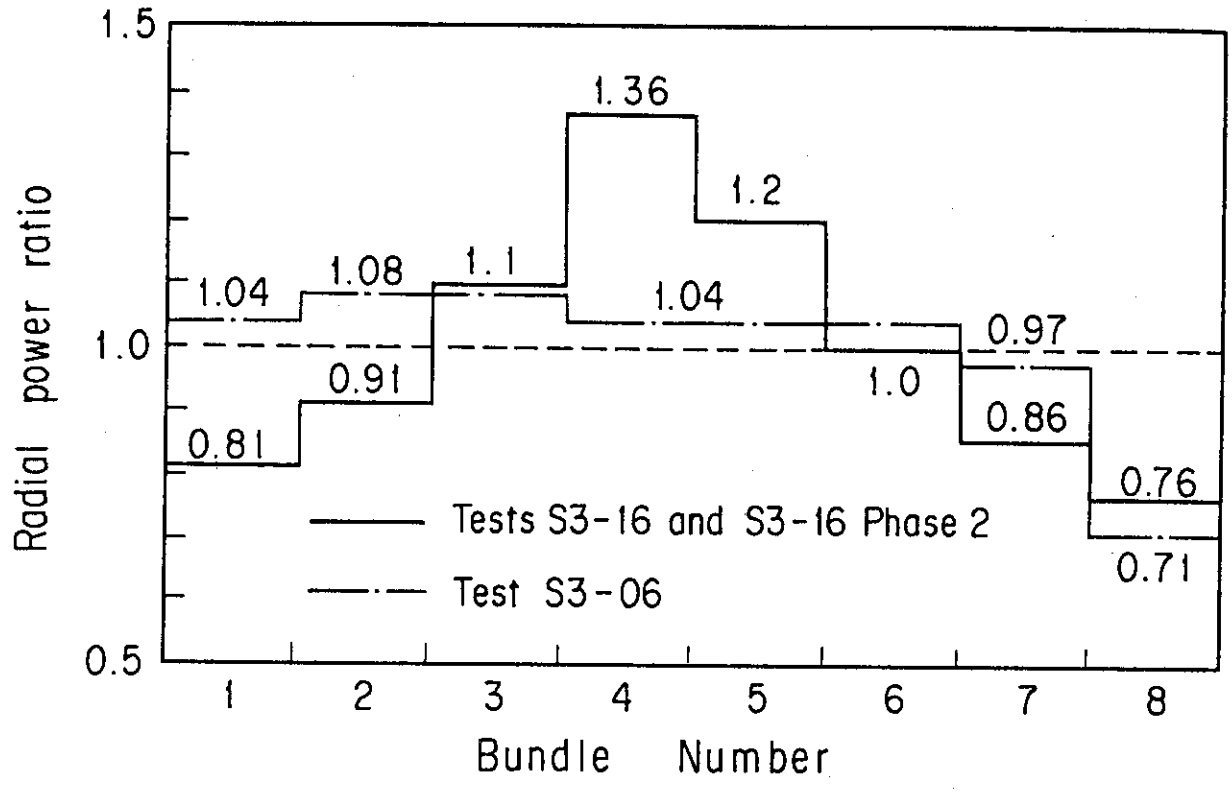

Fig. 2.3 Radial power distributions for Tests S3-06, S3-SH1, S3-16 and S3-16-Phase 2

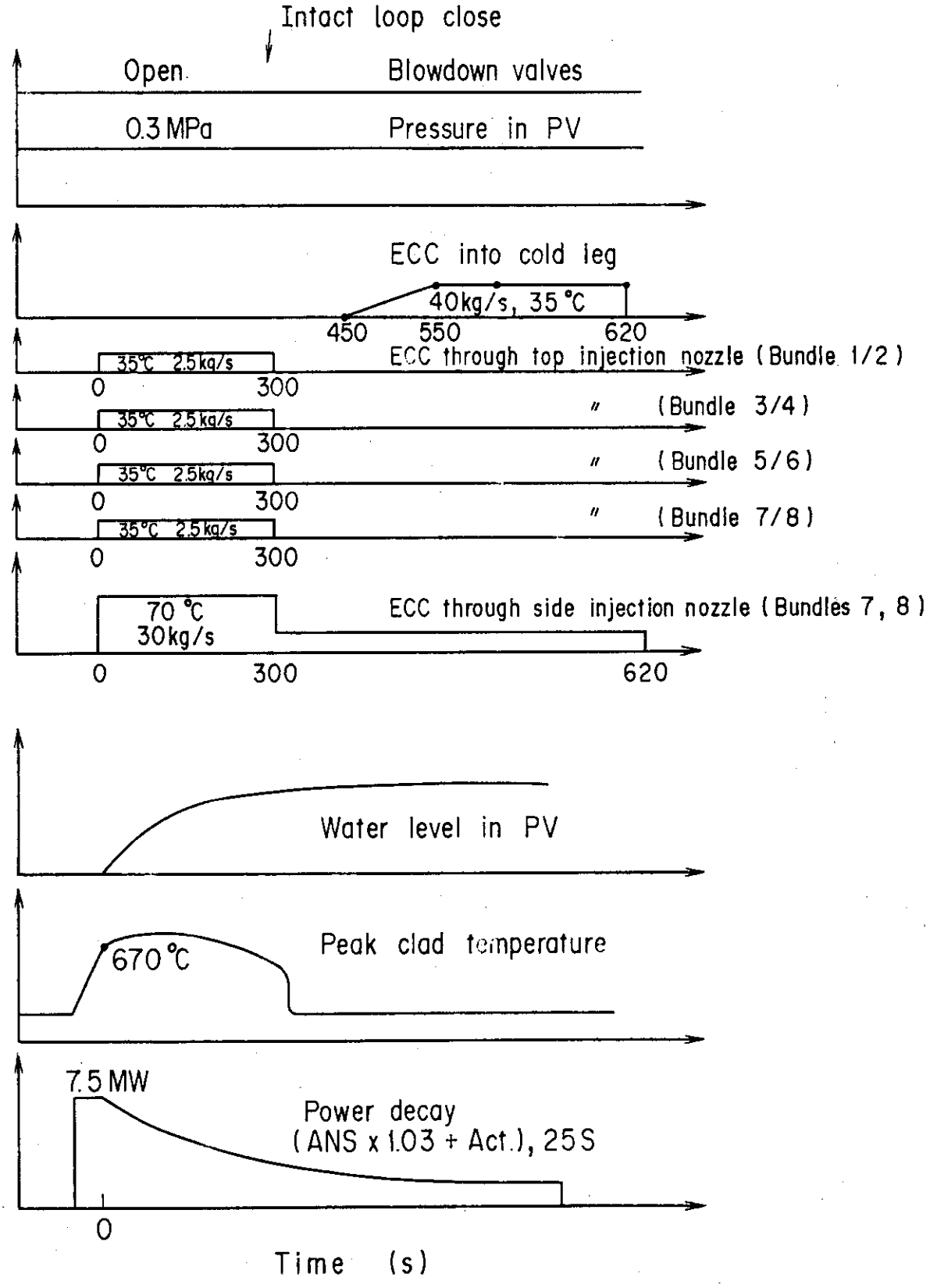

Test sequence of Run 710

Fig. 2.4 Test sequence of Test S3-06

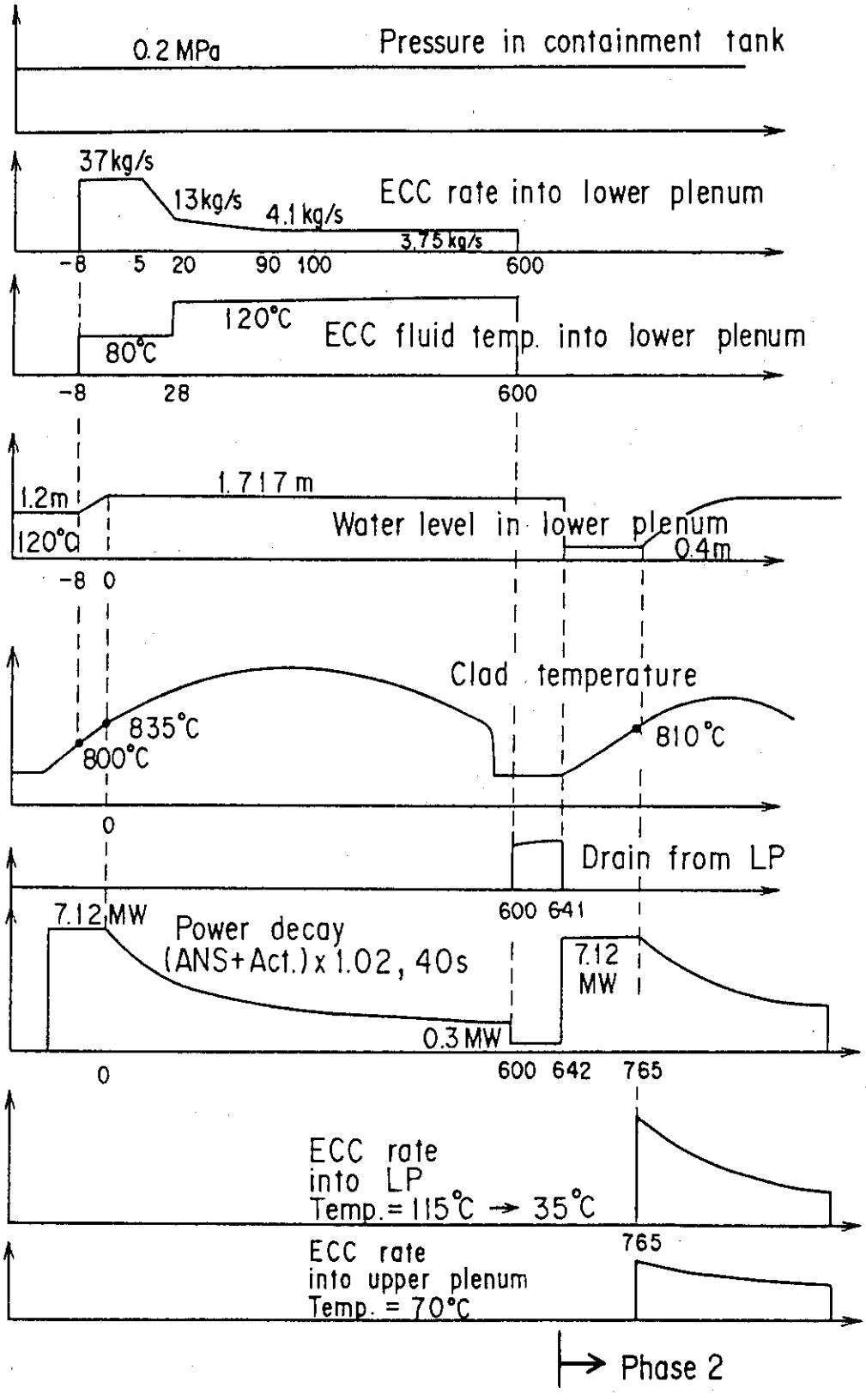

Fig. 2.5 Test sequence of Test S3-16-Phase 1 & 2

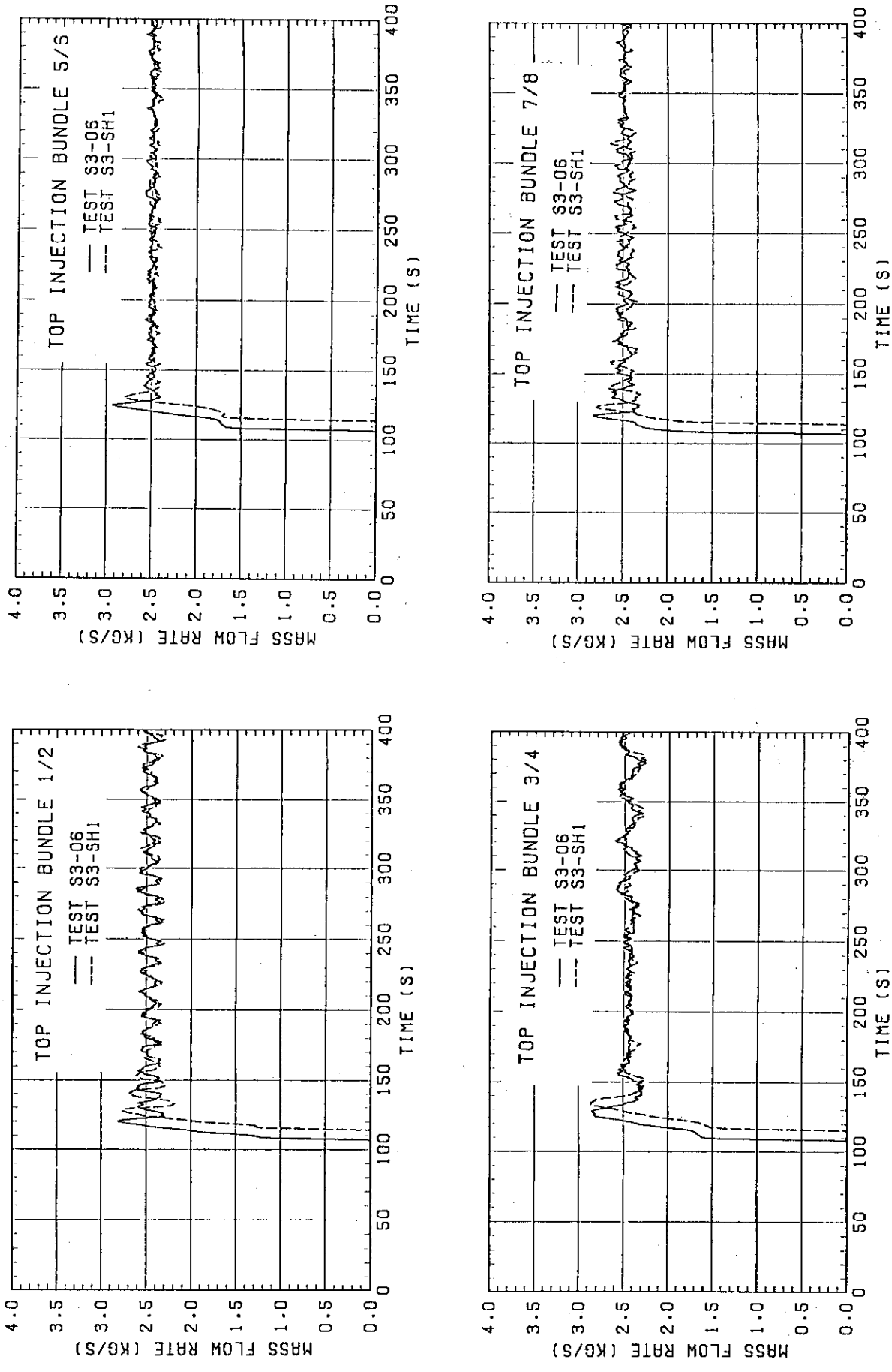

Fig. 3.1 ECC injection rates into upper plenum through top injection nozzles

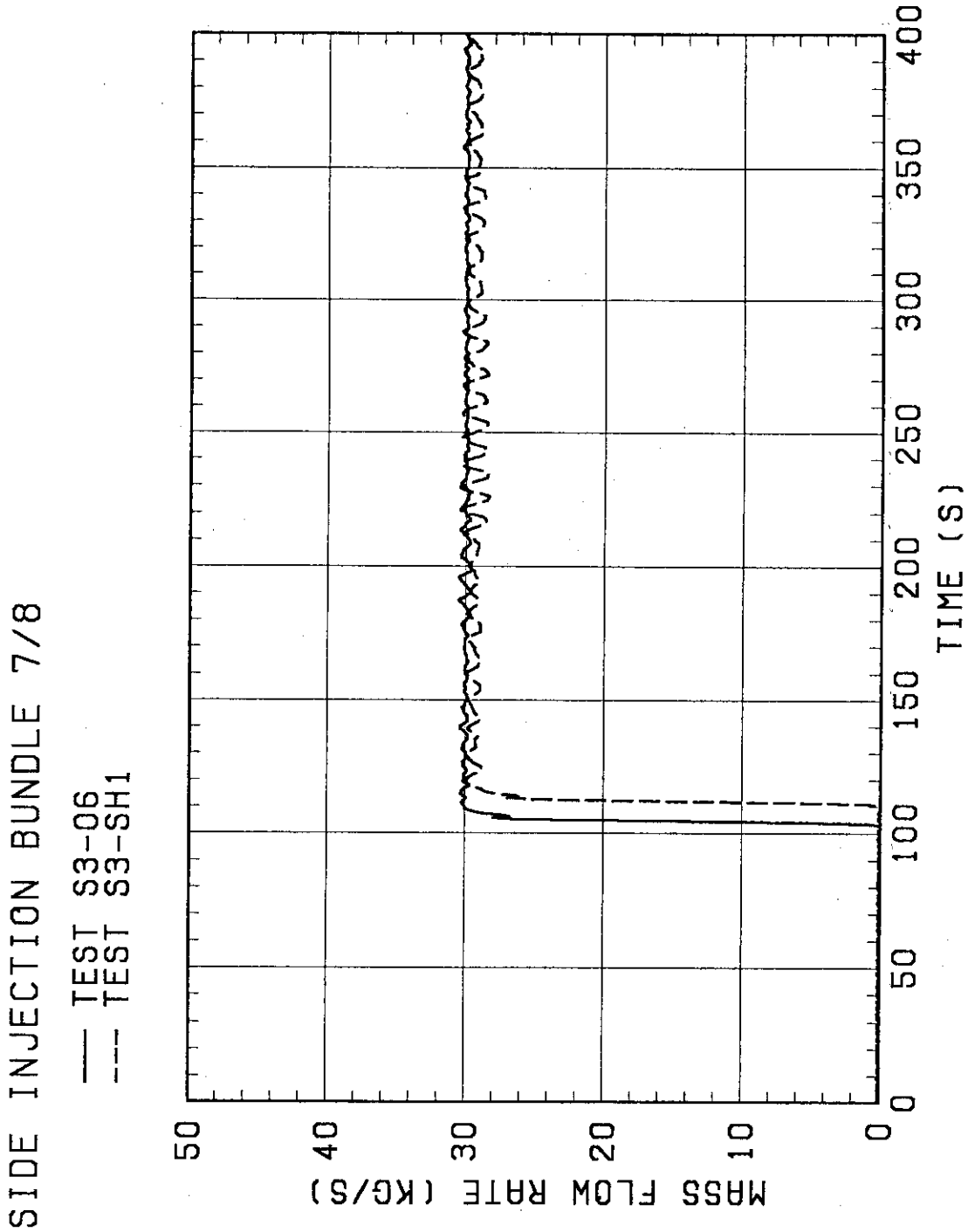

Fig. 3.2 ECC injection rates into plenum through side injection nozzles

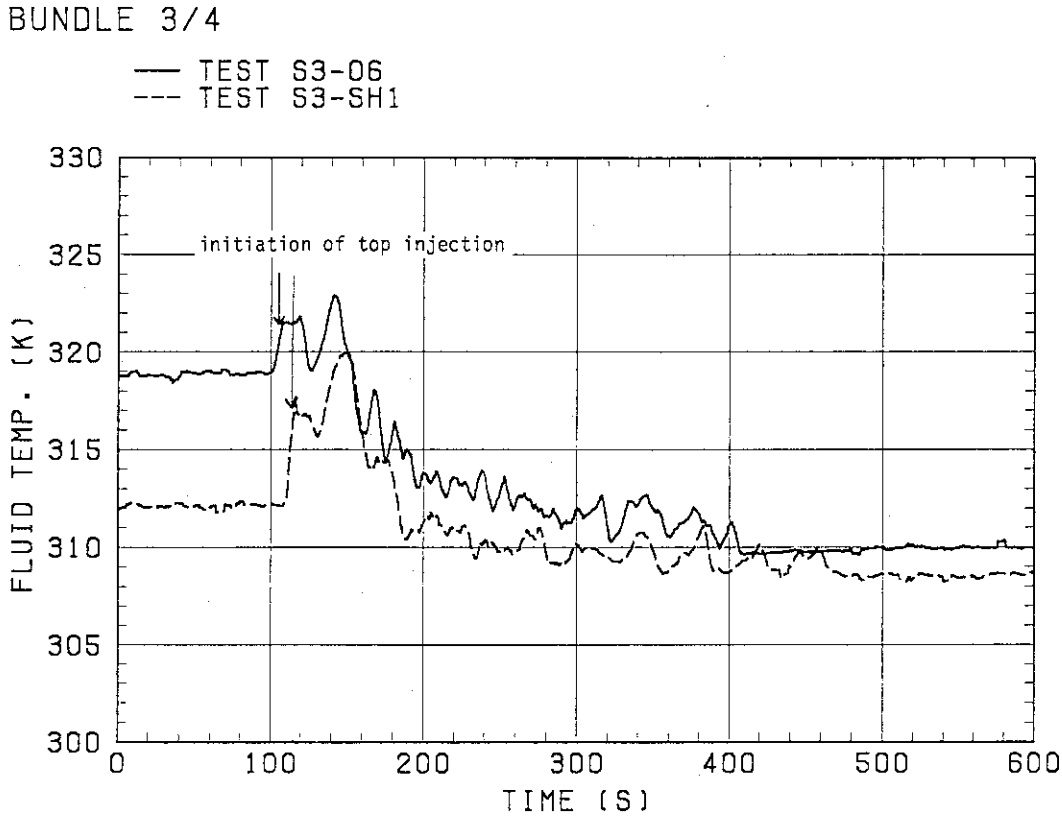

Fig. 3.3 Water temperatures for top incection

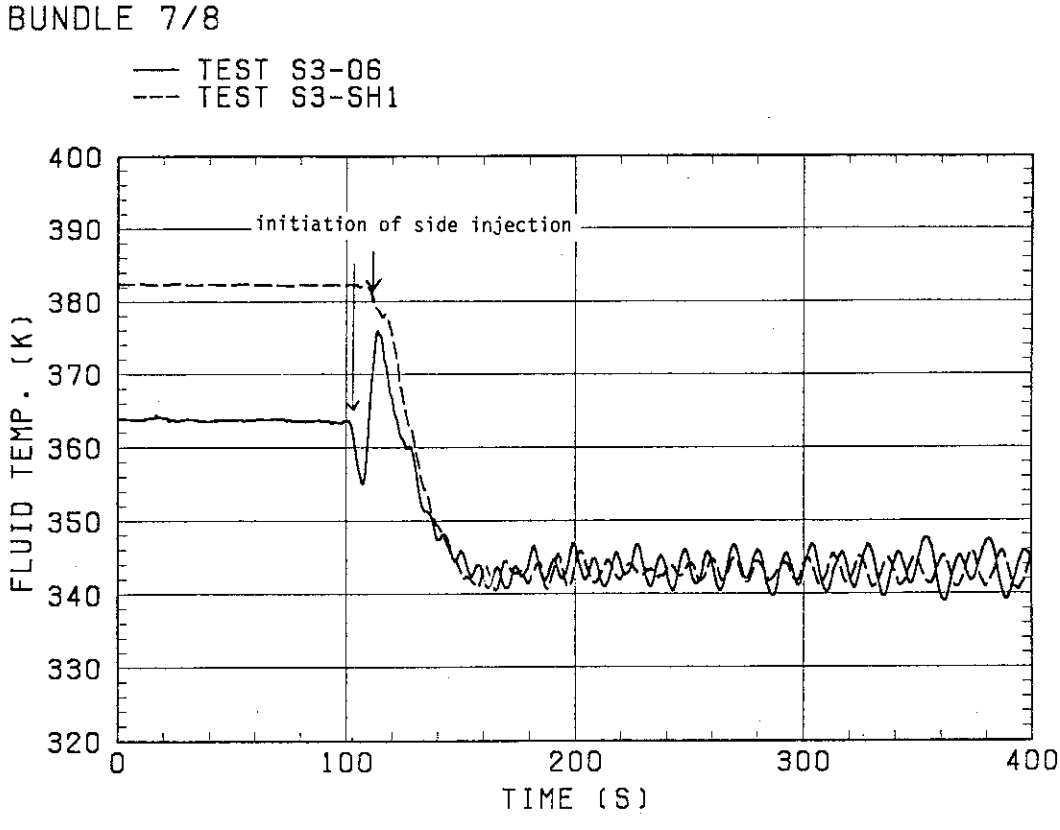

Fig. 3.4 Water temperatures for side injection

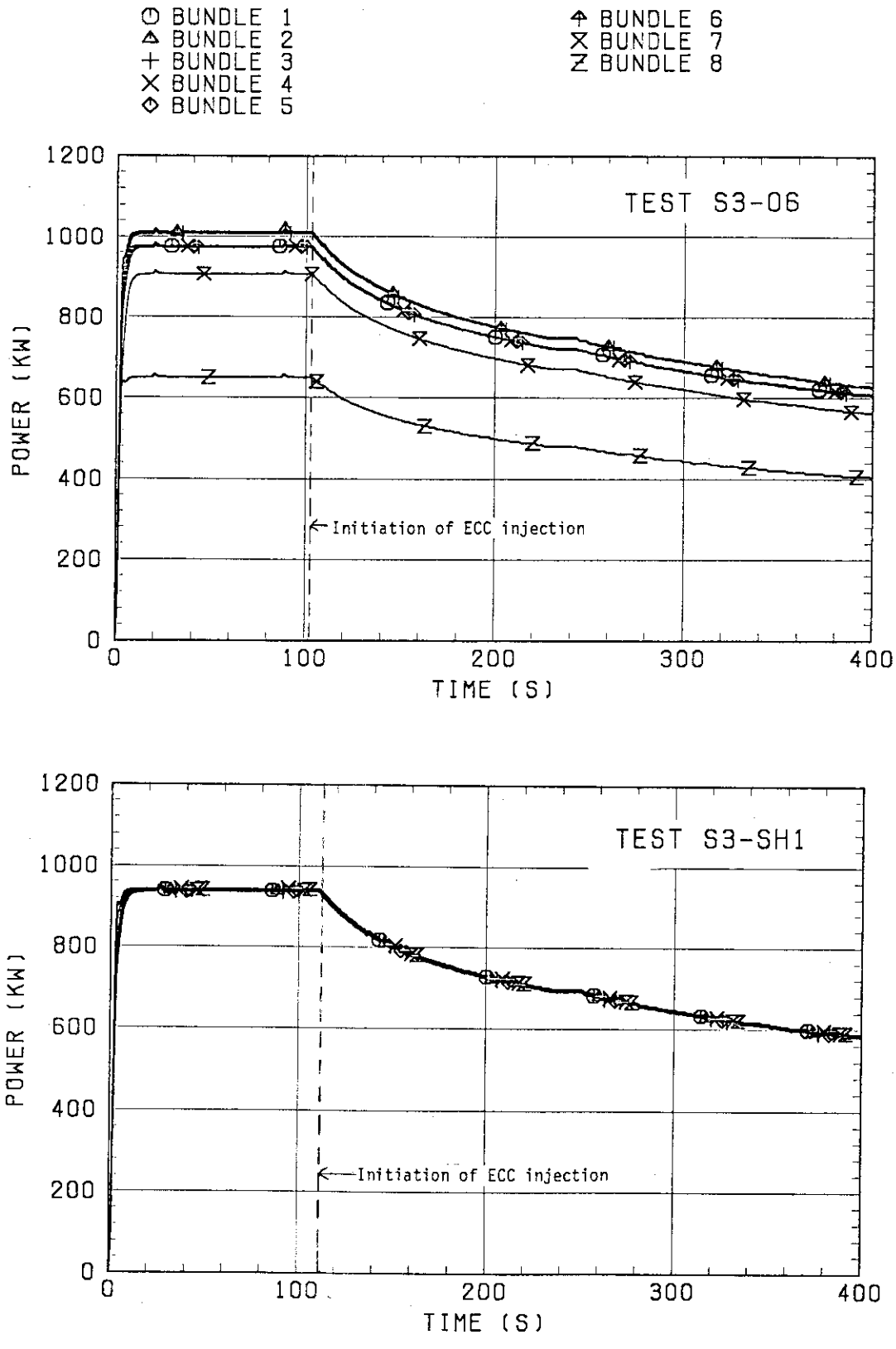

Fig. 3.5 Core heating power

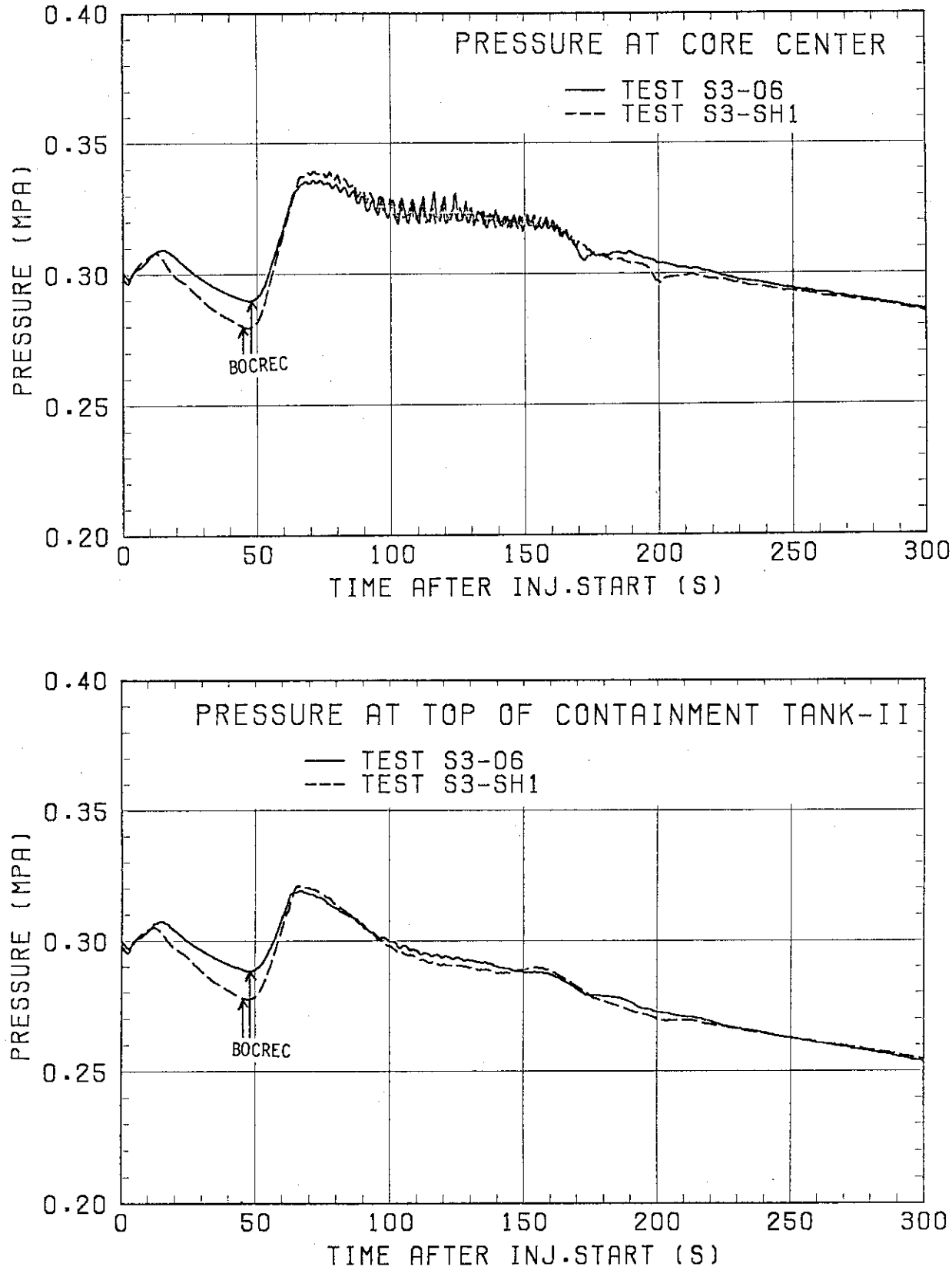

Fig. 3.6 Pressures at core center and top of containment tank-II

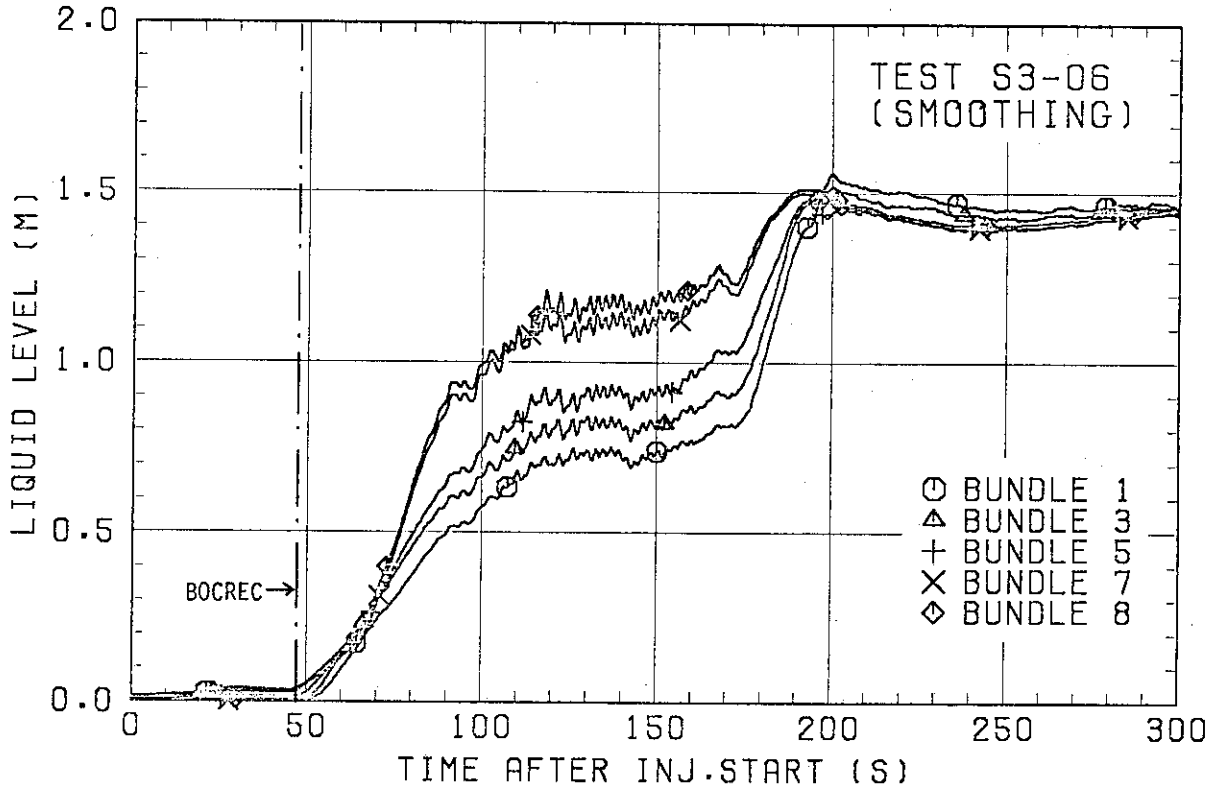

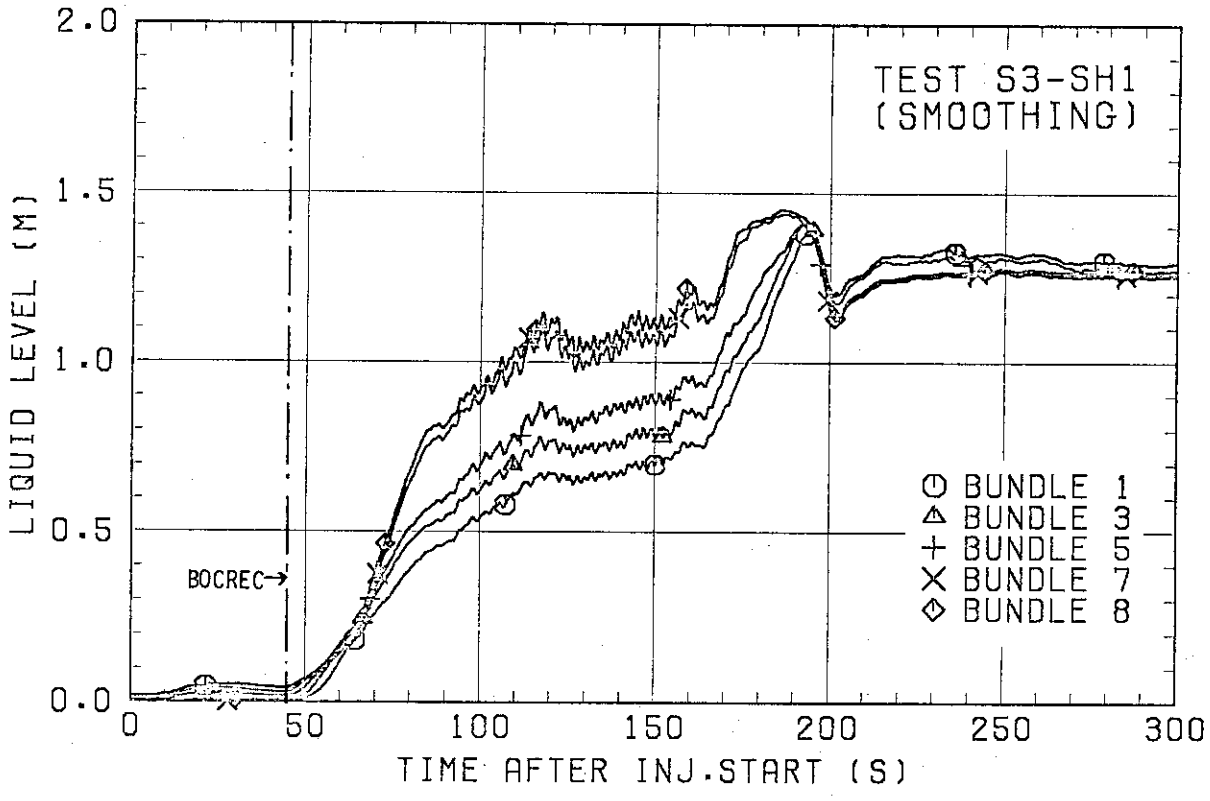

Fig. 3.7 Collapsed liquid in upper plenum

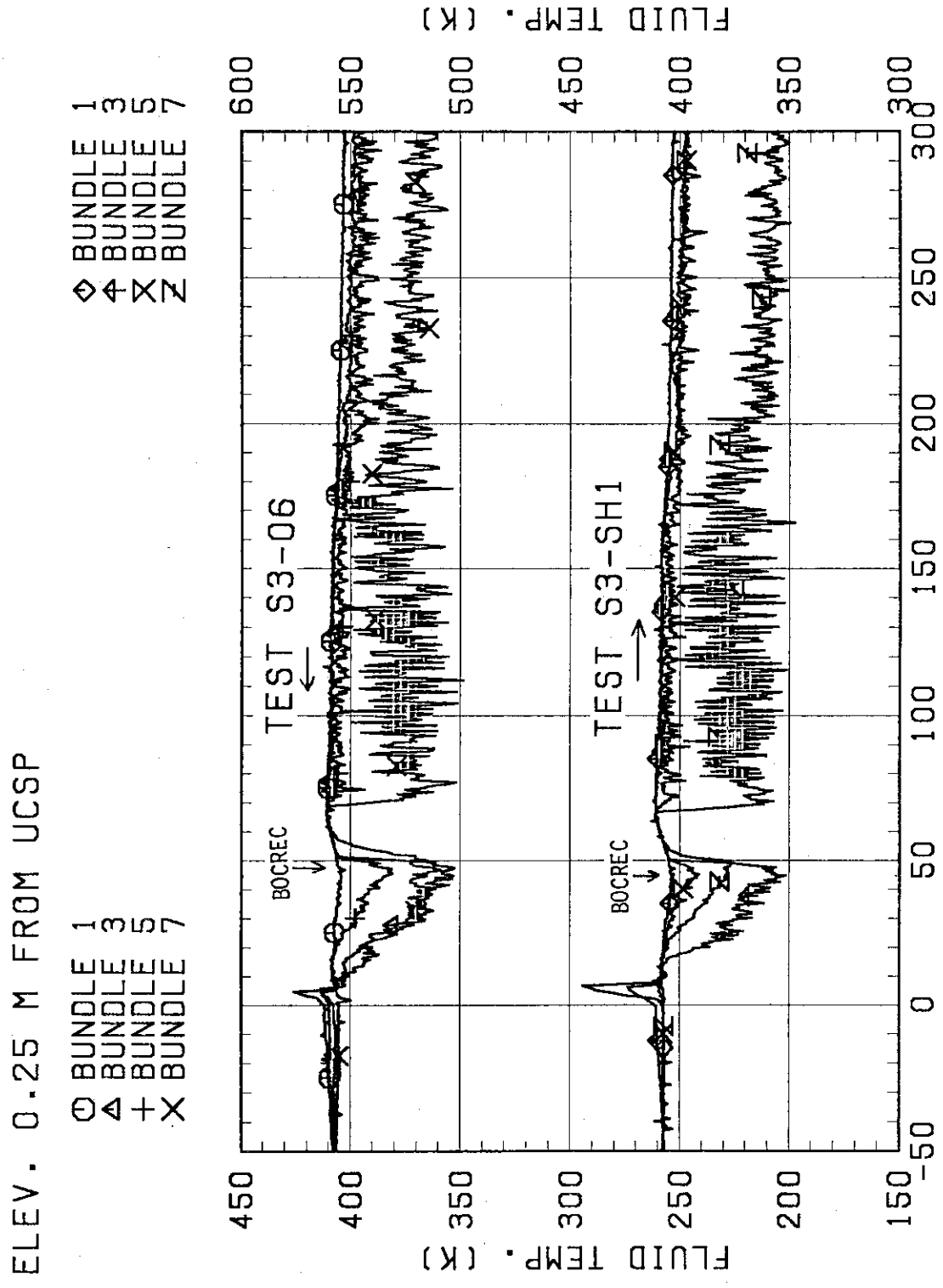

Fig. 3.8 Fluid temperatures in upper plenum at 0.25 m from UCSP

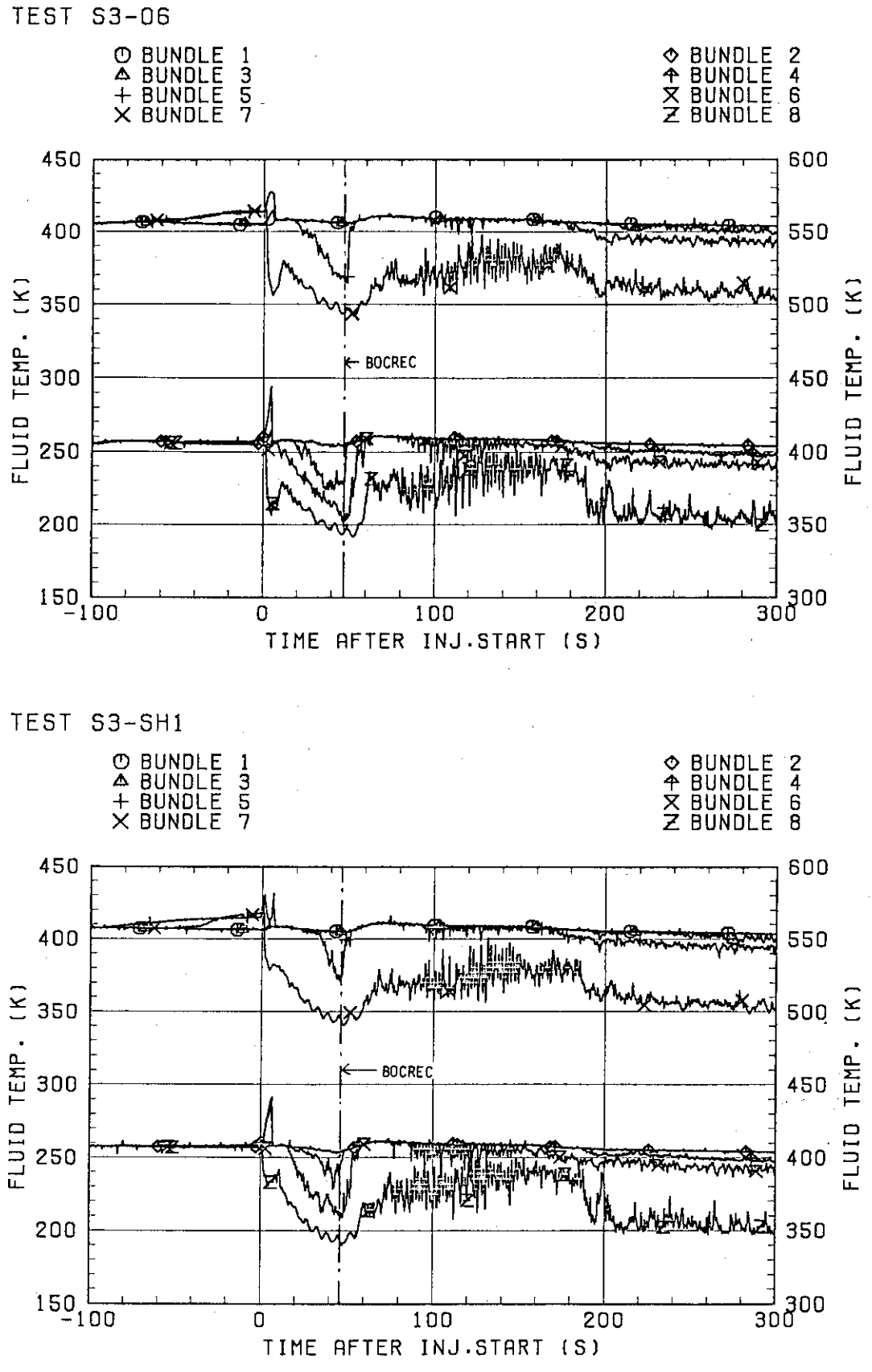

Fig. 3.9 Fluid temperatures at UCSP holes

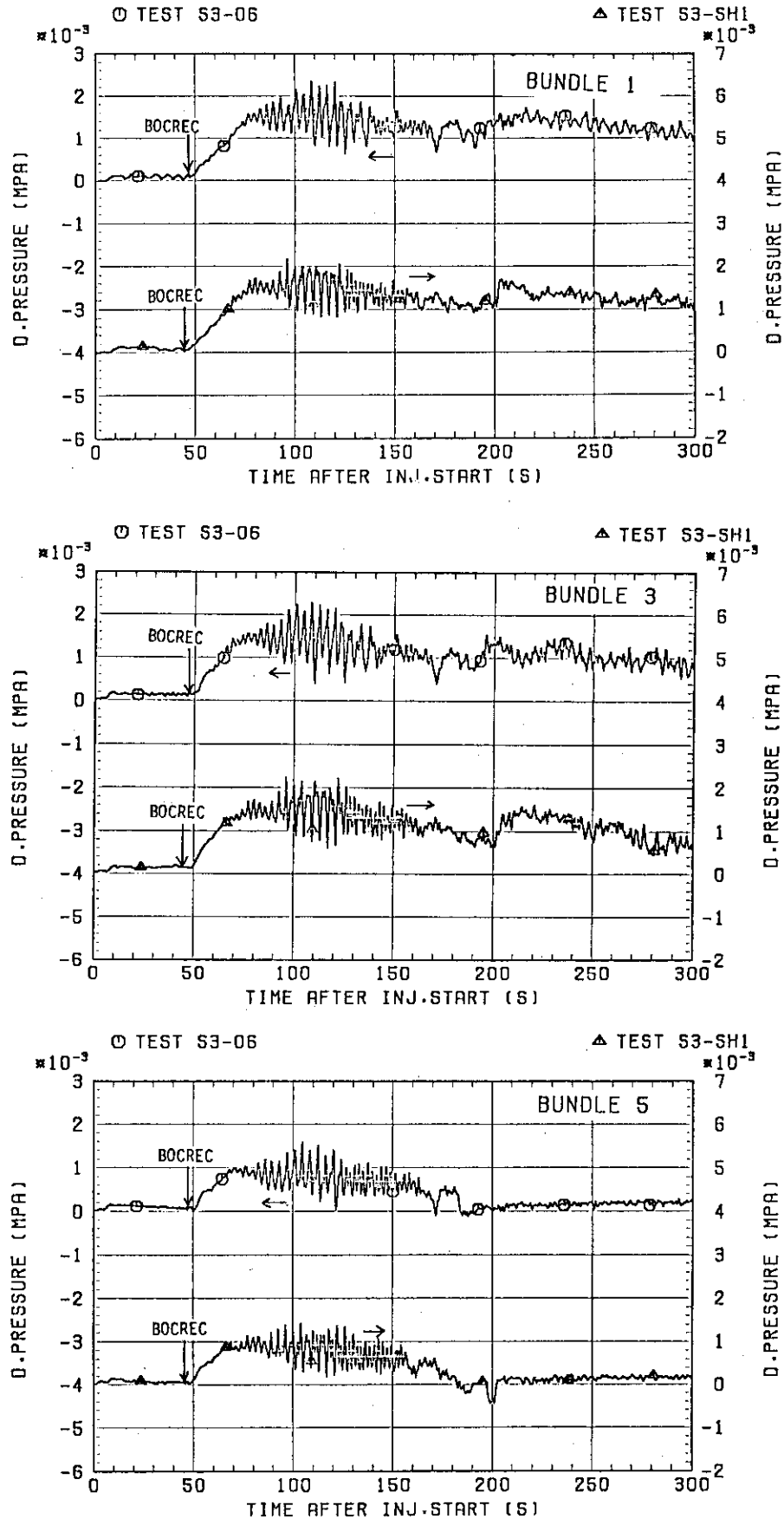

Fig. 3.10 Differential pressures across end box tie plate

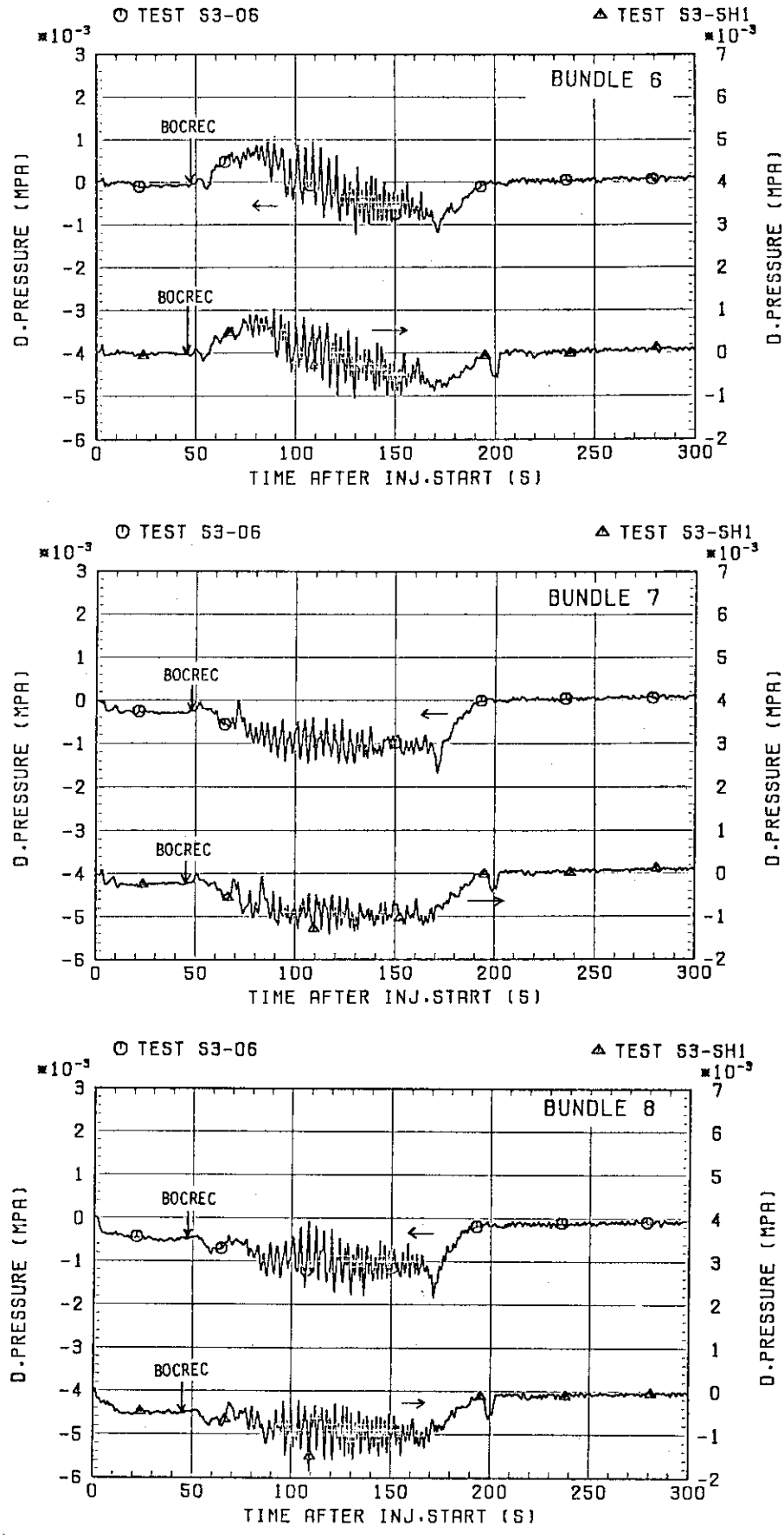

Fig. 3.10 (Continued)

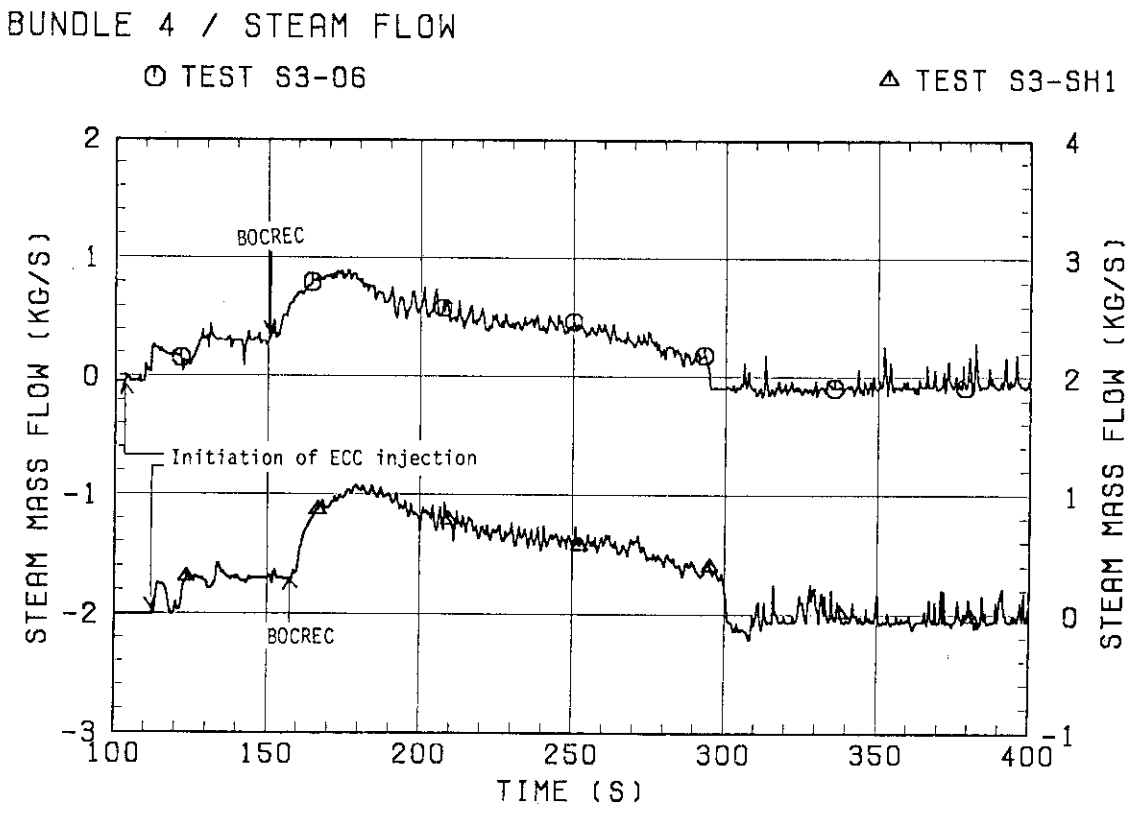

Fig. 3.11(a) Steam mass flow rate at end box tie plate in Bundle 4

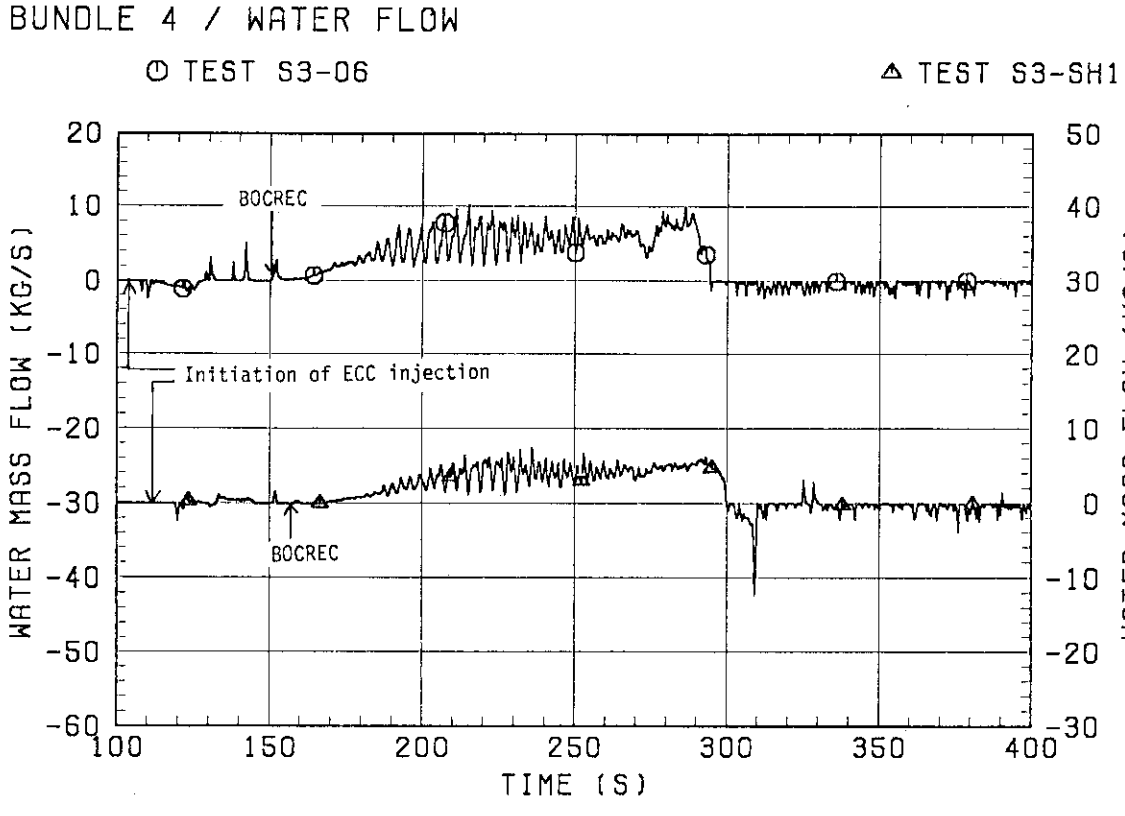

Fig. 3.11(b) Water mass flow rate at end box tie plate in Bundle 4

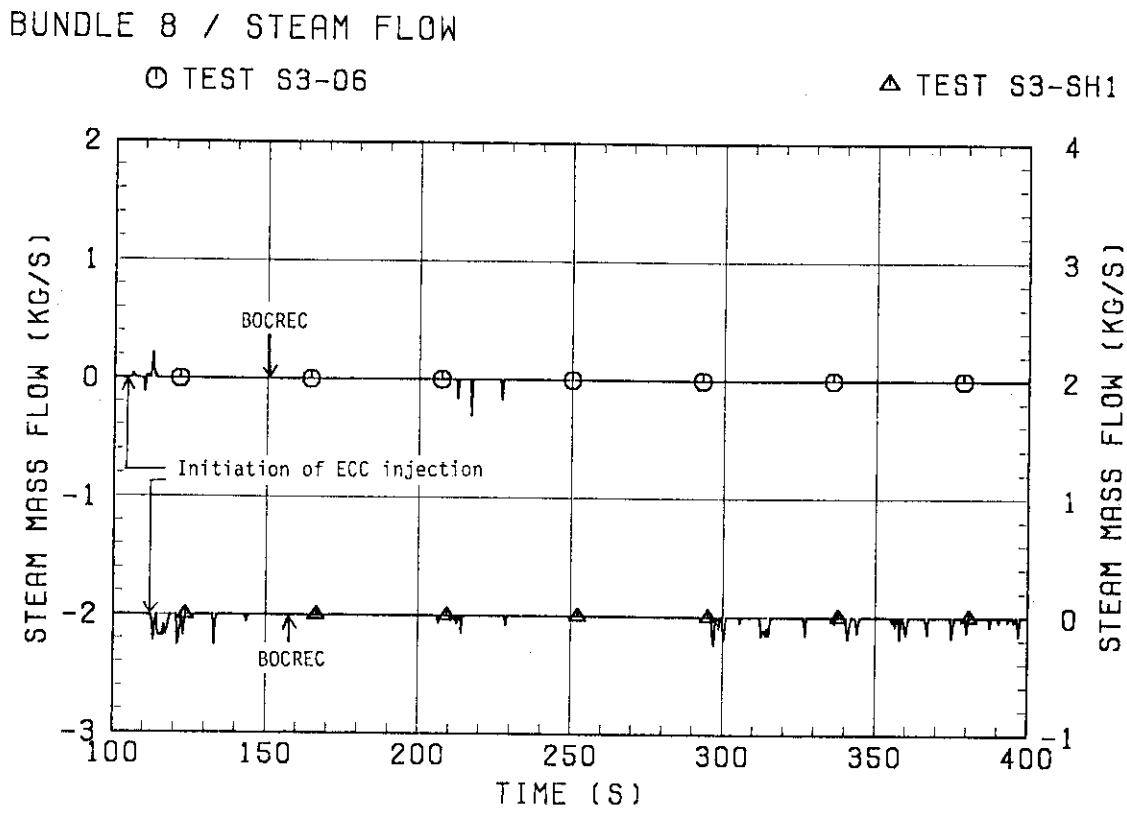

Fig. 3.11(c) Steam mass flow rate at end box tie plate in Bundle 8

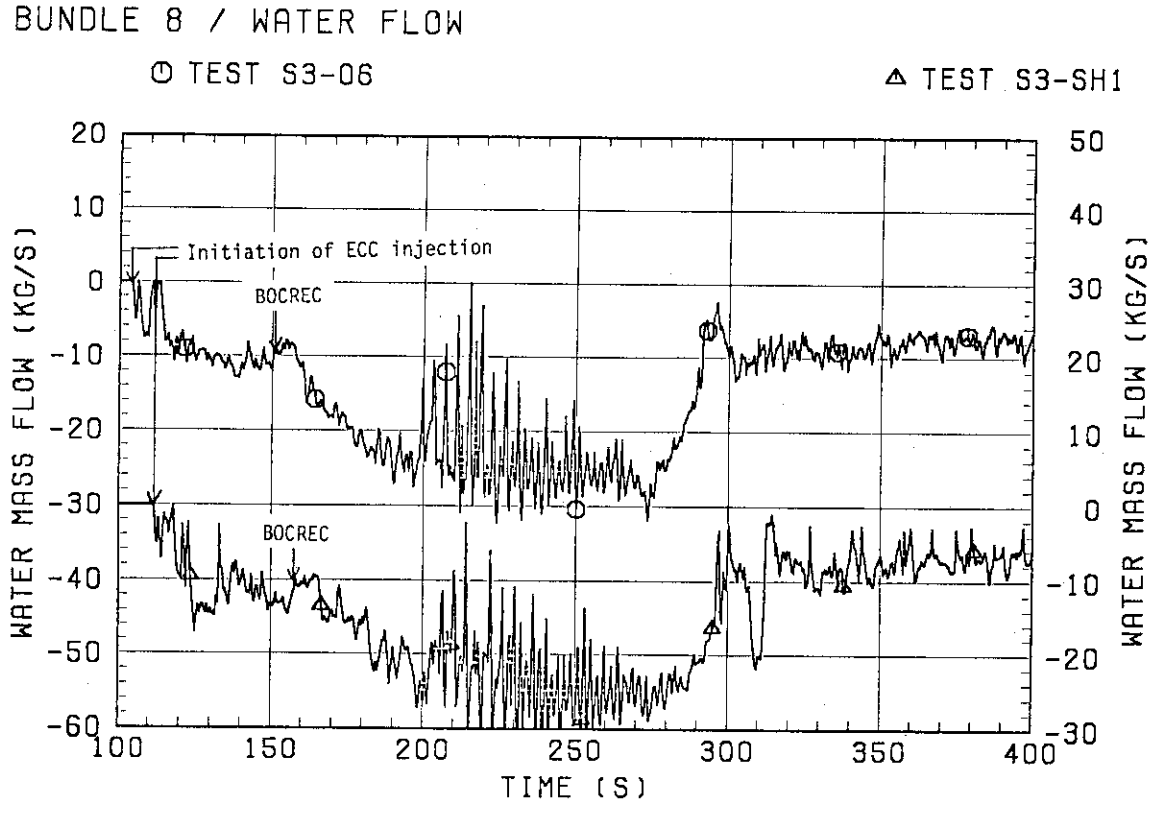

Fig. 3.11(d) Water mass flow rate at end box tie plate in Bundle 8

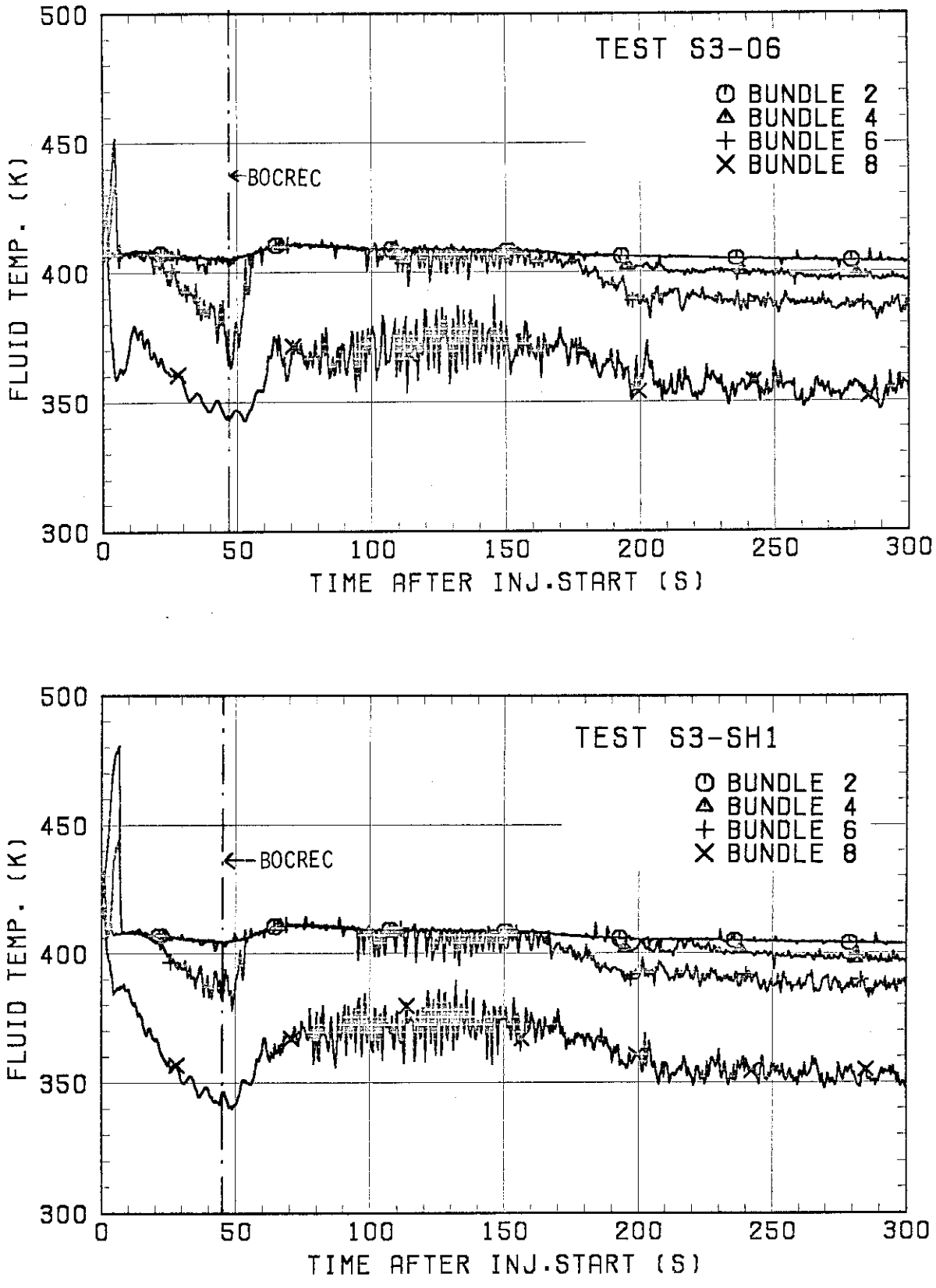

Fig. 3.12 Fluid temperatures just below end box tie plate

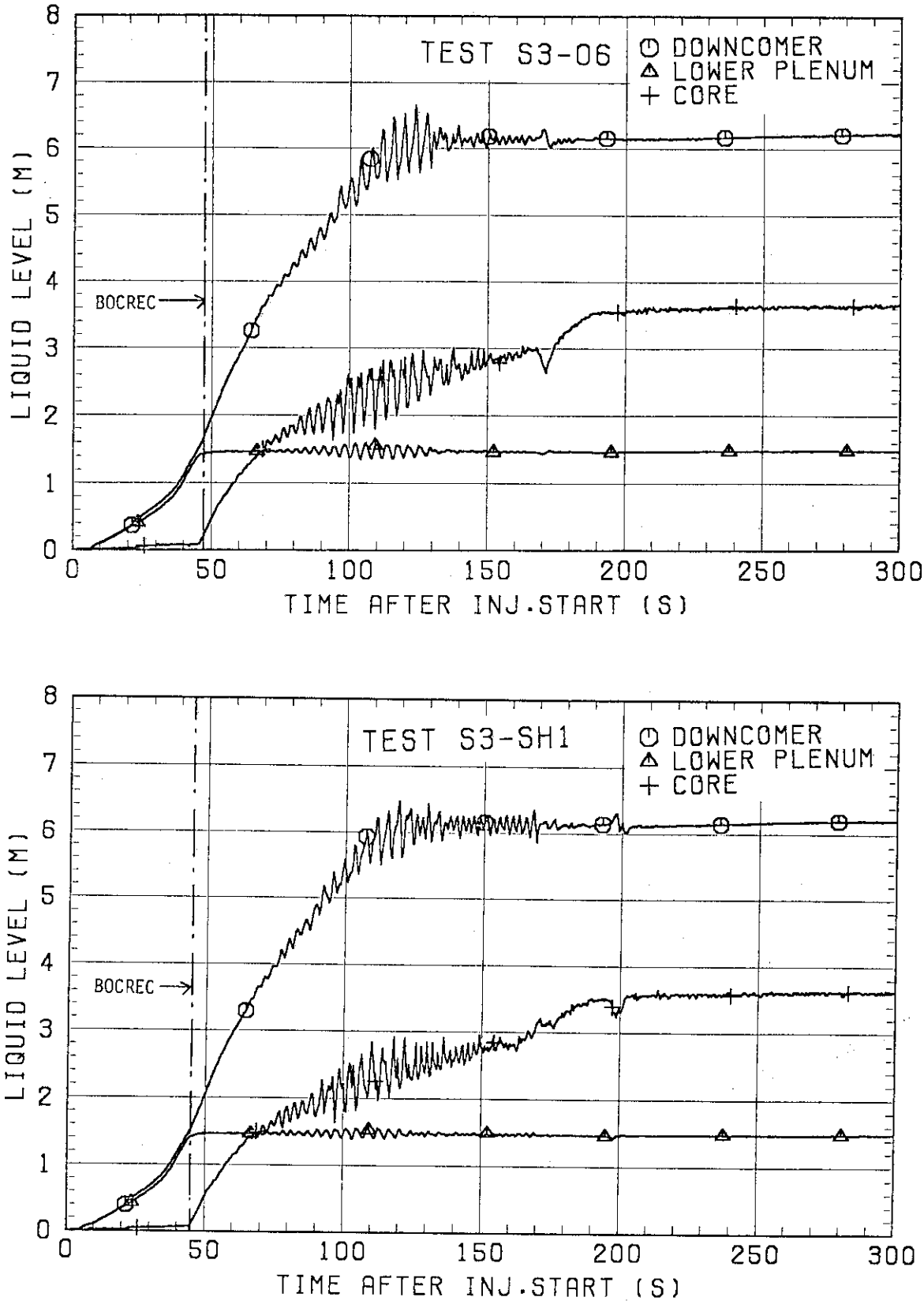

Fig. 3.13 Collapsed liquid levels in downcomer, lower plenum and core

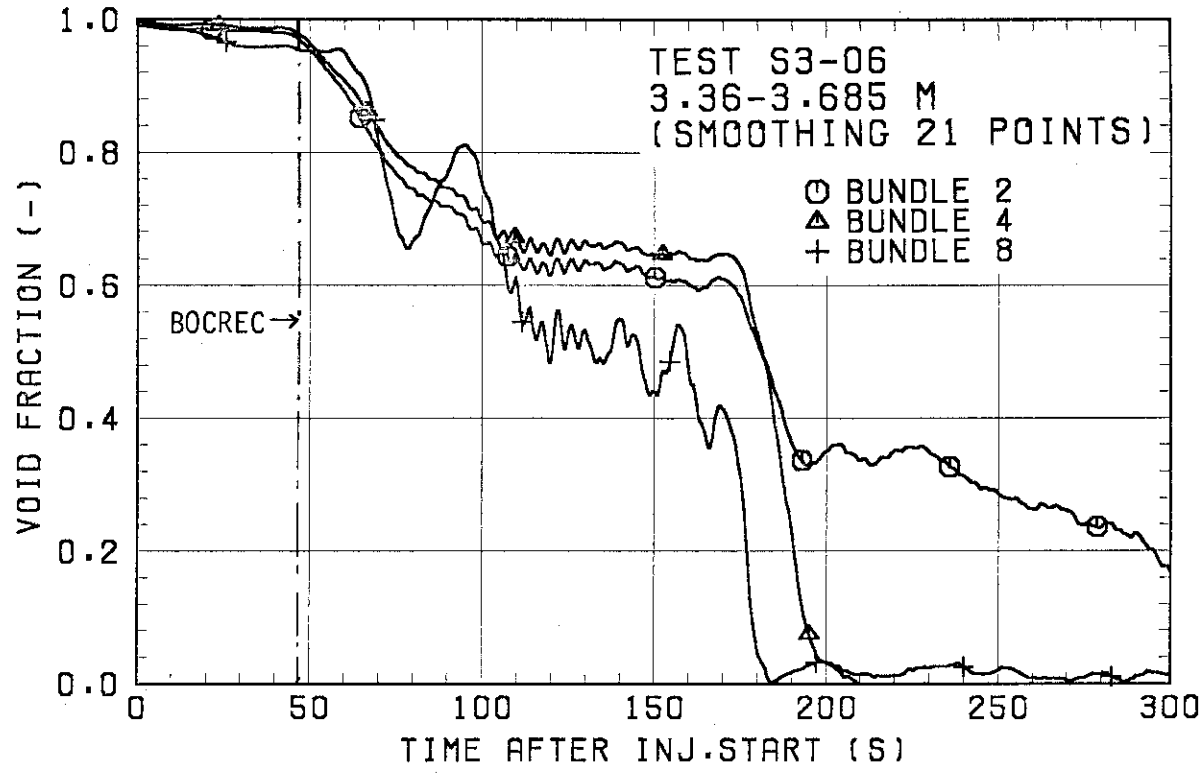

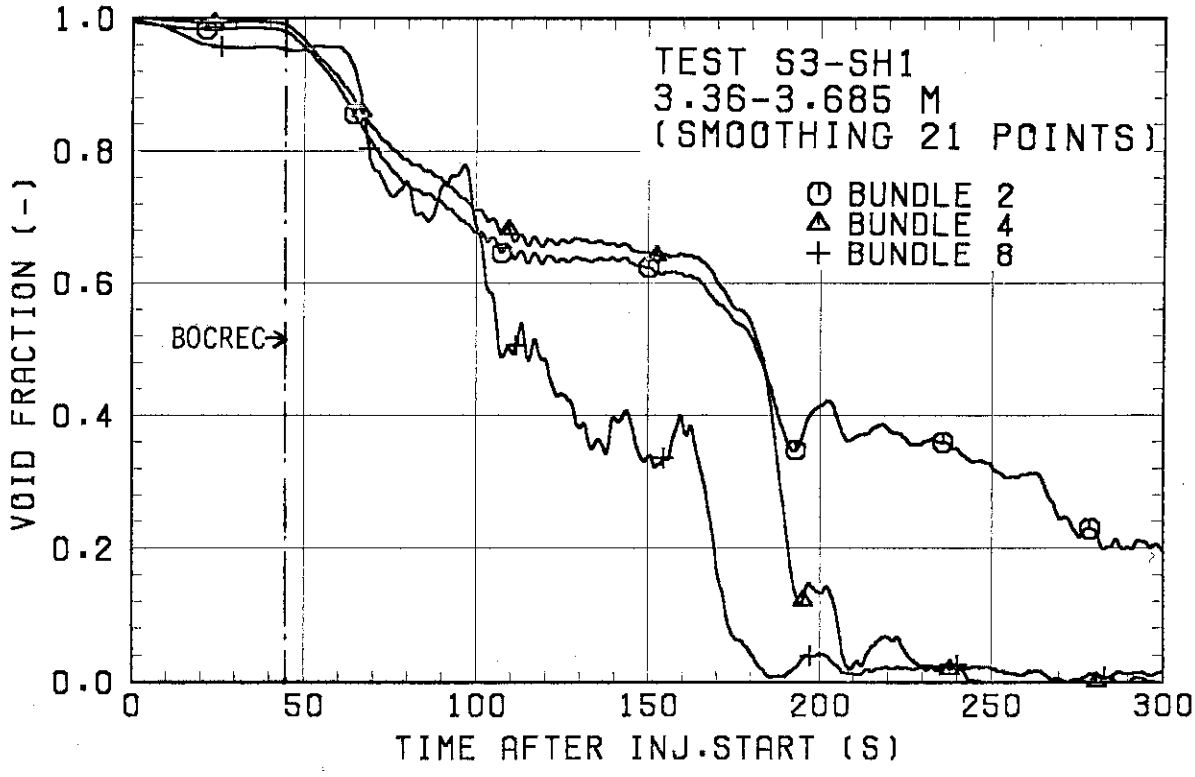

Fig. 3.14(a) Void fractions in core measured with D/P cells at upper elevation

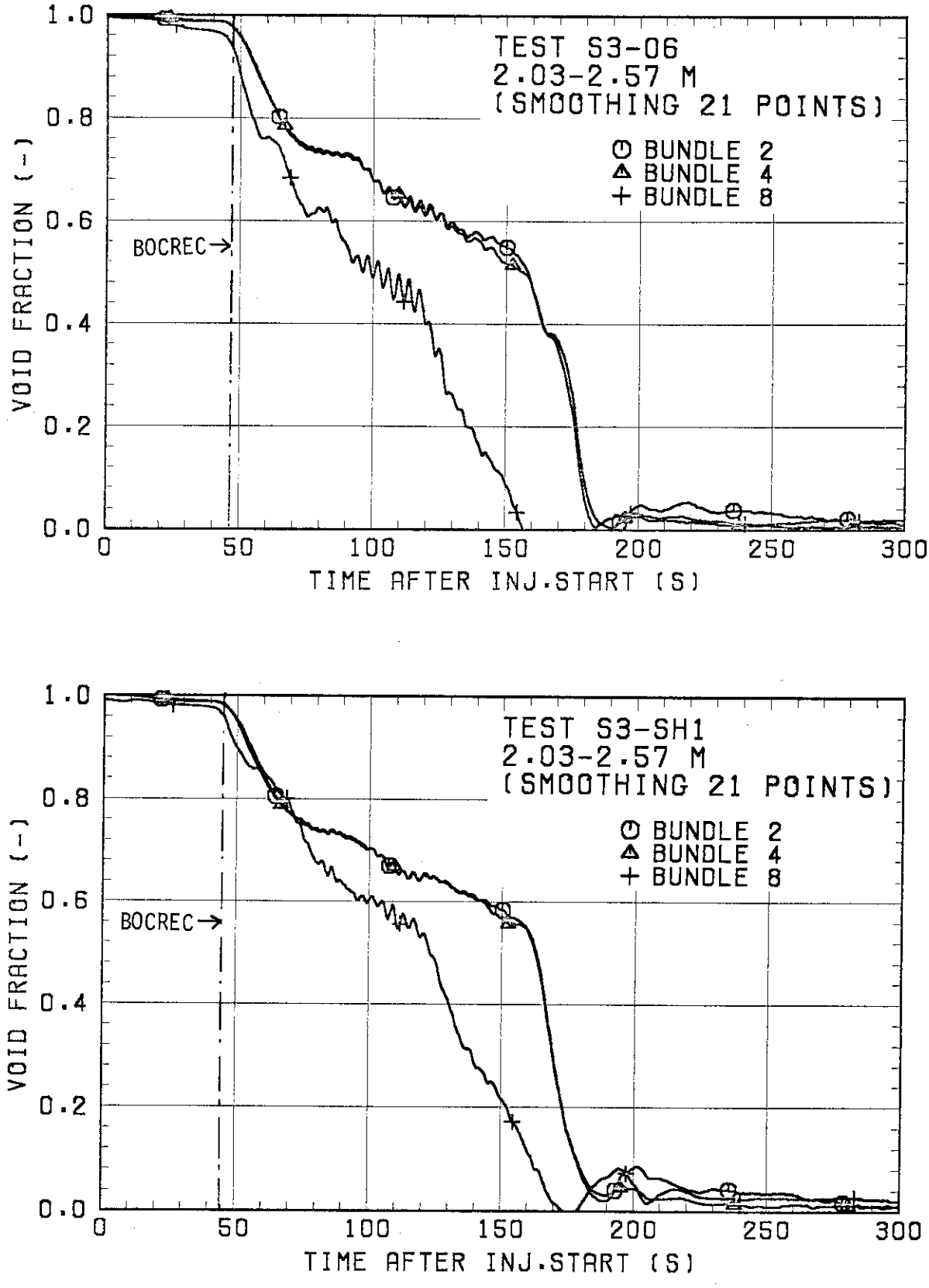

Fig. 3.14(b) Void fractions in core measured with D/P cells at cells elevation

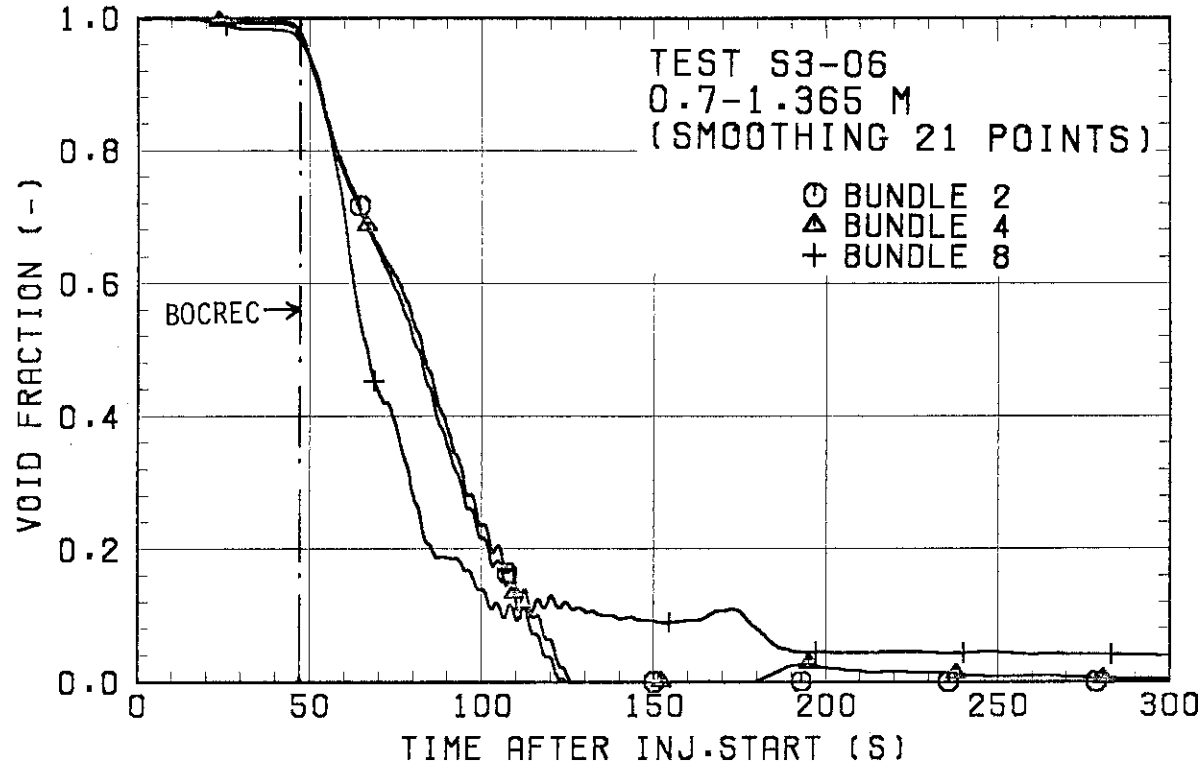

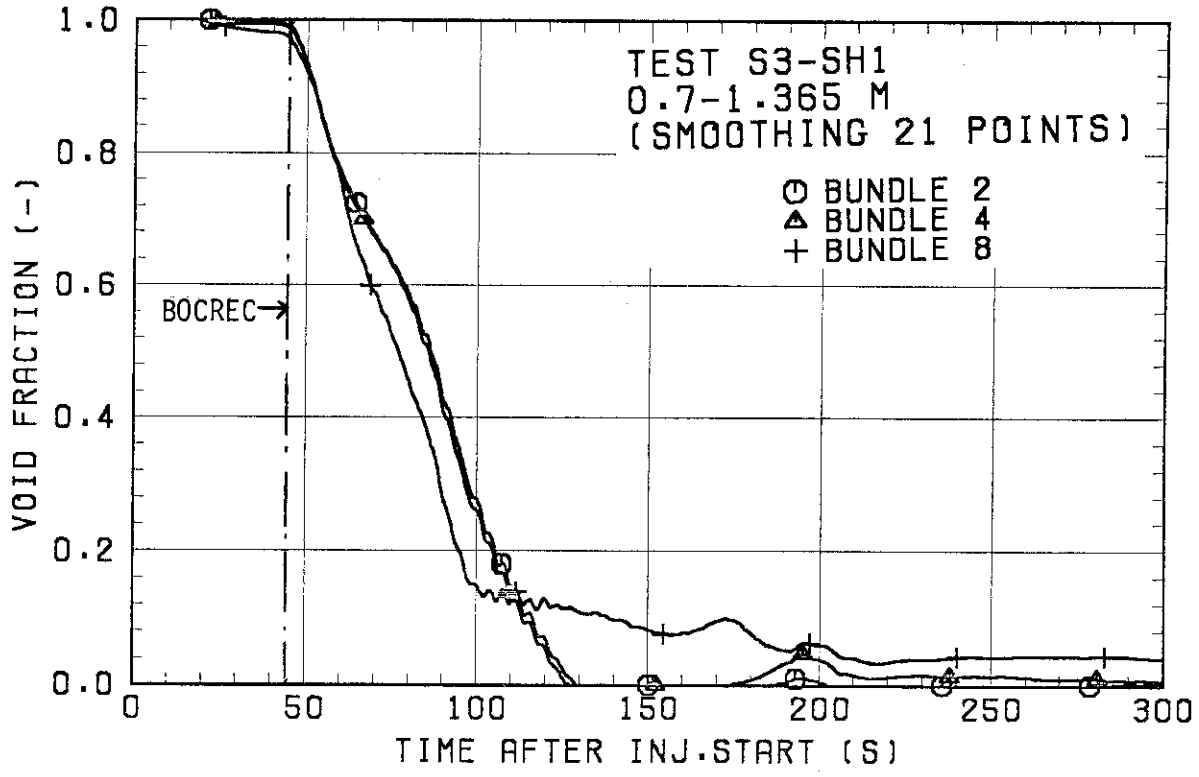

Fig. 3.14(c) Void fractions in core measured with D/P cells at lower elevation

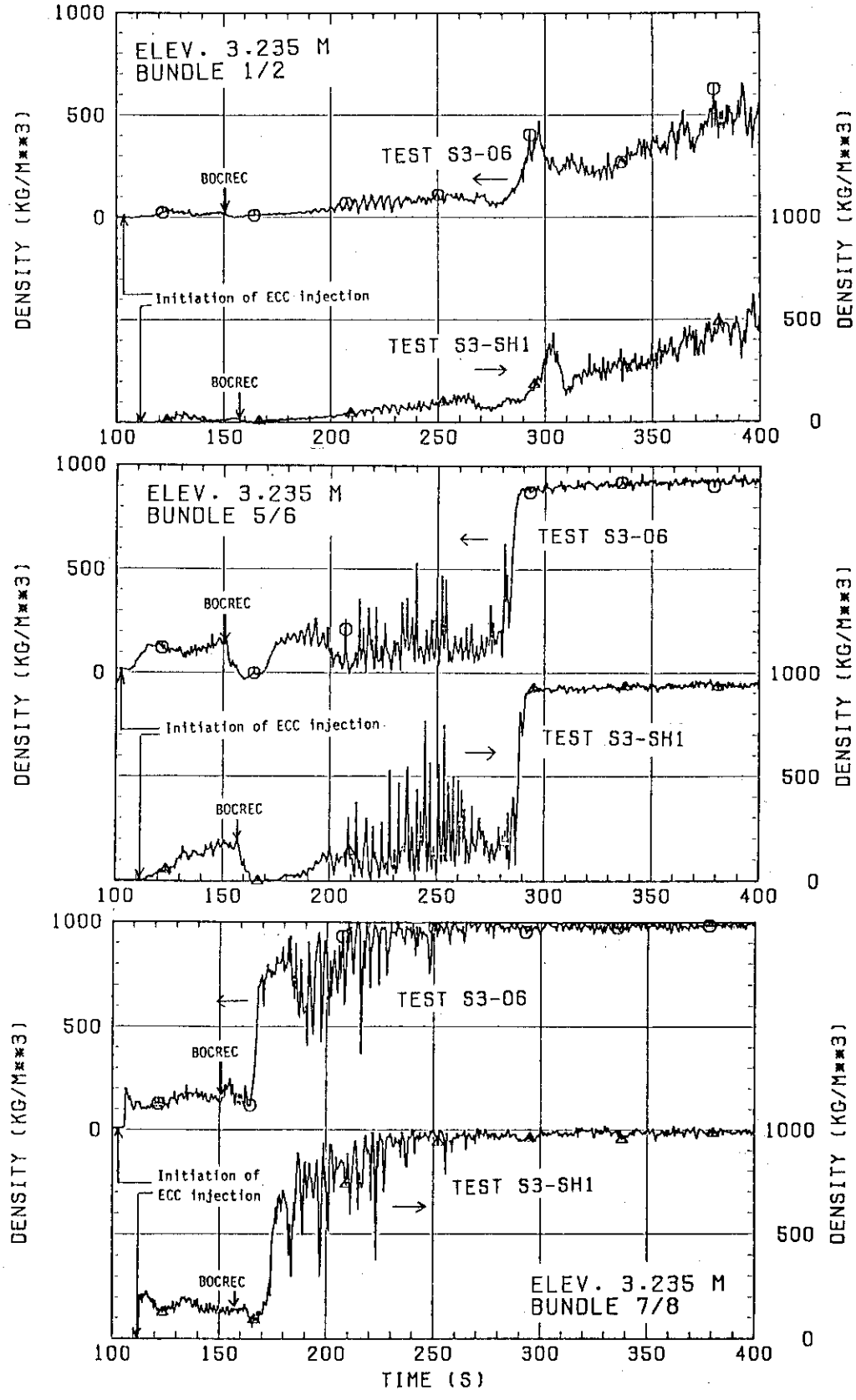

Fig. 3.15 Fluid densities in core measured with γ -densitometers

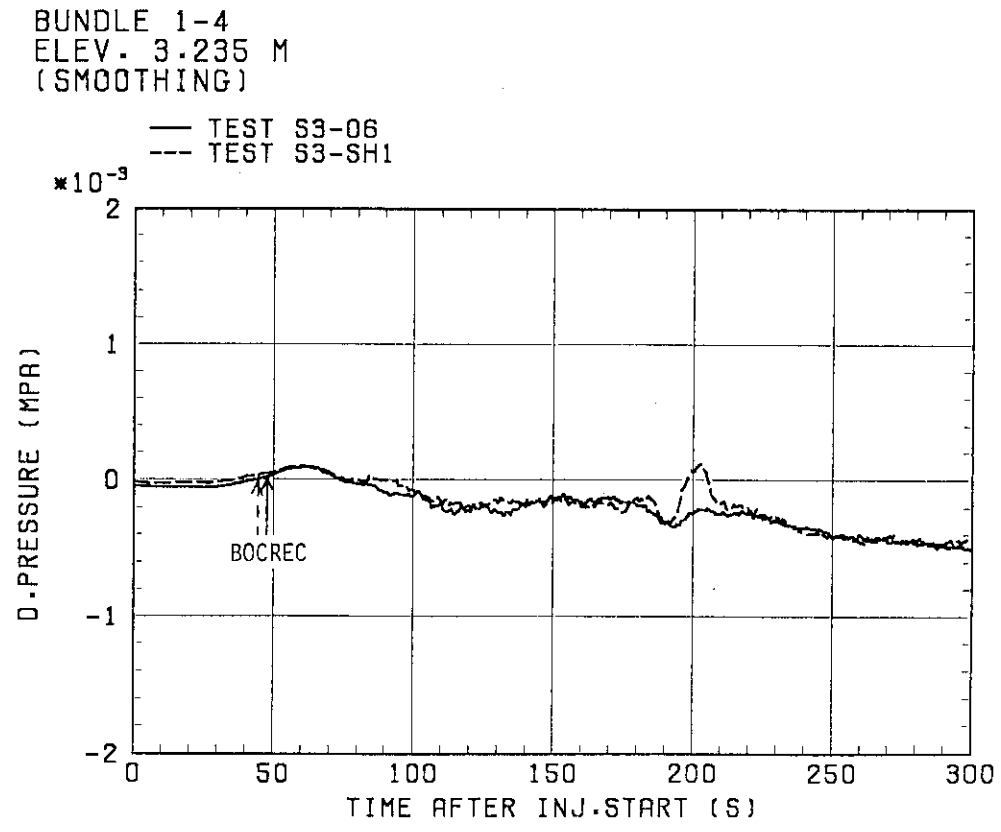

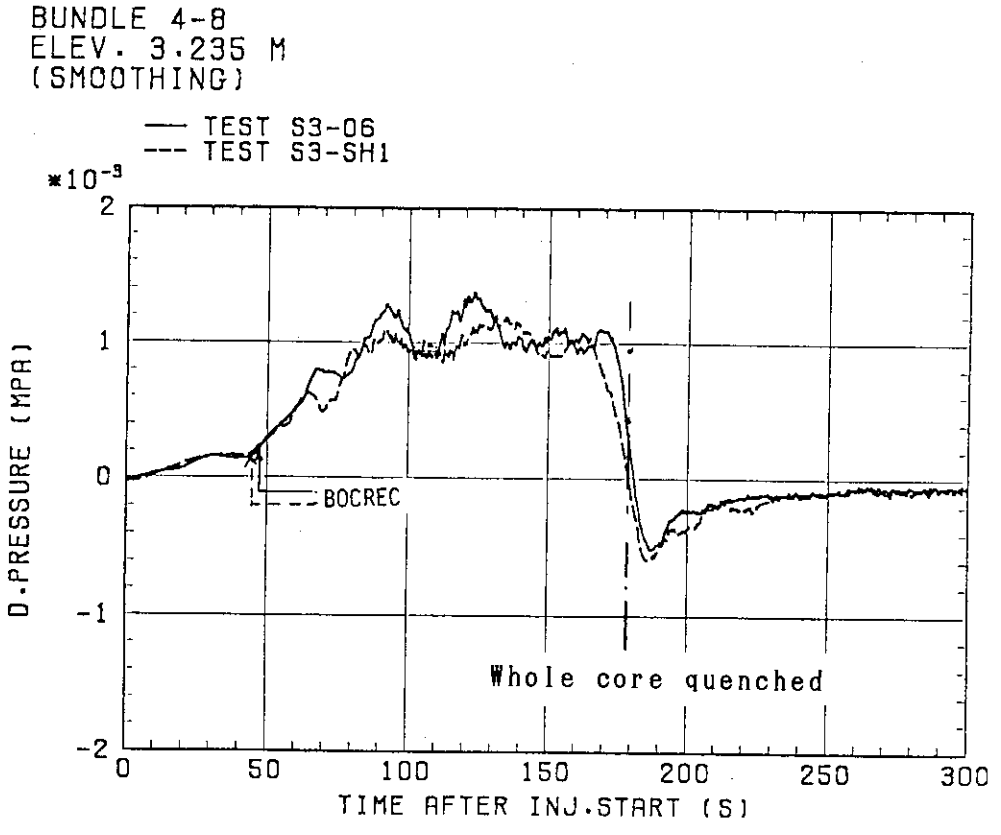

Fig. 3.16(a) Horizontal differential pressures in core at 3.235 m

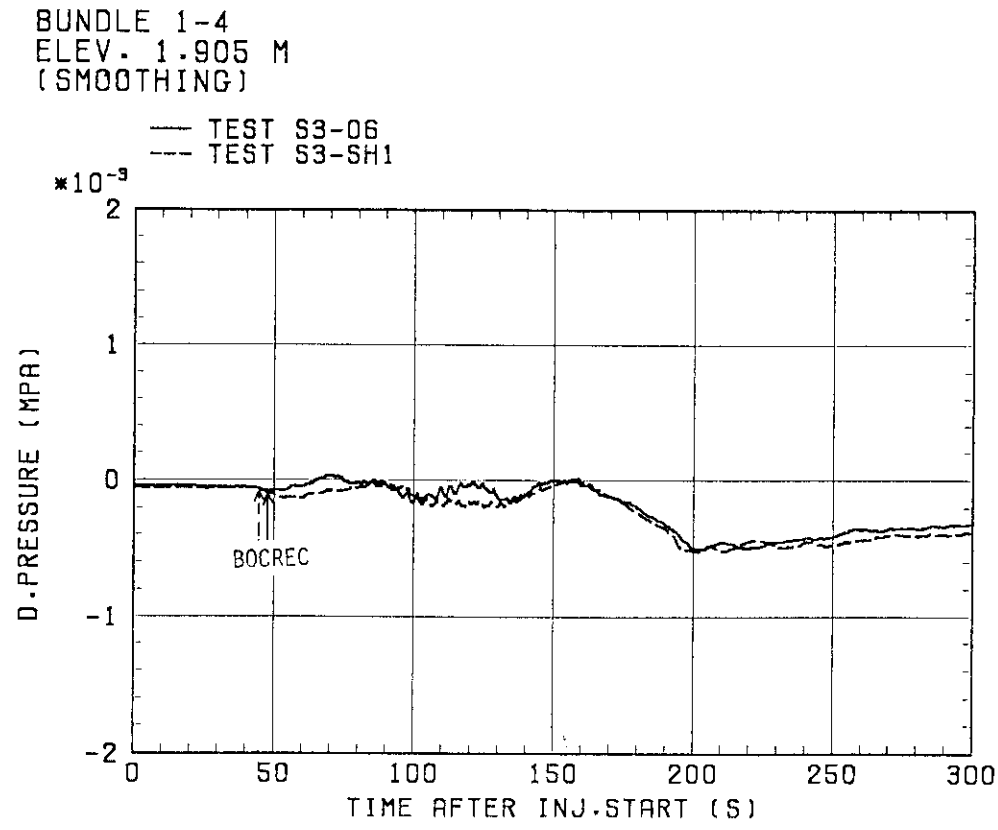

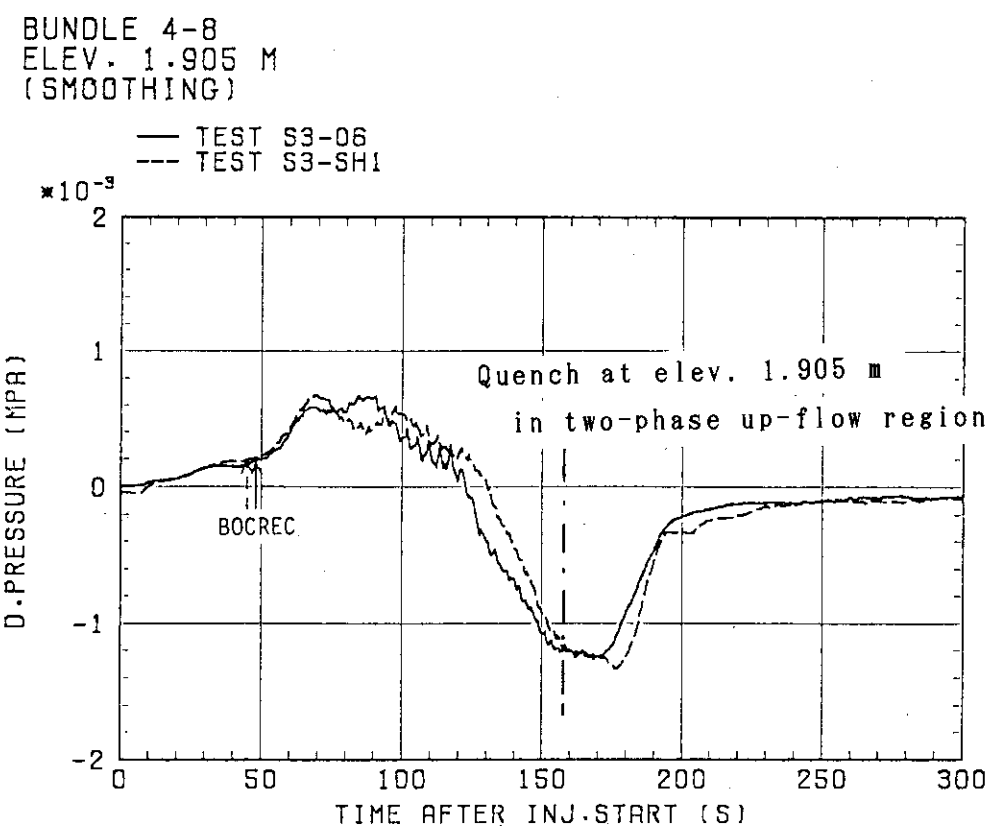

Fig. 3.16(b) Horizontal differential pressures in core at 1.905 m

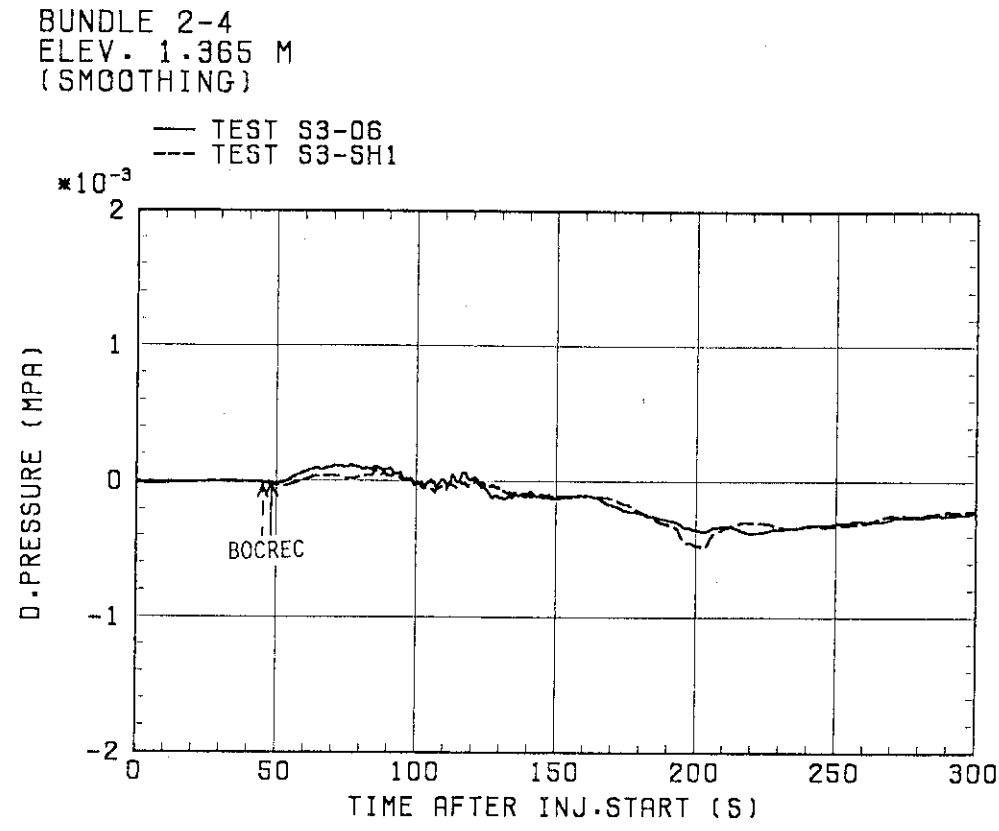

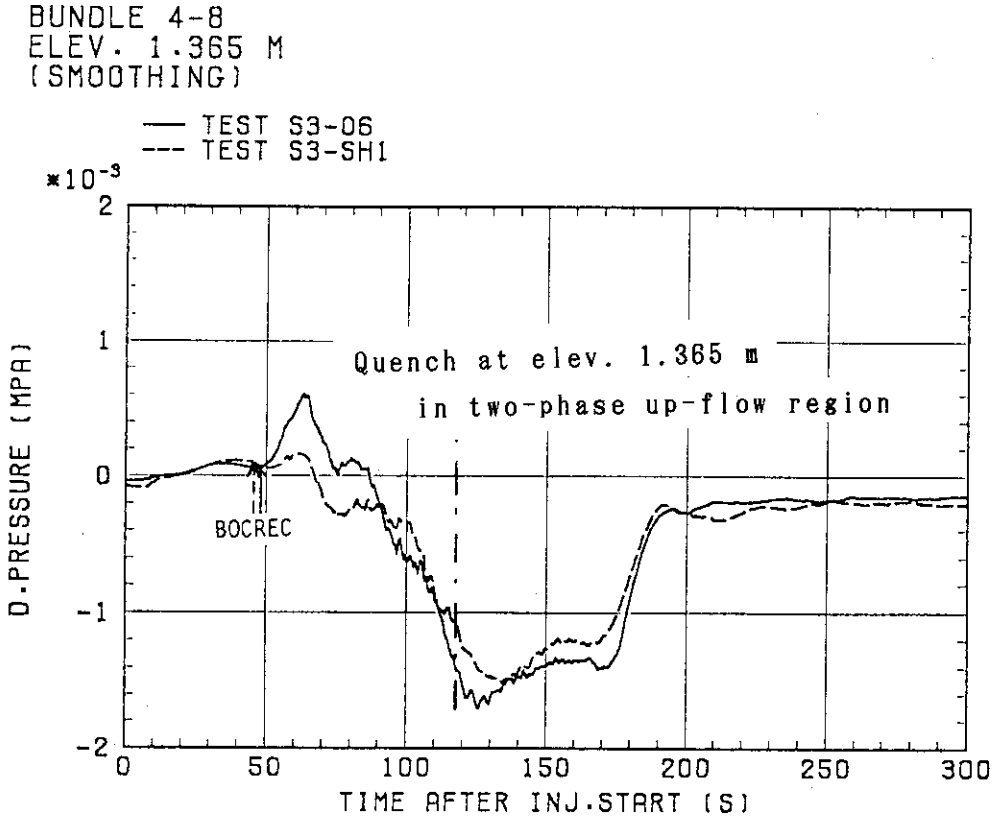

Fig. 3.16(c) Horizontal differential pressures in core at 1.365 m

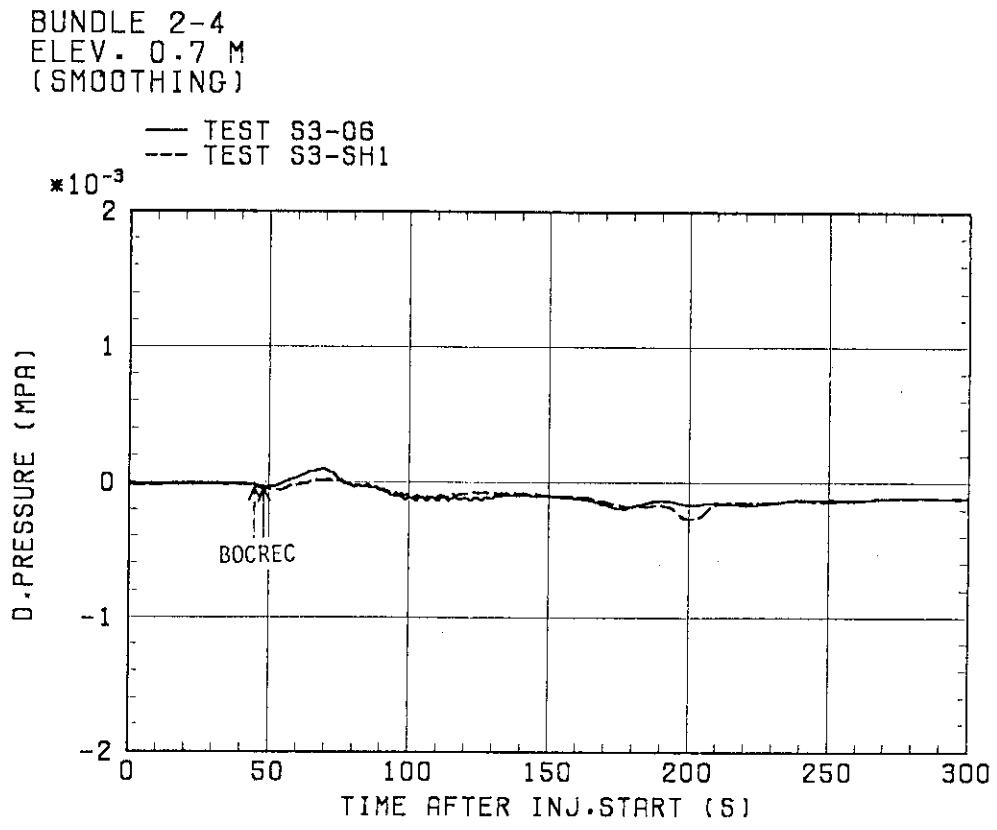

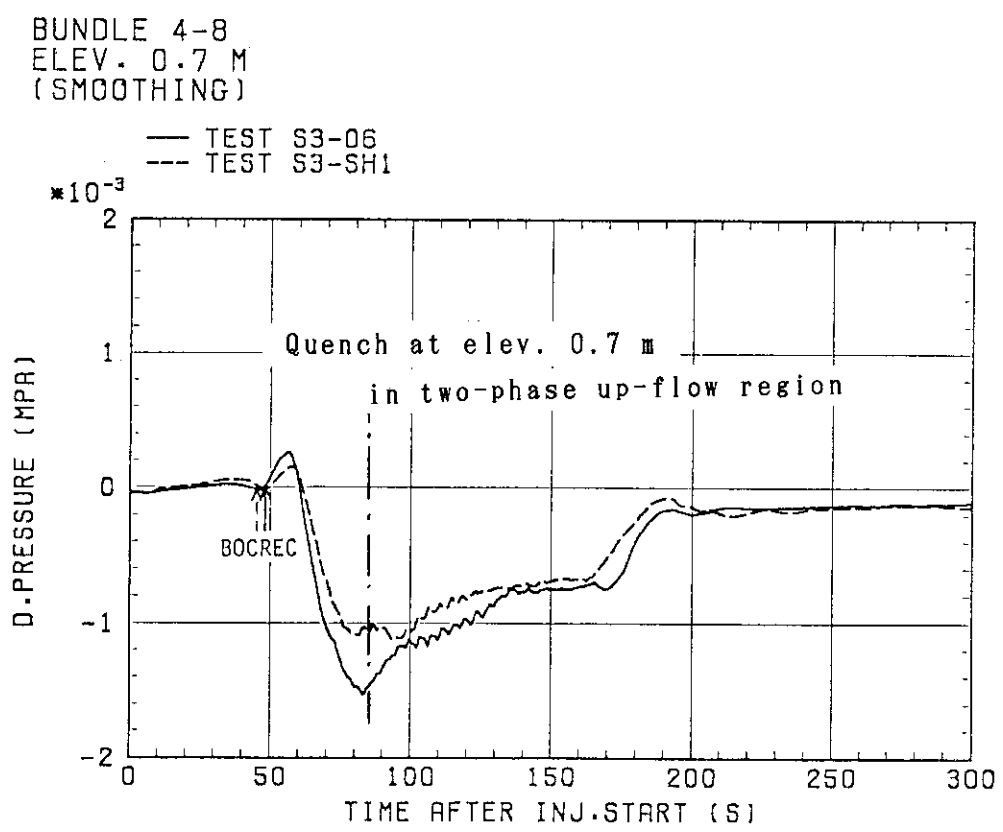

Fig. 3.16(d) Horizontal differential pressures in core at 0.7 m

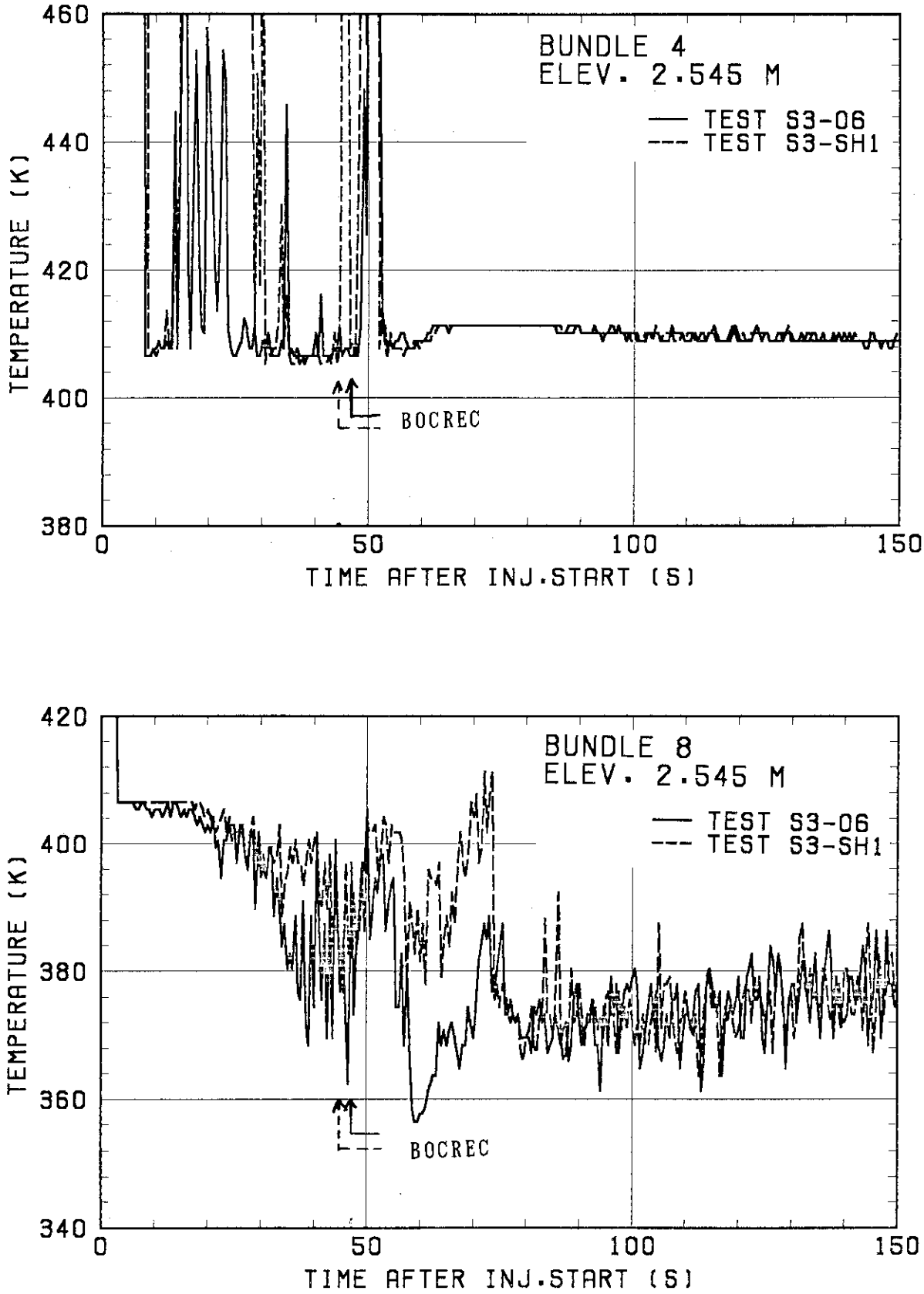

Fig. 3.17 Fluid temperatures in core

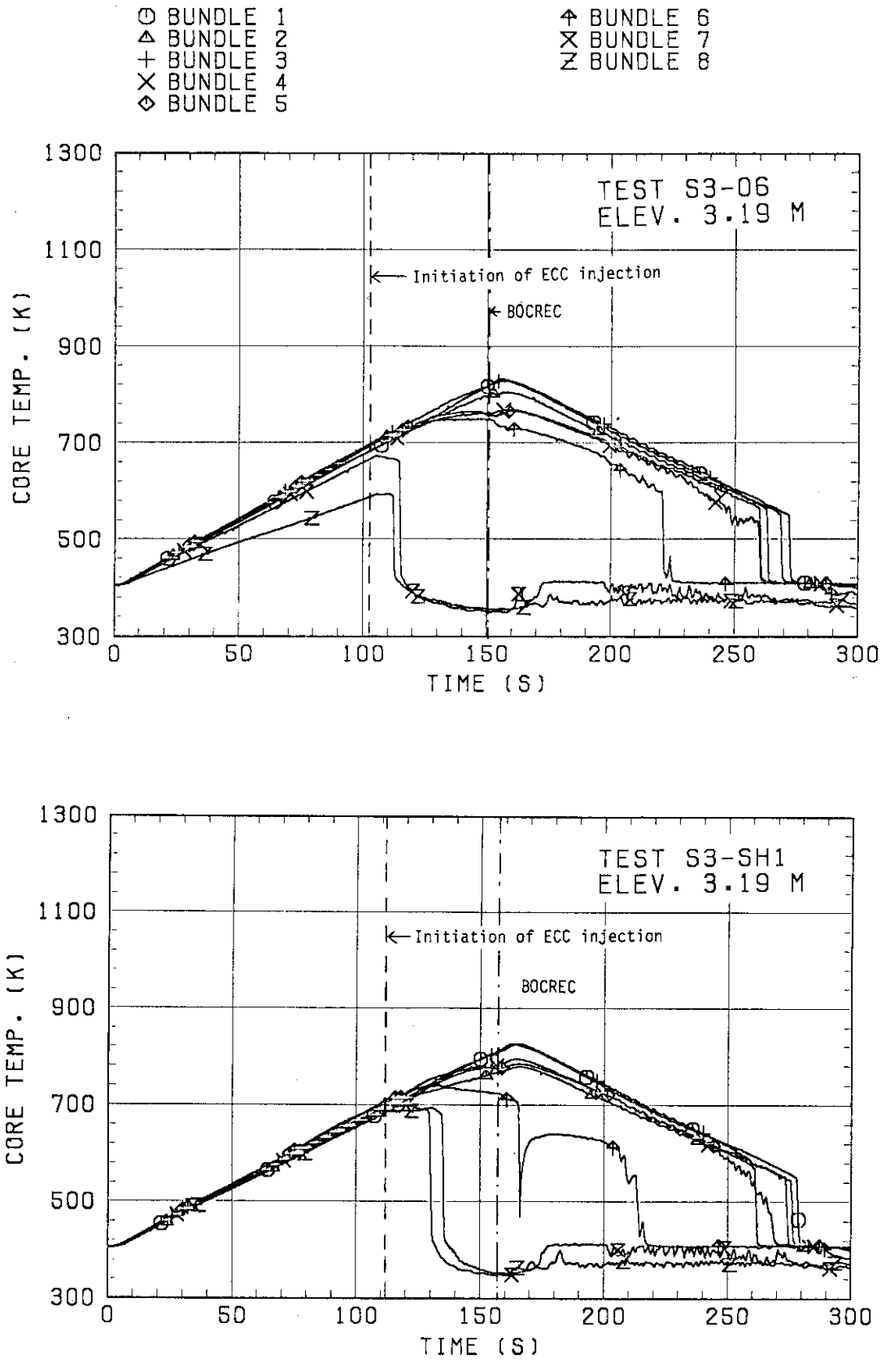

Fig. 3.18(a) Heater rod temperatures at 3.19 m

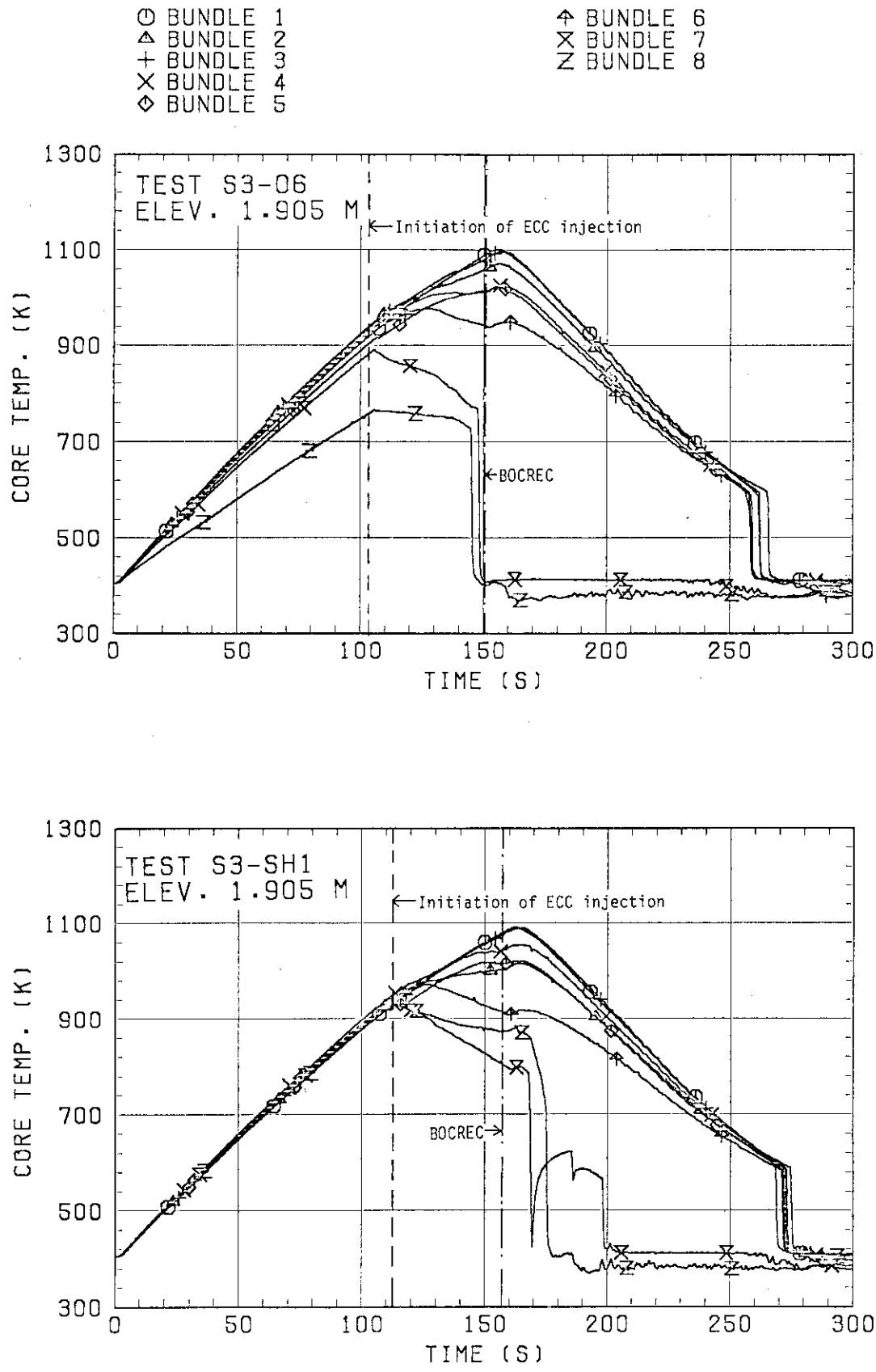

Fig. 3.18(b) Heater rod temperatures at 1.905 m

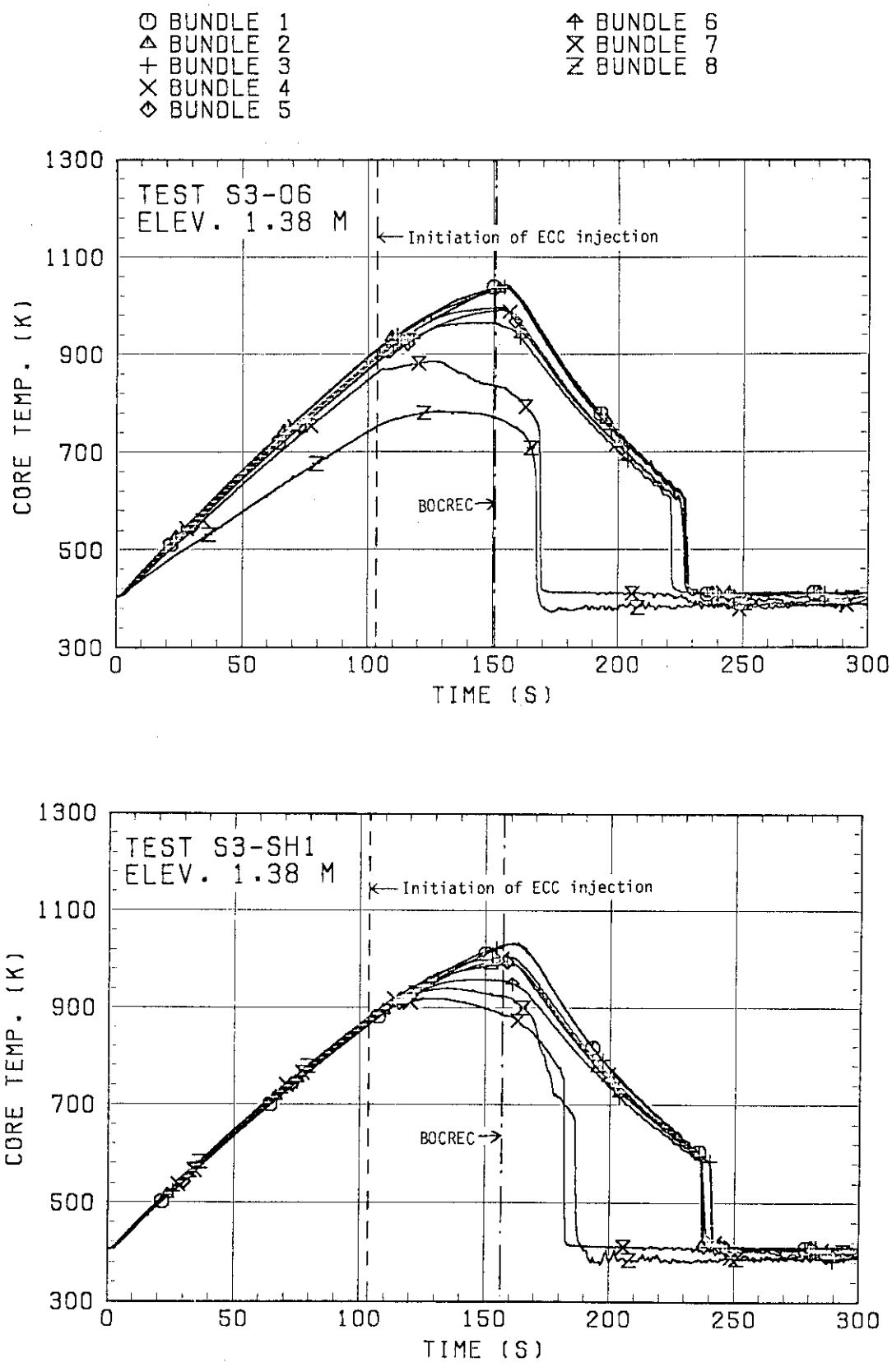

Fig. 3.18(c) Heater rod temperatures at 1.38 m

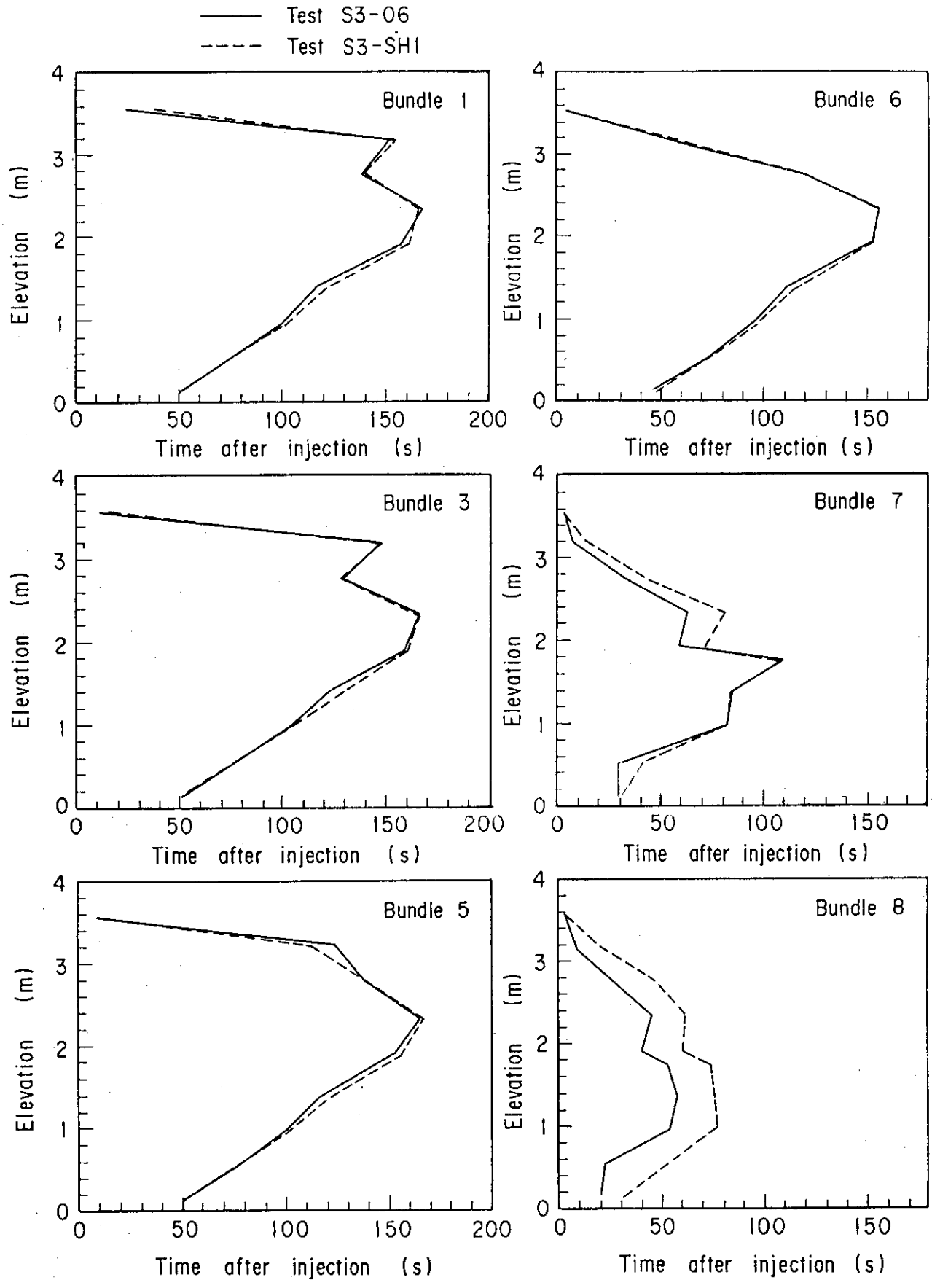

Fig. 3.19 Quench front propagation profiles

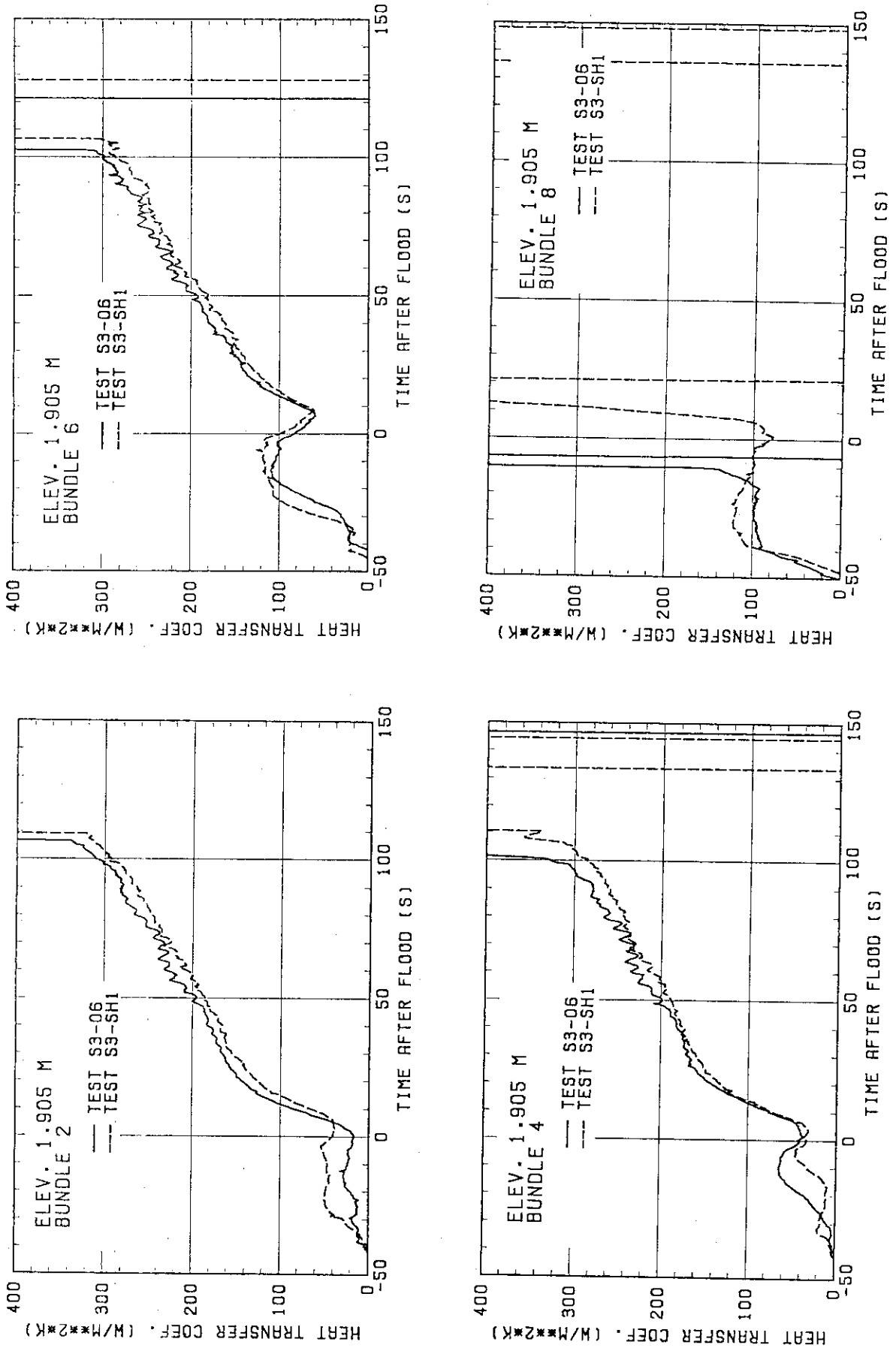

Fig. 3.20 Heat transfer coefficients in Bundles 2, 4, 6 and 8 at 1.905 m

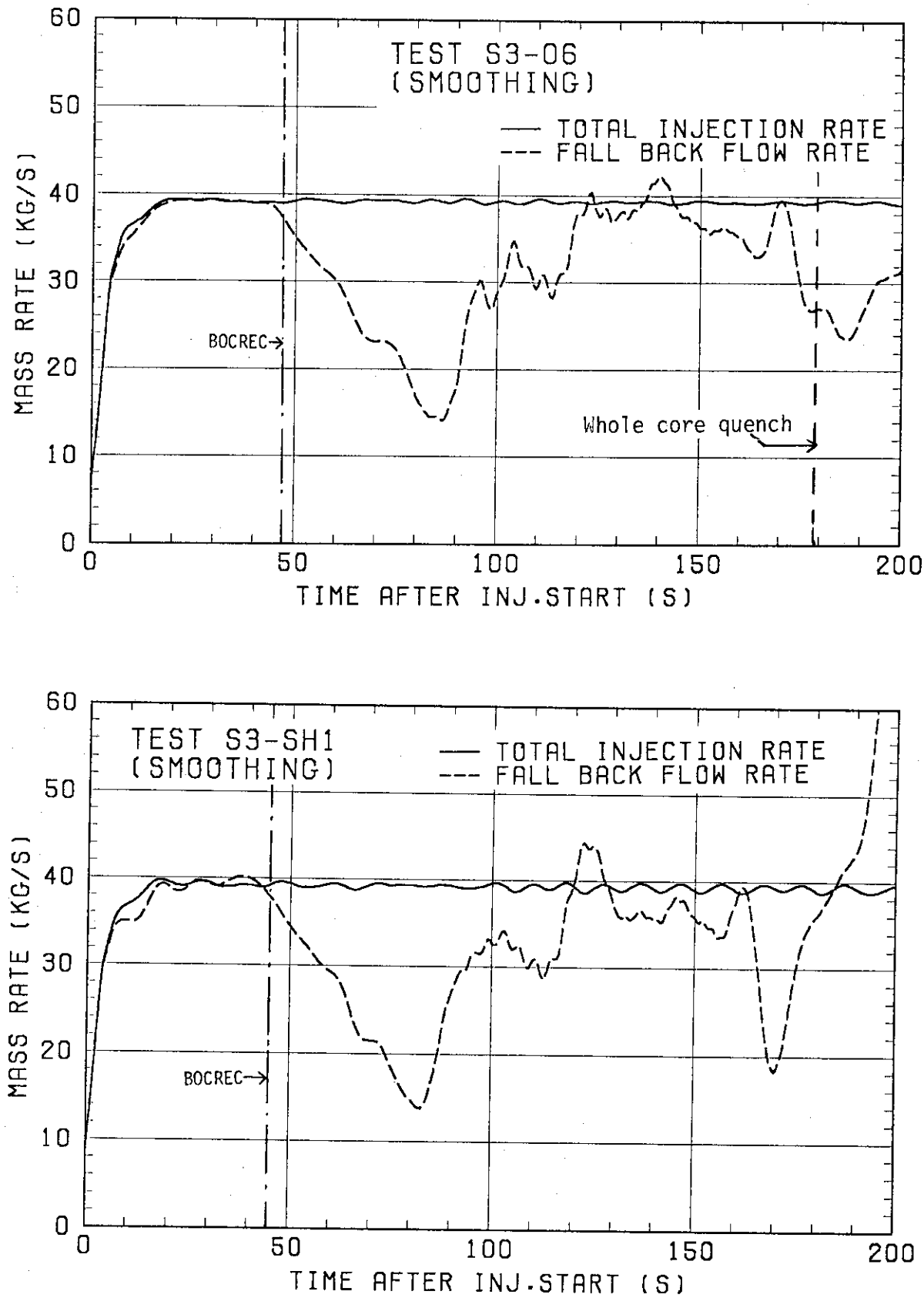

Fig. 3.21 Fall back mass flow rate obtained by mass balance method and total ECC injection rate

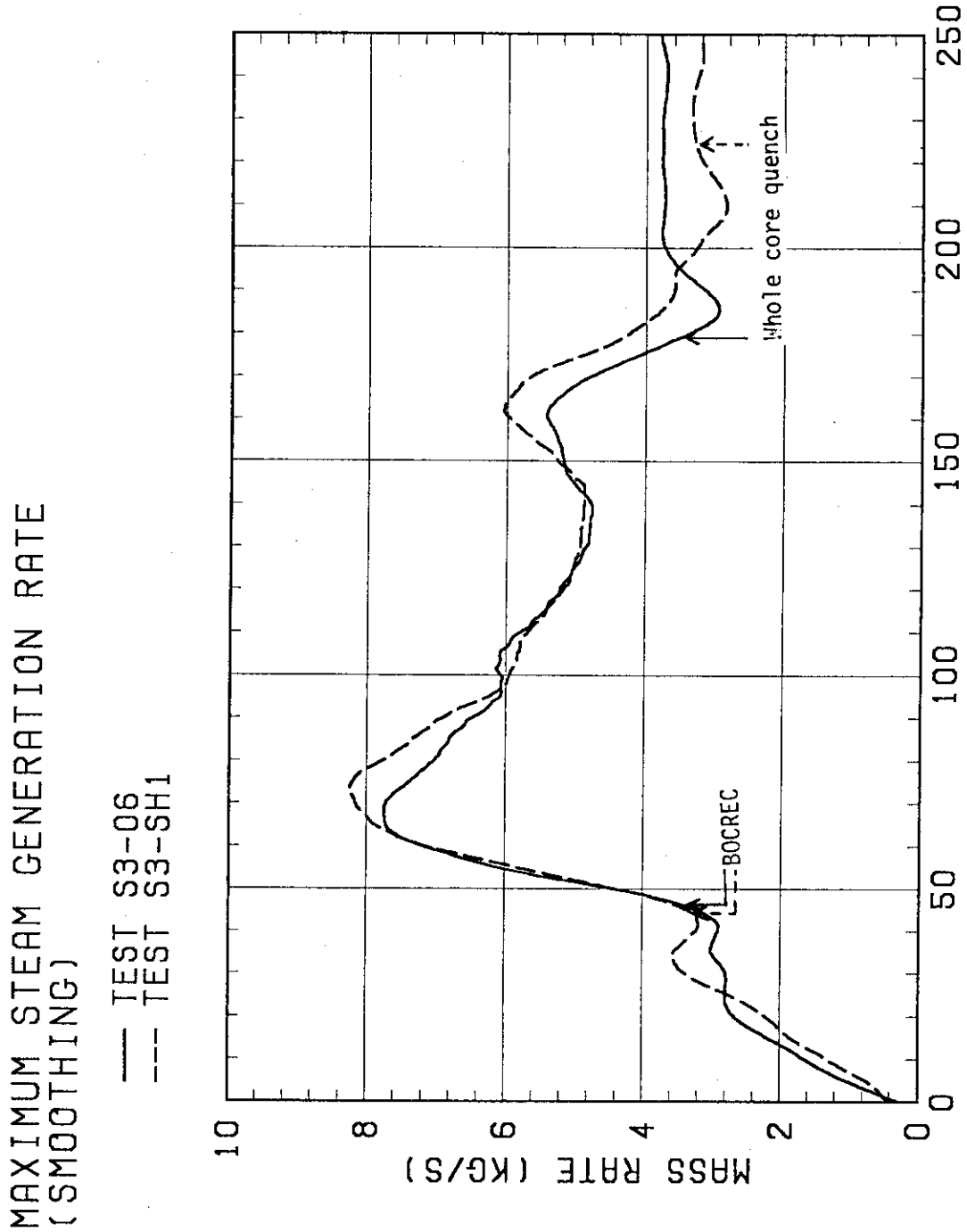

Fig. 3.22 Maximum steam generation rate

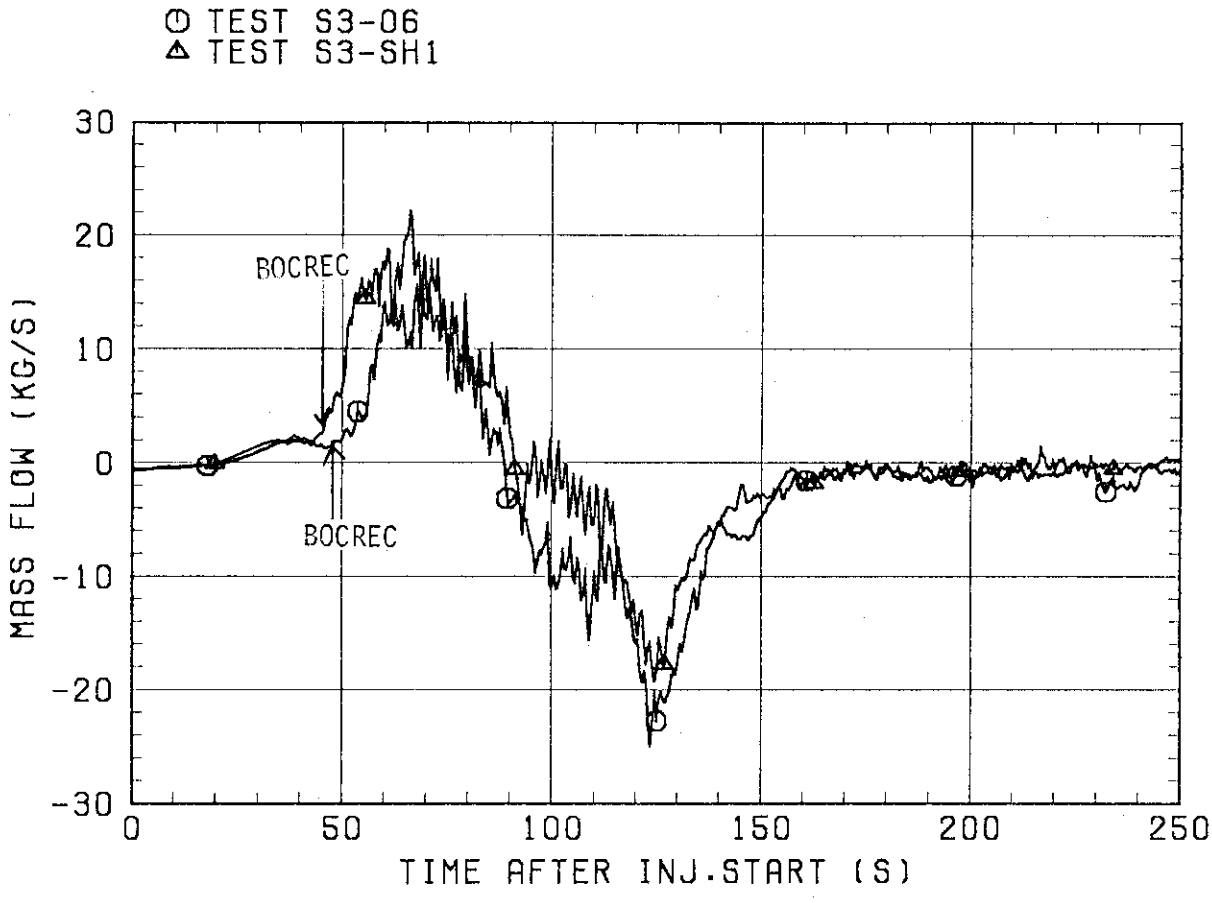

Fig. 3.23 Mass Flow Rate in Hot Leg

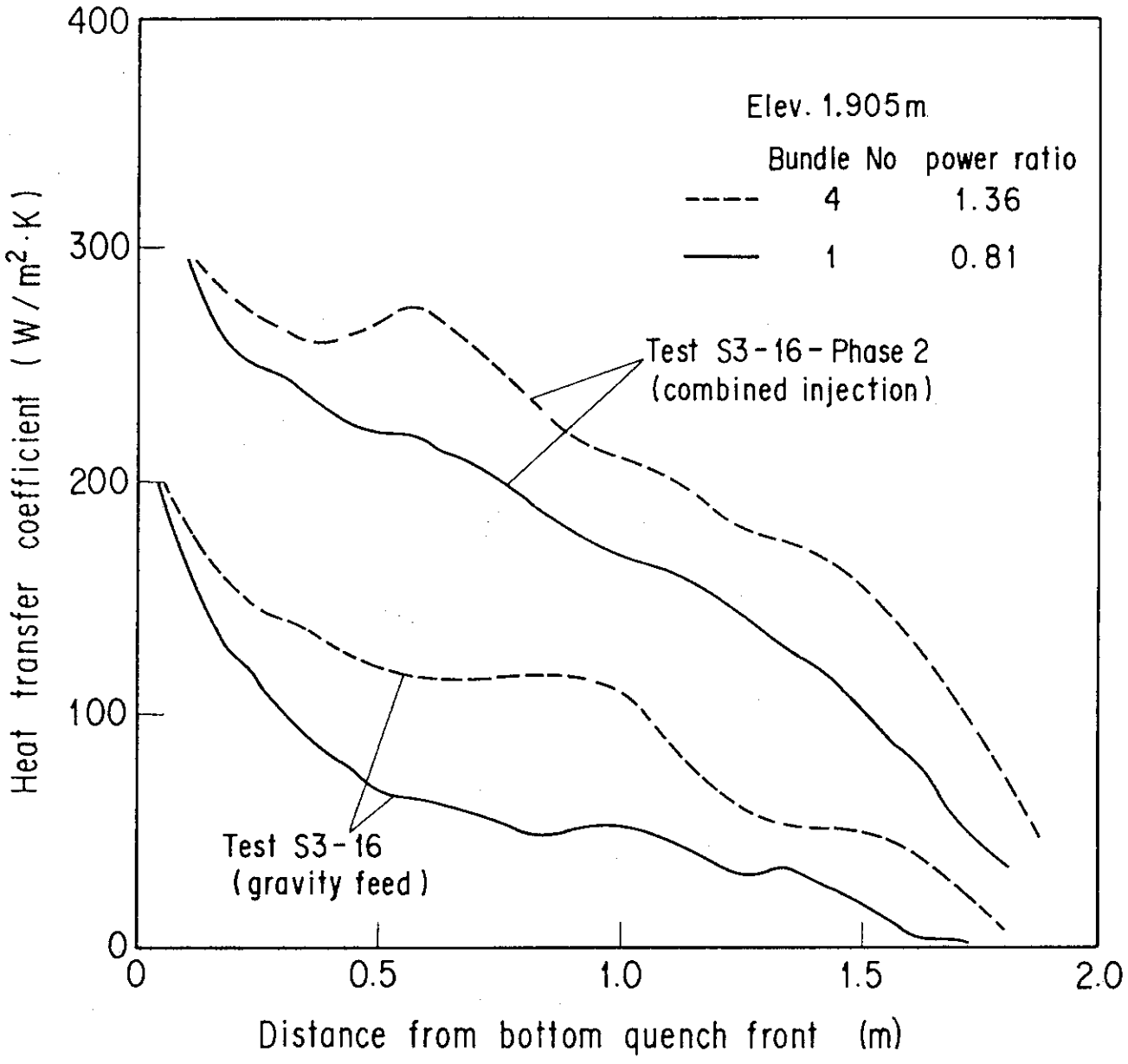

Fig. 3.24 Comparison of heat transfer coefficients in high and low power bundles for combined injection test and gravity injection test

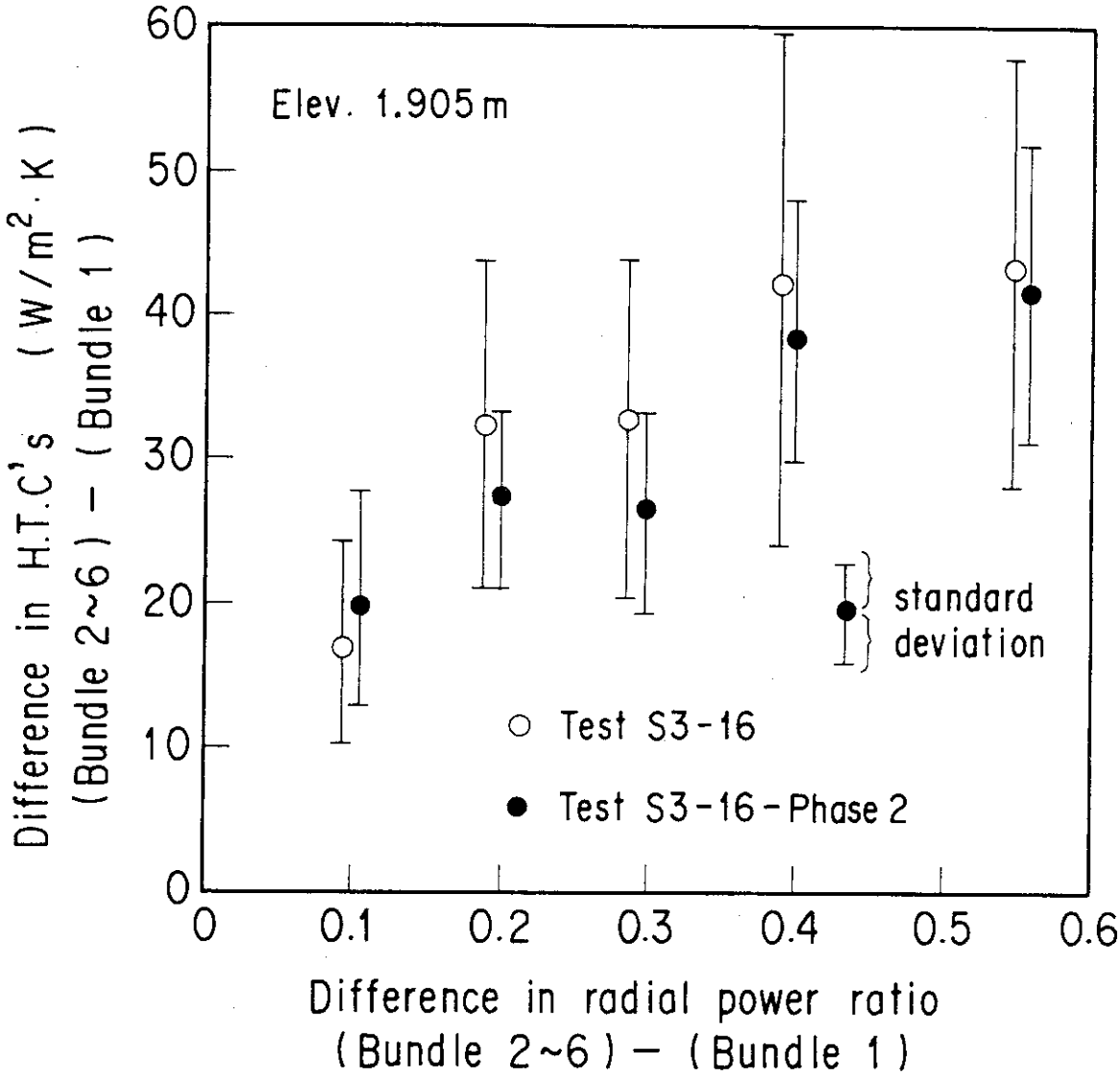

Fig. 3.25 Difference in heat transfer coefficients between bundles vs. difference in radial power ratios between bundles

Appendix A Slab Core Test Facility (SCTF) Core-III

A.1 Test Facility

The overall schematic diagram of SCTF is shown in Fig. A-1. The principal dimensions of the facility is shown in Table A-1, and the comparison of dimensions between SCTF and the reference PWR is shown in Fig. A-2.

A.1.1 Pressure Vessel

The pressure vessel is of slab geometry as shown in Fig. A-3. The height of the components in the pressure vessel is almost the same as the reference reactor's, and the flow area and the fluid volume of each component are scaled down based on the nominal core flow area scaling, 1/21.

The core consists of 8 bundles arranged in a row and each bundle includes heater rods and non-heated rods with 16×16 array. The core is enveloped by the honeycomb thermal insulator which is attached on the back surface of core wall plate.

The downcomer is located at one end of the pressure vessel which corresponds to the periphery of the actual reactor pressure vessel. The core baffle region located between the core and the downcomer is isolated for Core-III to minimize uncertainty in actual core flow. The cross sections of the pressure vessel at the upper head, upper plenum, core and lower plenum are shown in Fig. A-4.

A.1.2 Interface between Core and Upper Plenum

The interface between the core and the upper plenum consists of upper core support plate (UCSP), end box and various structures in the end box such as control rod spider which is paired with the control rod guid assembly (CRGA) and its support column bottom and special baffle plate spider which is paired with the hold-down bridge. These structures are exactly the same as those for a German PWR except some minor modifications.

Figure A-5 shows arrangement of the UCSP, the end box and the top grid spacer. The configuration of the end box is shown in Fig. A-6.

Detail of the end boxes with drag transducer device and other internals is shown in Fig. A-7. The UCSP shown in Fig. A-8 has two kinds of holes, i.e., the square holes correspond to the end boxes with control rod spider and the circular holes correspond to the end boxes with special baffle plate spider.

A.1.3 Upper Plenum and Upper Head

The vertical and horizontal cross sections of the upper plenum are shown in Figs. A-9 and A-4, respectively. In the SCTF Core-III, the slab cut of the upper plenum of a German (KWU) PWR is simulated. The splitted and staggered arrangement of the CRGA support columns was chosen to make good simulation of horizontal flow in the upper plenum.

As shown in Fig. A-10, there are three kinds of CRGA support column. Support column-1 is installed above Bundles 3 and 5 and connected to the CRGA support column bottom with the transition cone. Cross section of the CRGA support calumn changes from a circle to a half circle in this transition cone. Support column 2 is installed above Bundles 6 and 7 and the bottom is closed with the half conical bottom seal plate with many flow holes. Support column 3 is essentially the same as support column 2 but the edge of one side is cut off in order to install above Bundle 1. Each CRGA support column has ten or eleven baffle plates with flow holes. Top flow paths to the upper head bottom and to the upper plenum top are also provided.

Figure A-11 shows vertical cross section of the bottom part of the upper plenum and the interface between the core and the upper plenum. There are eight side flow injection nozzles and eight side flow extraction nozzles just at the opposite side of the upper plenum bottom, corresponding to each bundle.

The upper plenum is separated from the upper head by an upper support plate. Four top injection nozzles penetrate the upper head and open the top of upper plenum as shown in Fig. A-12. Outlet part of the top injection nozzle has a rectangular cross section and double mesh screen with 45 degree cross angle is attached at the mouth.

A.1.4 Simulated Core

The simulated core for the SCTF Core-III consists of 8 heater rod bundles arranged in a row. Each bundle has 236 electrically heated rods and 20 non-heated rods. The arrangement of rods in a bundle is shown in Fig. A-13. The dimensions of the heater rods are based on 15×15 fuel rods bundle for a PWR and the heated length and the outer diameter of each heater rod are 3.613 m and 10.7 mm, respectively. A heater rod consists of a nichrome heater element, boron nitride (BN) or magnesium oxide (MgO) depending on elevation in the heated zone and Nichrofer 7216 (equivalent to Inconel 600) sheath. The sheath thickness is about 1.0 mm and is thicker than the actual fuel cladding because of the requirements for thermocouple installation. The heater element is a helical coil and has a 17 step chopped cosine axial power profile as shown in Fig. A-14. The peaking factor is 1.4.

Non-heated rods are either pipes or solid rods of stainless steel with 13.8 mm O.D. The heater rods and non-heated rods are fixed at the top of the core allowing downward expansion. In Fig. A-15, relative elevation of rods and spacers is shown.

For better simulation of flow resistance in the lower plenum, the simulated fuel rods end in the lower plenum and do not penetrate through the bottom plate of the lower plenum as shown in Fig. A-15.

A.1.5 Primary Loops

Primary loops consist of a hot leg equivalent to four hot legs in area, a steam/water separator for simulating single steam phase flow downstream of the steam generator and for measuring flow rate of carry over water, an intact cold leg equivalent to three intact loops, a broken cold leg on the pressure vessel side and a broken cold leg on the steam/water separator side. These two broken cold legs are connected to two containment tanks through break valves, respectively. The arrangement of the primary loops is shown in Fig. A-16. The flow area of each loop is scaled down based on the core flow area scaling, 1/21. It should be emphasized that the cross section of the hot leg is an elongated circle with an actual height to realize proper flow pattern in the hot leg. The steam/water separator has a steam generator inlet plenum simulator to correctly simulate the flow

characteristics of carryover water into the U-tubes. The cross section of the hot leg and the configuration of the steam genrator inlet plenum simulator are shown in Fig. A-17.

A pump simulator and a loop seal part are provided for the intact cold leg. The arangement of the intact cold leg is shown in Fig. A-18. The pump simulator consists of the casing and duct simulators and an orifice plate as shown in Fig. A-19. The loop resistance is adjusted with the orifice plates attached to the intact cold leg, the steam/water separator side and pressure vessel side broken cold legs and the pump simulator.

A.1.6 ECC Water Injection System

Three kinds of ECCSs are provided, i.e., the accumulator injection system (Acc), low pressure coolant injection system (LPCI) and combined injection system. Available injection locations for the former two are the intact and broken cold legs, the hot leg, the lower plenum and the downcomer. On the other hand, those for the last one are the top and bottom-side of the upper plenum and the intact and broken cold legs.

A.1.7 Containment Tanks and Auxiliary System

Two containment tanks are provided to SCTF. The containment tank-I is connected with the downcomer through the pressure vessel side broken cold leg and the containment tank-II is connected with the steam/water separator through the steam/water separator side broken cold leg. Especially in the containment tank-I, carryover water from the downcomer is measured by the differentiation of the liquid level. These containment tanks and auxiliary system such as a pressurizer for injecting water from the Acc tanks, etc. are shared with CCTF.

A.2 Instrumentation

The instrumentation in SCTF has been provided both by JAERI and USNRC. The JAERI-provided instrumentation includes the measurement of temperatures, pressures, differential pressures, liquid levels, flow velocities, and heating powers. USNRC has provided film probes, impedance probes, string probes, liquid level detectors (LLDs), fluid distribution grids (FDGs), turbine meters, drag disks, densitometers, spool pieces, drag bodies, break through detectors and video optical probes. Locations of the JAERI-provided instruments are shown in Figs. A-20 through A-43.

Table A-1 Principal Dimensions of the SCTF

1.	Core Dimension		
	(1) Quantity of Bundle	8 Bundles	
	(2) Bundle Array	1 × 8	
	(3) Bundle Pitch	230 mm	
	(4) Rod Array in a Bundle	16 × 16	
	(5) Rod Pitch in a Bundle	14.3 mm	
	(6) Quantity of Heater Rod in a Bundle	236 rods	
	(7) Quantity of Non-Heated Rod in a Bundle	20 rods	
	(8) Total Quantity of Heater Rods	236×8=1,888	rods
	(9) Total Quantity of Non-Heated Rods	20×8=160	rods
	(10) Effective Heated Length of Heater Rod	3613 mm	
	(11) Diameter of Heater Rod	10.7 mm	
	(12) Diameter of Non-Heated Rod	13.8 mm	
2.	Flow Area & Fluid Volume		
	(1) Core Flow Area	0.25	m^2
	(2) Core Fluid Volume	0.903	m^3
	(3) Baffle Region Flow Area (isolated)	(0.096)	m^2
	(4) Baffle Region Fluid Volume (nominal)	0.355	m^3
	(5) Cross-Sectional Area of Core Additional Fluid Volumes Including Gap between Core Barrel and Pressure Vessel Wall and Various Penetration Holes	0.07 ~ 0.10	m^2 m^2
	(6) Downcomer Flow Area	0.158	m^2
	(7) Upper Annulus Flow Area	0.158	m^2
	(8) Upper Plenum Horizontal Flow Area (max.)	0.541	m^2
	(9) Upper Plenum Vertical Flow Area	0.525	m^2
	(10) Upper Plenum Fluid Volume	1.156	m^3
	(11) Upper Head Fluid Volume	0.86	m^3
	(12) Lower Plenum Fluid Volume (excluding below downcomer)	1.305	m^3
	(13) Steam Generator Inlet Plenum Simulator Flow Area	0.626	m^2
	(14) Steam Generator Inlet Plenum Simulator Fluid Volume	0.931	m^3
	(15) Steam Water Separator Fluid Volume	5.3	m^3
	(16) Flow Area at the Top Plate of Steam Generator Inlet Plenum Simulator	0.195	m^2
	(17) Hot Leg Flow Area	0.0826	m^2

Table A-1 (continued)

(18)	Intact Cold Leg Flow Area (Diameter = 297.9 mm) Inverted U-Tube with 0.0314 m^2 Cross-Sectional Area (Diameter = 200 mm) and 10 m Height from the Top of Steam Generator Inlet Plenum Simulator Can Be Added As an Option.	0.0697 m^2
(19)	Broken Cold Leg Flow Area (Diameter = 151.0 mm)	0.0197 m^2
(20)	Containment Tank-I Fluid Volume	30 m^3
(21)	Containment Tank-II Fluid Volume	50 m^3
(22)	Flow Area of Exhausted Steam Line from Containment Tank-II to the Atmosphere	see Fig. 3-63

3. Elevation & Height

(1)	Top Surface of Upper Core Support Plate (UCSP)	0 mm
(2)	Bottom Surface of UCSP	- 40 mm
(3)	Top of the Effective Heated Length of Heater Rod	- 444 mm
(4)	Bottom of the Effective Heated Length of Heater Rod	-4,057 mm
(5)	Bottom of the Skirt in the Lower Plenum	-5,270 mm
(6)	Bottom of Intact Cold Leg	+ 724 mm
(7)	Bottom of Hot Leg	+1,050 mm
(8)	Top of Upper Plenum	+2,200 mm
(9)	Bottom of Steam Generator Inlet Plenum Simulator	+1,933 mm
(10)	Centerline of Loop Seal Bottom	-2,281 mm
(11)	Bottom Surface of End Box	- 263 mm
(12)	Top of Upper Annulus of Downcomer	+2,234 mm
(13)	Height of Steam Generator Inlet Plenum Simulator	1,595 mm
(14)	Height of Loop Seal	3,140 mm
(15)	Inner Height of Hot Leg Pipe	737 mm
(16)	Bottom of Lower Plenum	-5,772 mm
(17)	Top of Upper Head	+2,887 mm

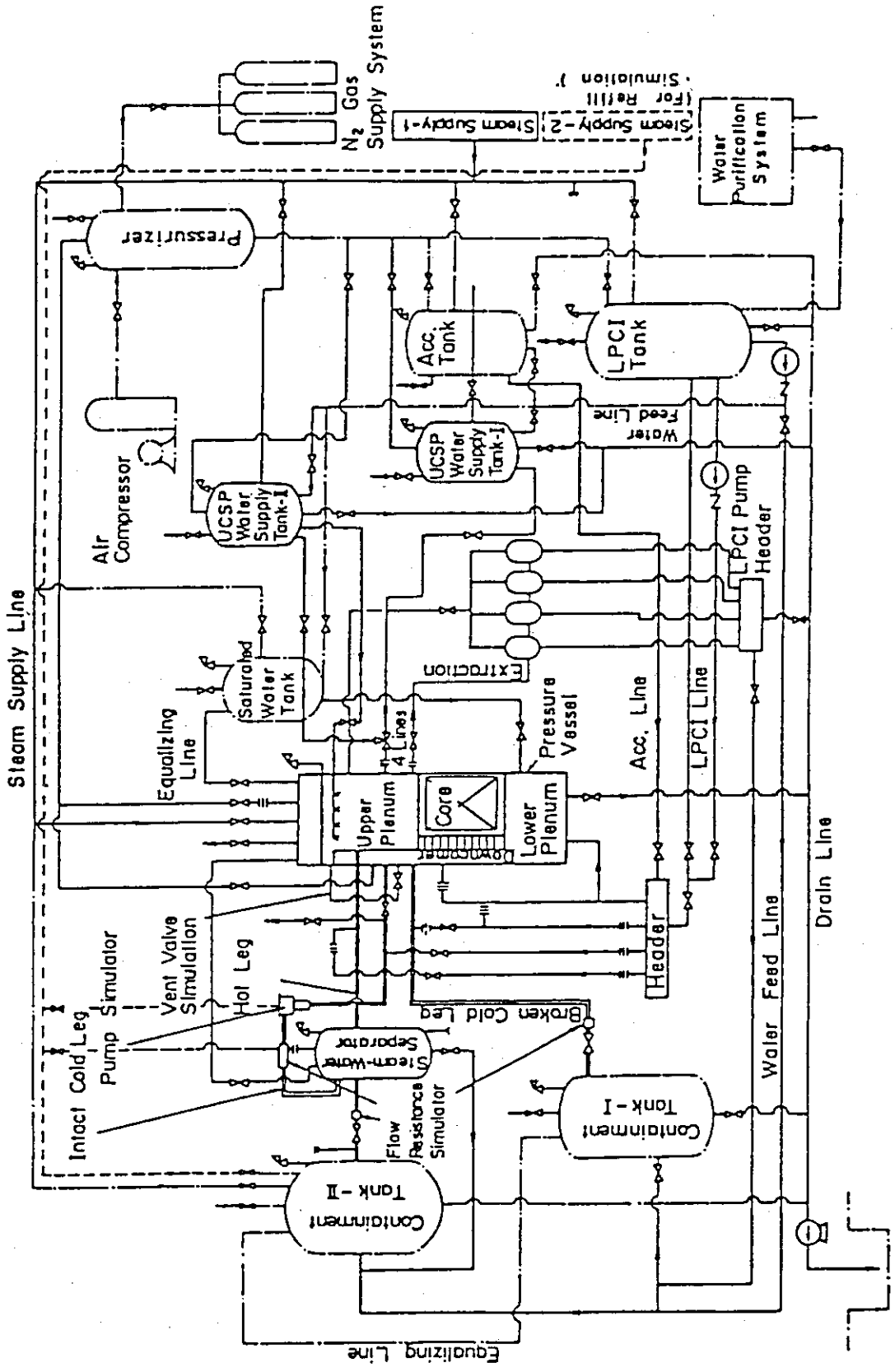

Fig. A-1 Schematic Diagram of Slab Core Test Facility

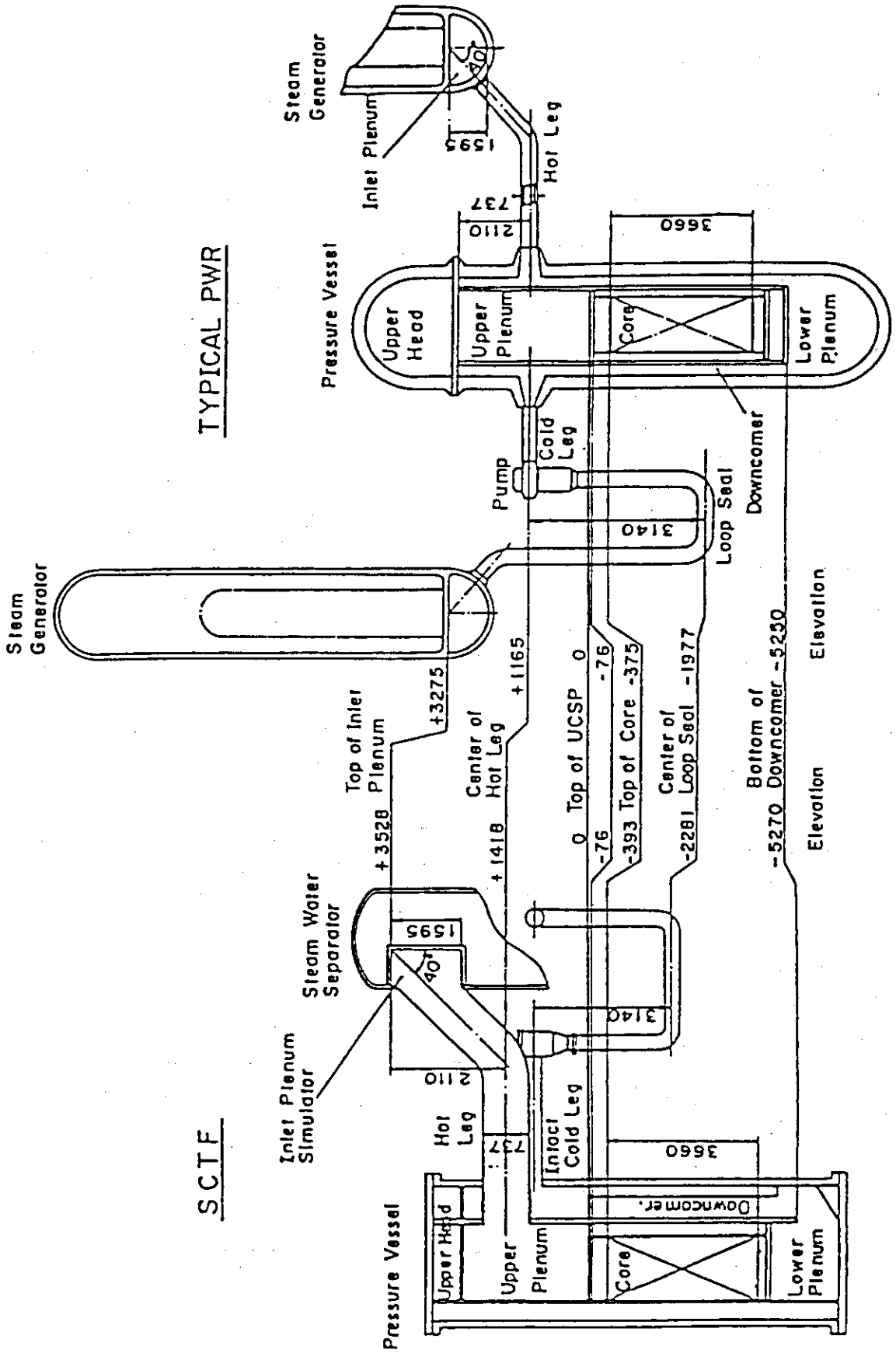

Fig. A-2 Comparison of Dimensions between SCTF and a Reference PWR

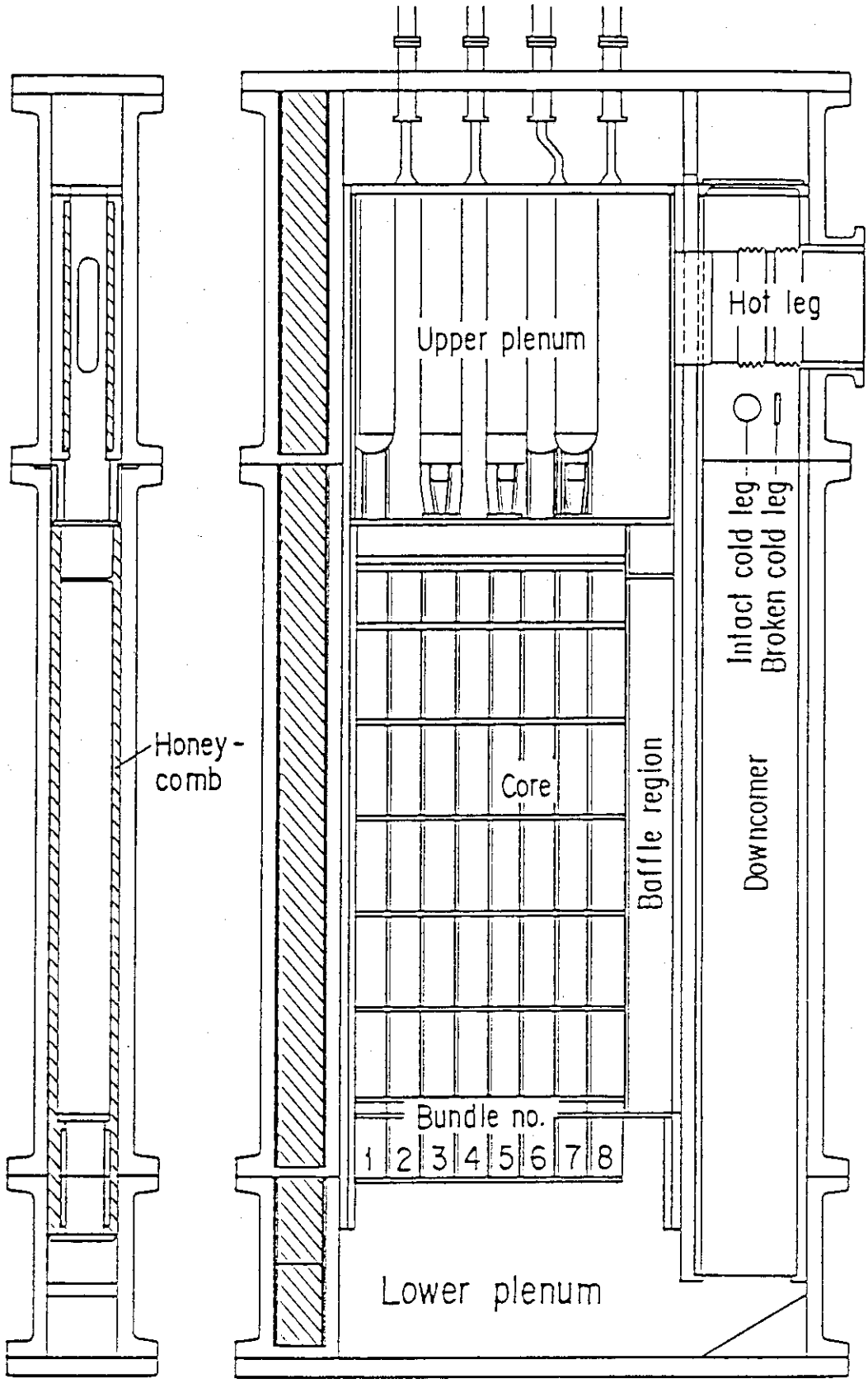

Fig. A-3 Vertical Cross Sections of Pressure Vessel

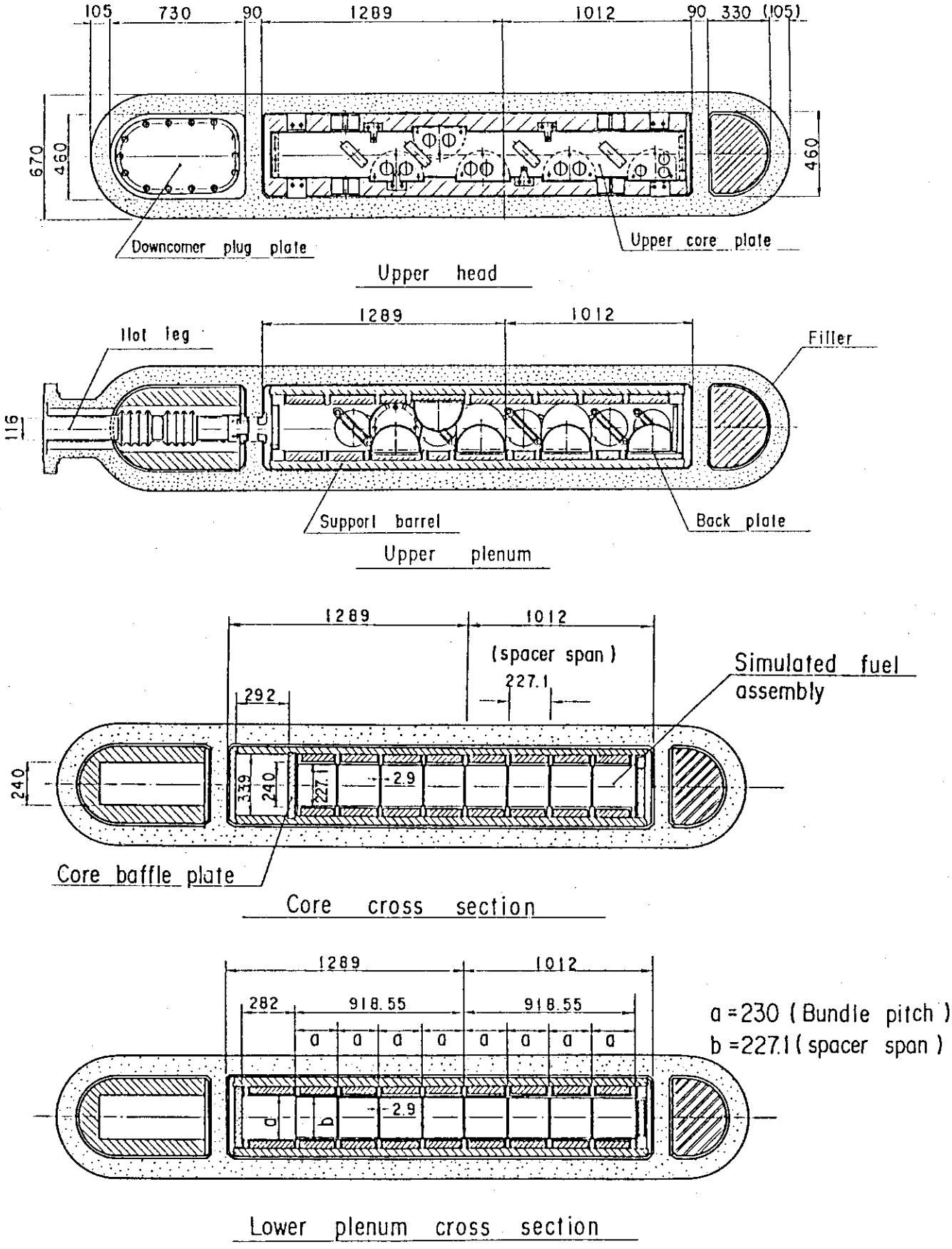

Fig. A-4 Horizontal Cross Sections of Pressure Vessel

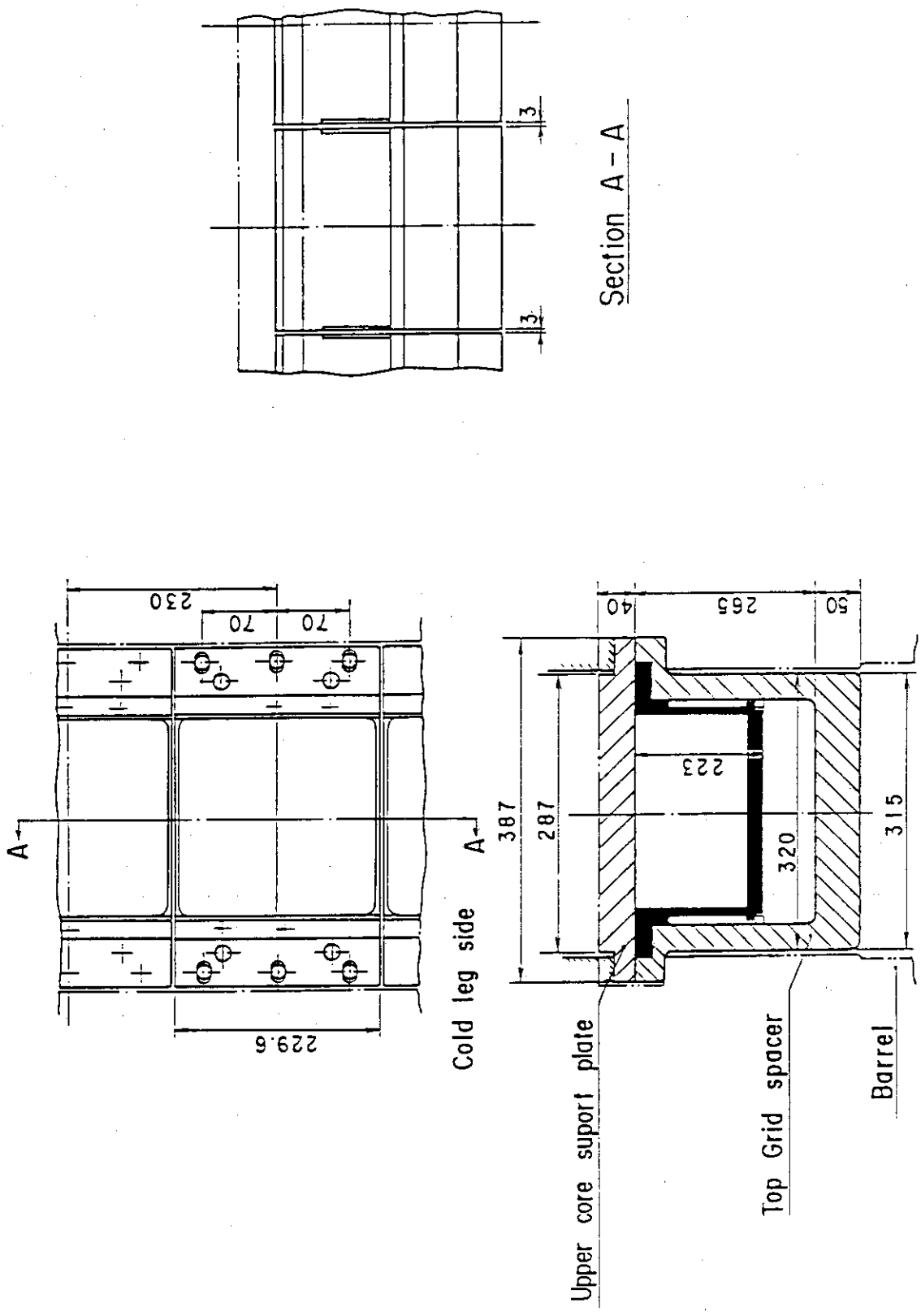

Fig. A-5 Arrangement and Principal Dimension of End Boxes and Top Grid Spacers

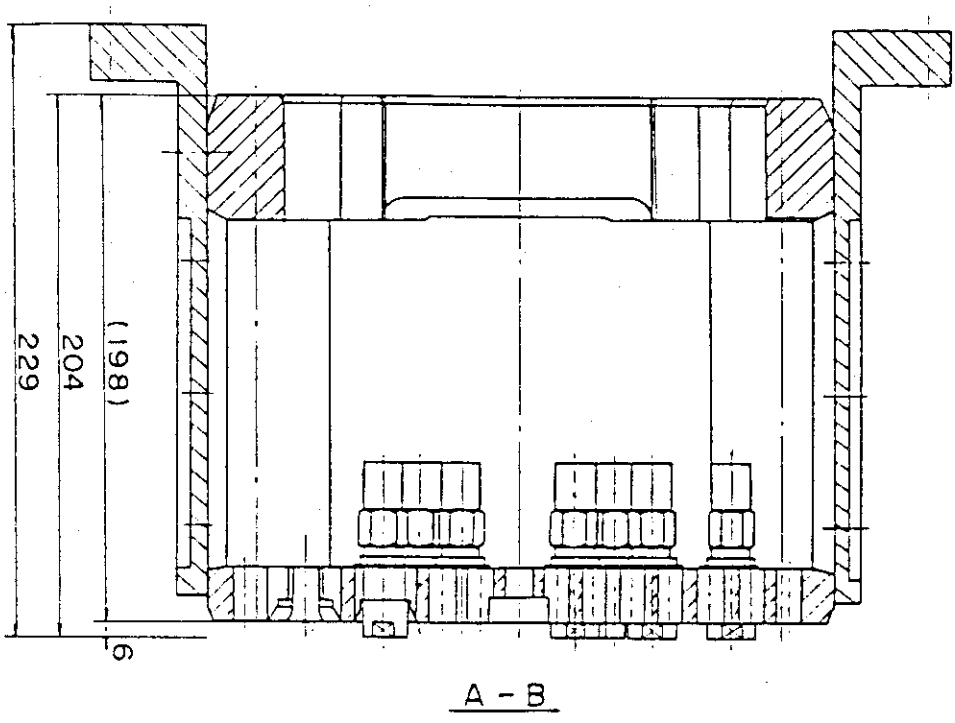

Fig. A-6 Configuration and Dimension of End Boxes

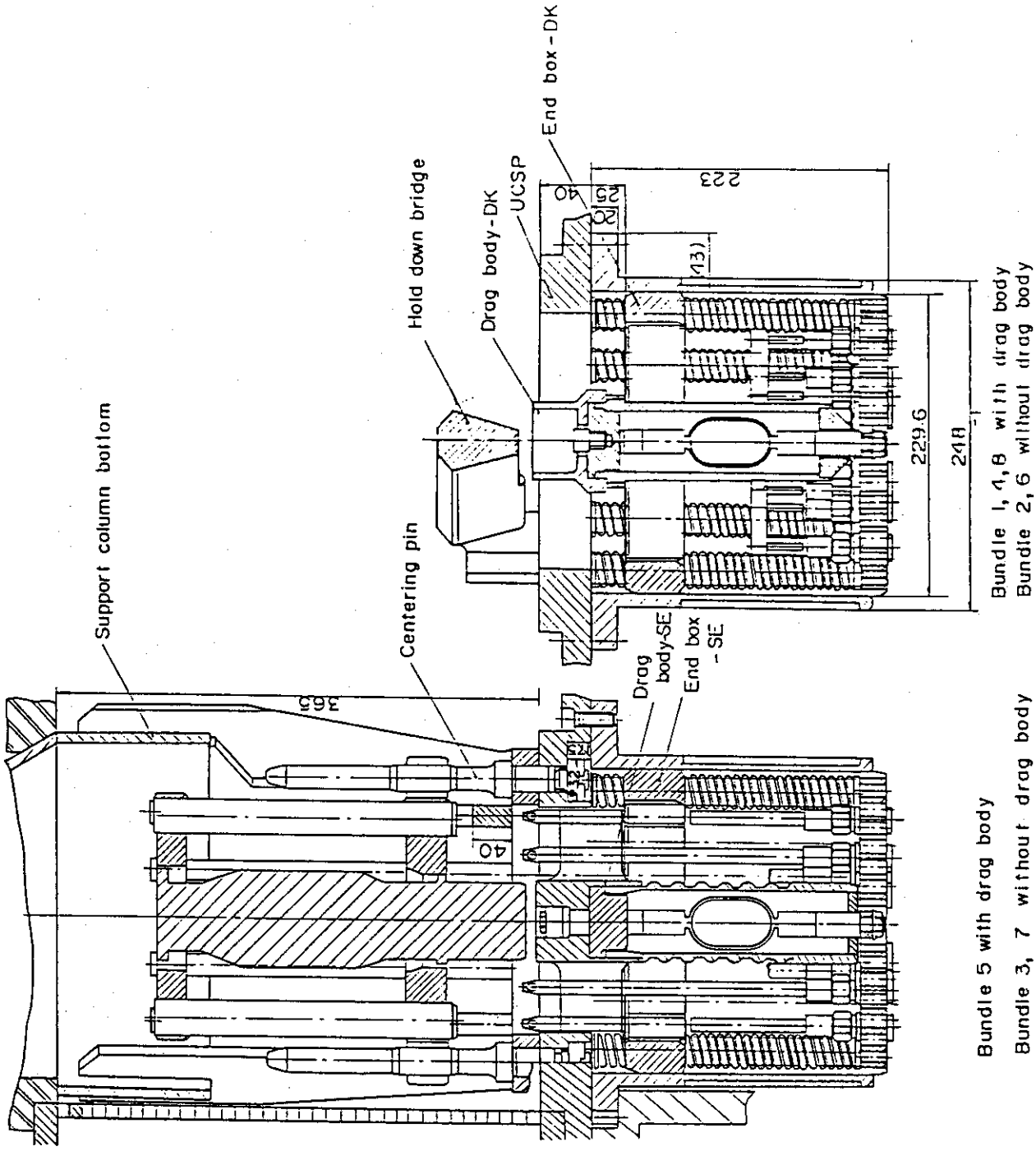

Fig. A-7 Detail of End Boxes with Drag Bodies

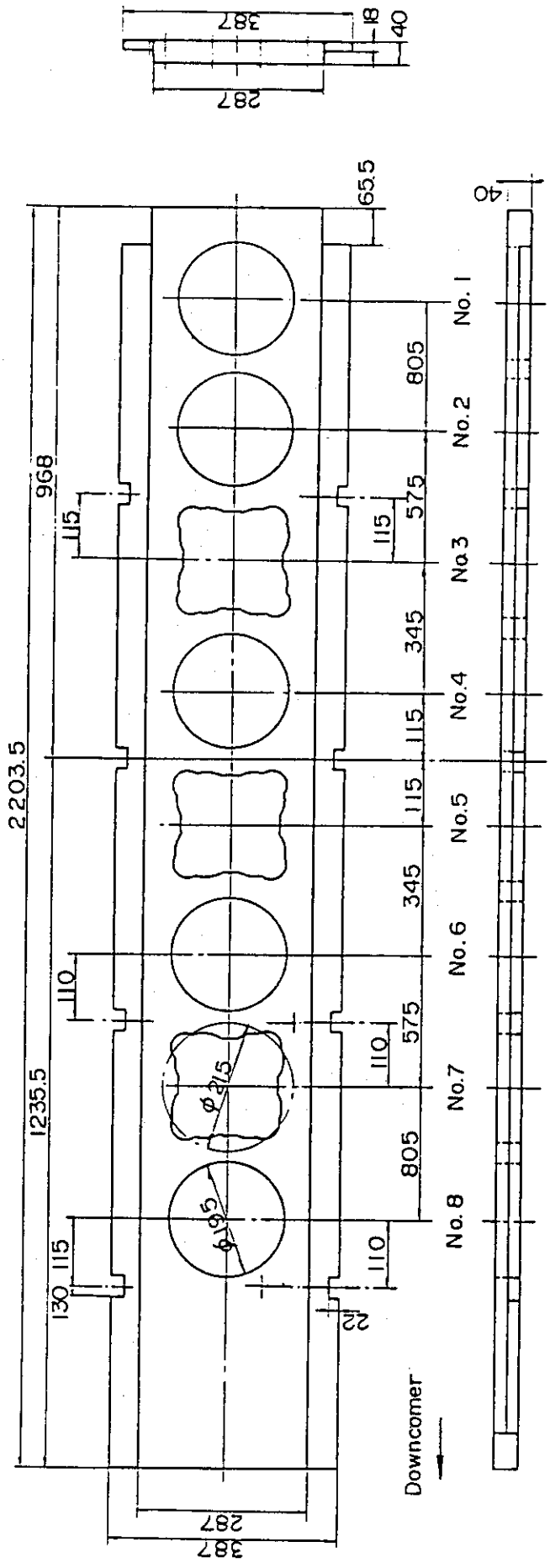

Fig. A-8 Dimension of Upper Core Support Plate

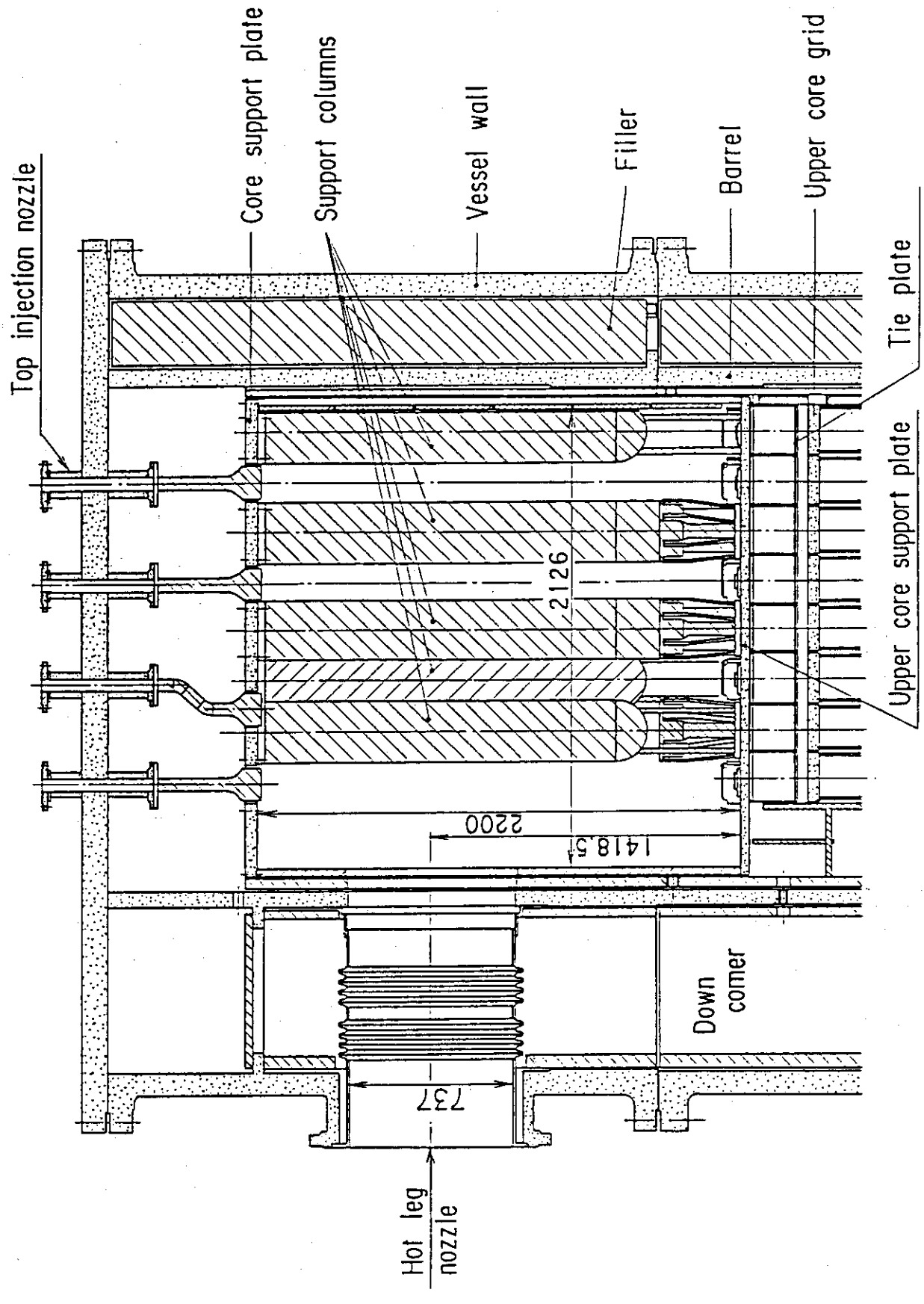

Fig. A-9 Vertical Cross Section of Upper Plenum Internals

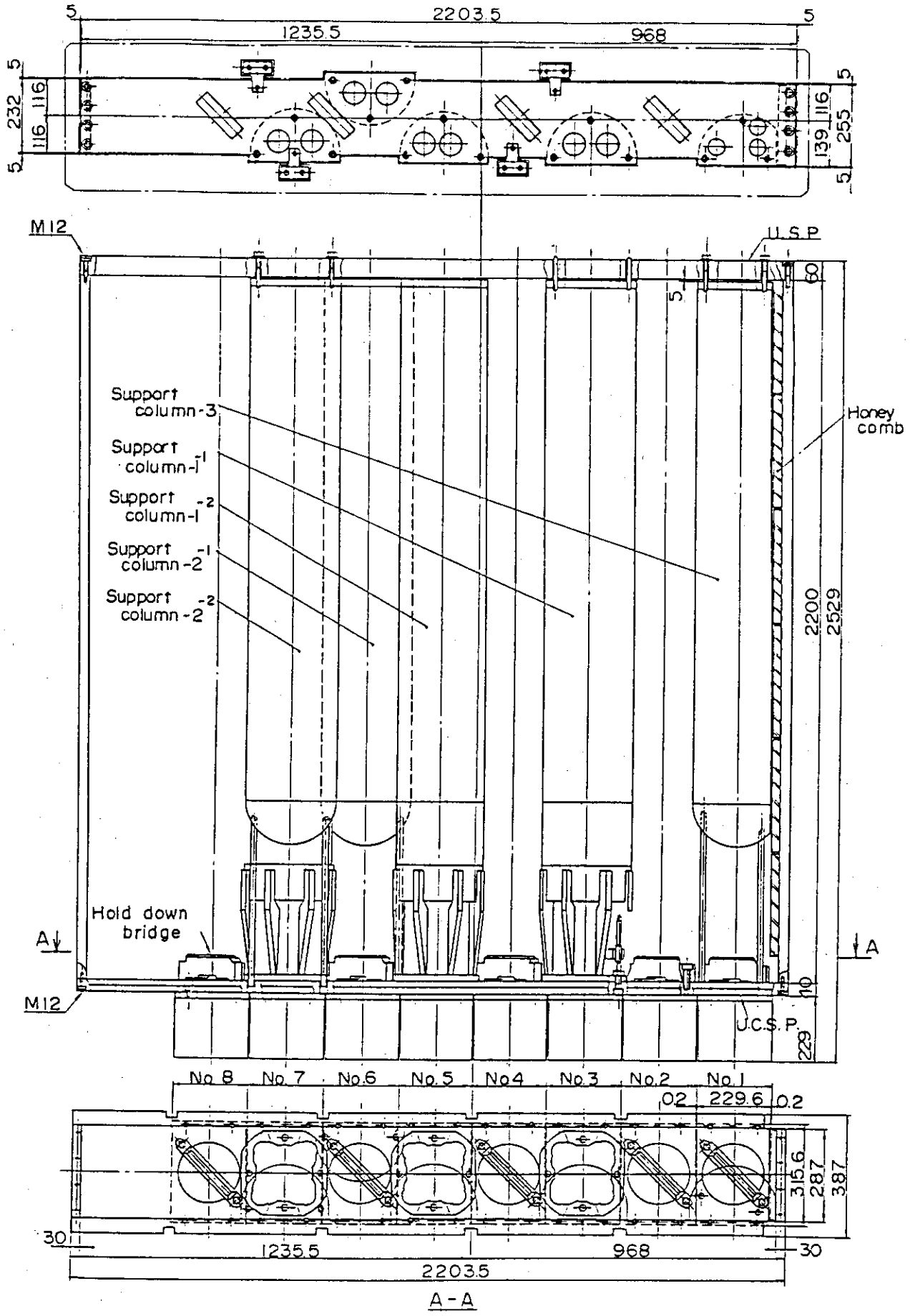

Fig. A-10 Three Kinds of CRGA Support Column

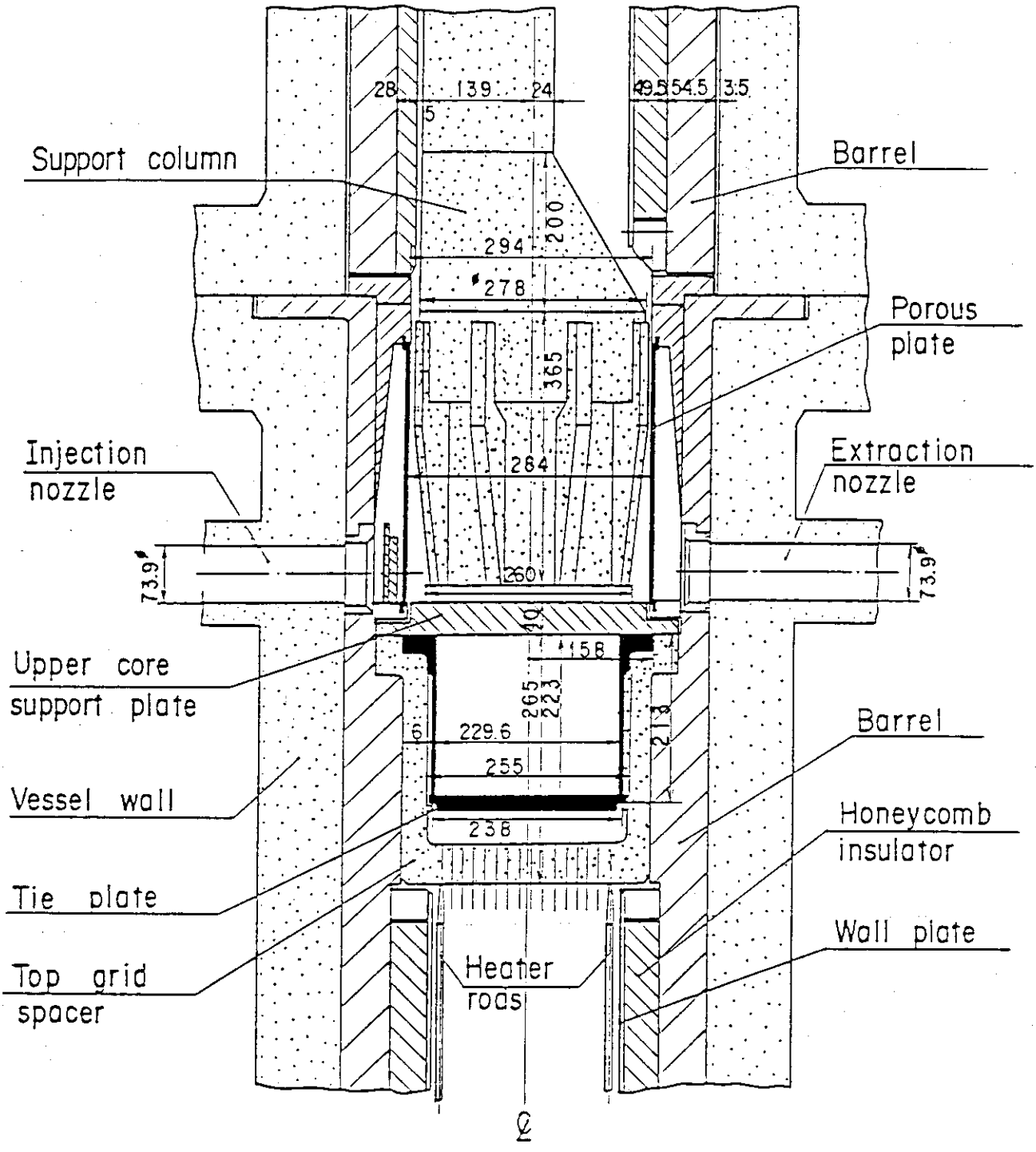

Fig. A-11 Vertical Cross Section of Interface between Core and Upper Plenum

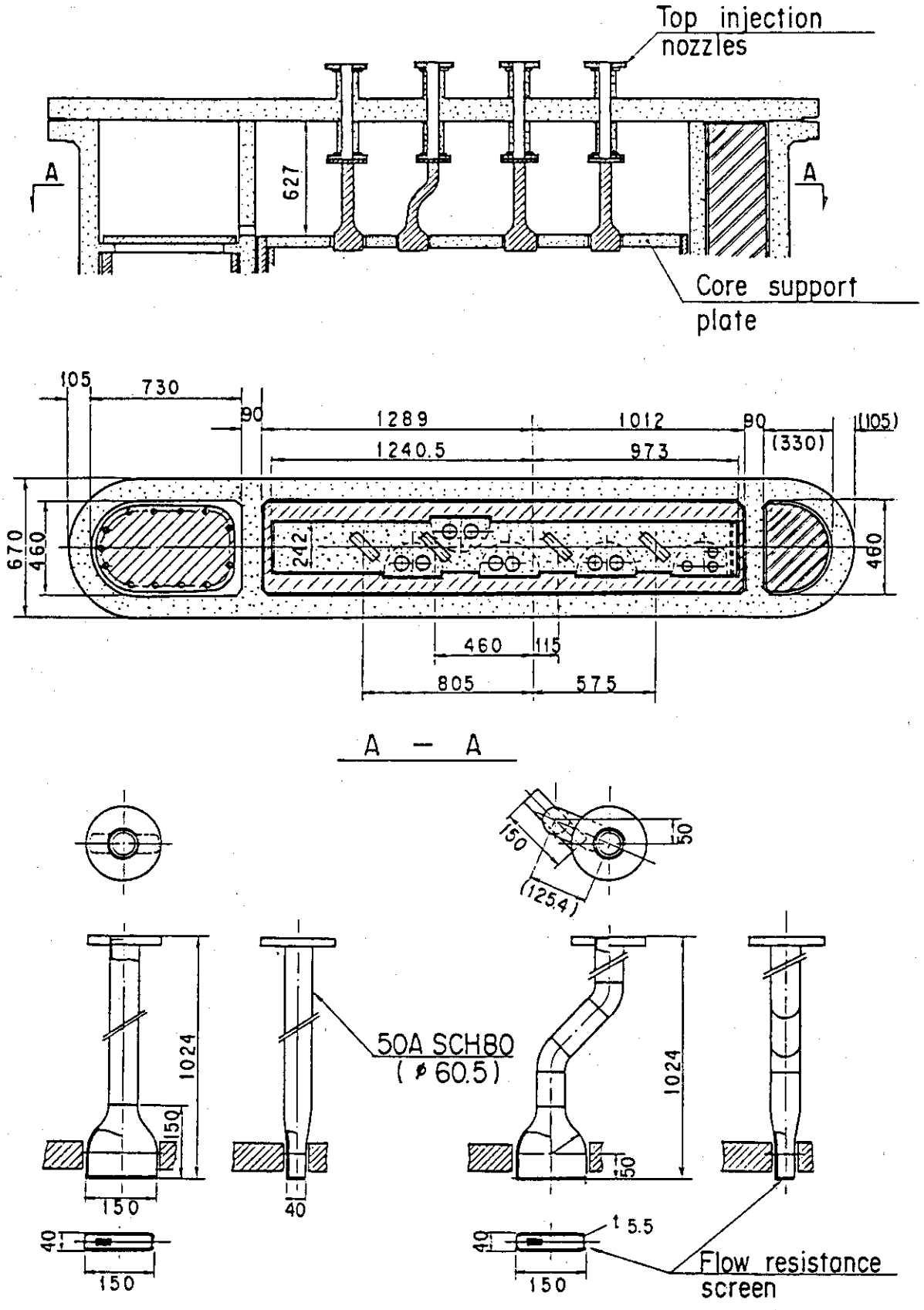

Fig. A-12 Schematic of Upper Head

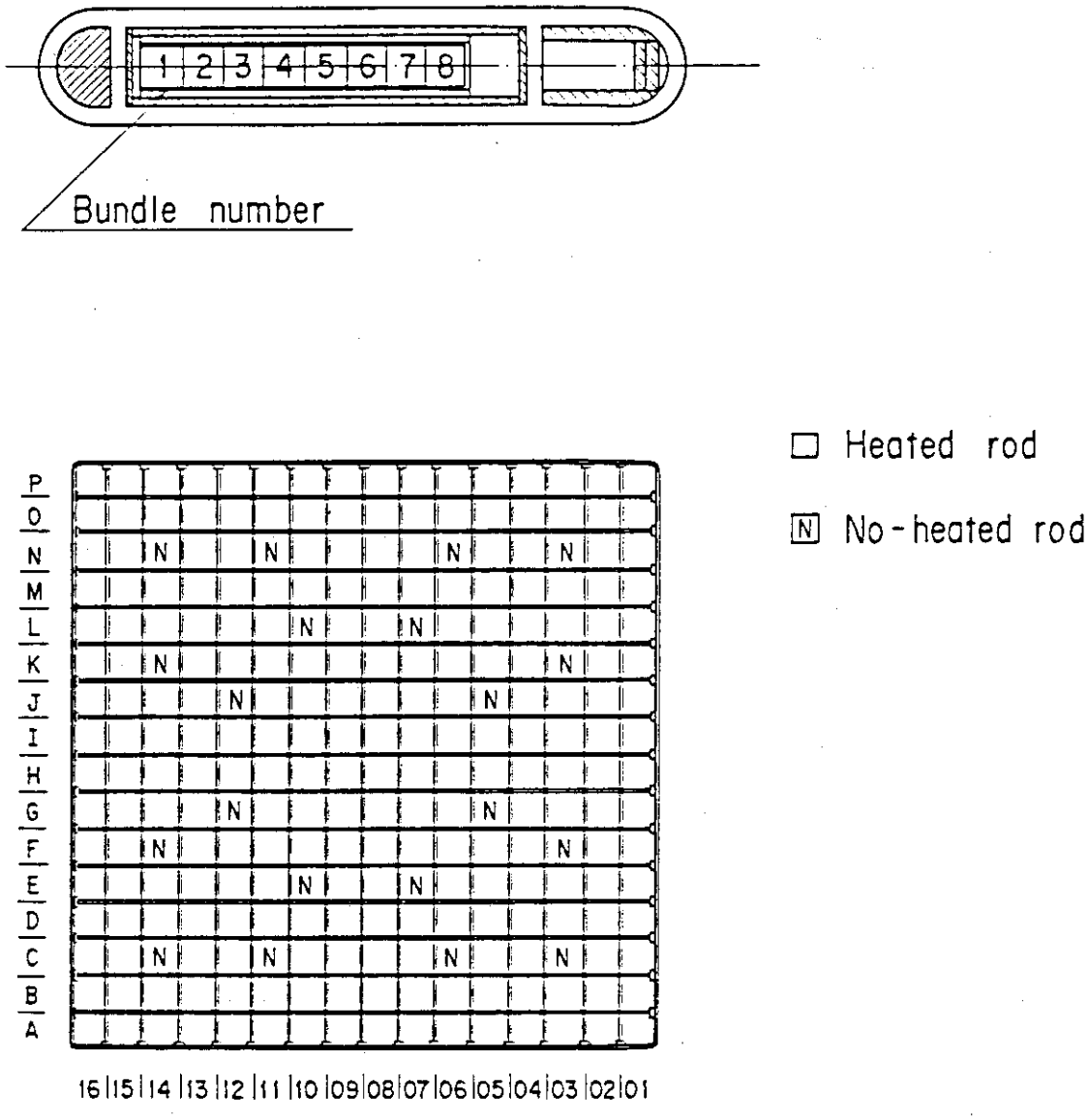

Fig. A-13 Arrangement of Heater Rod Bundles

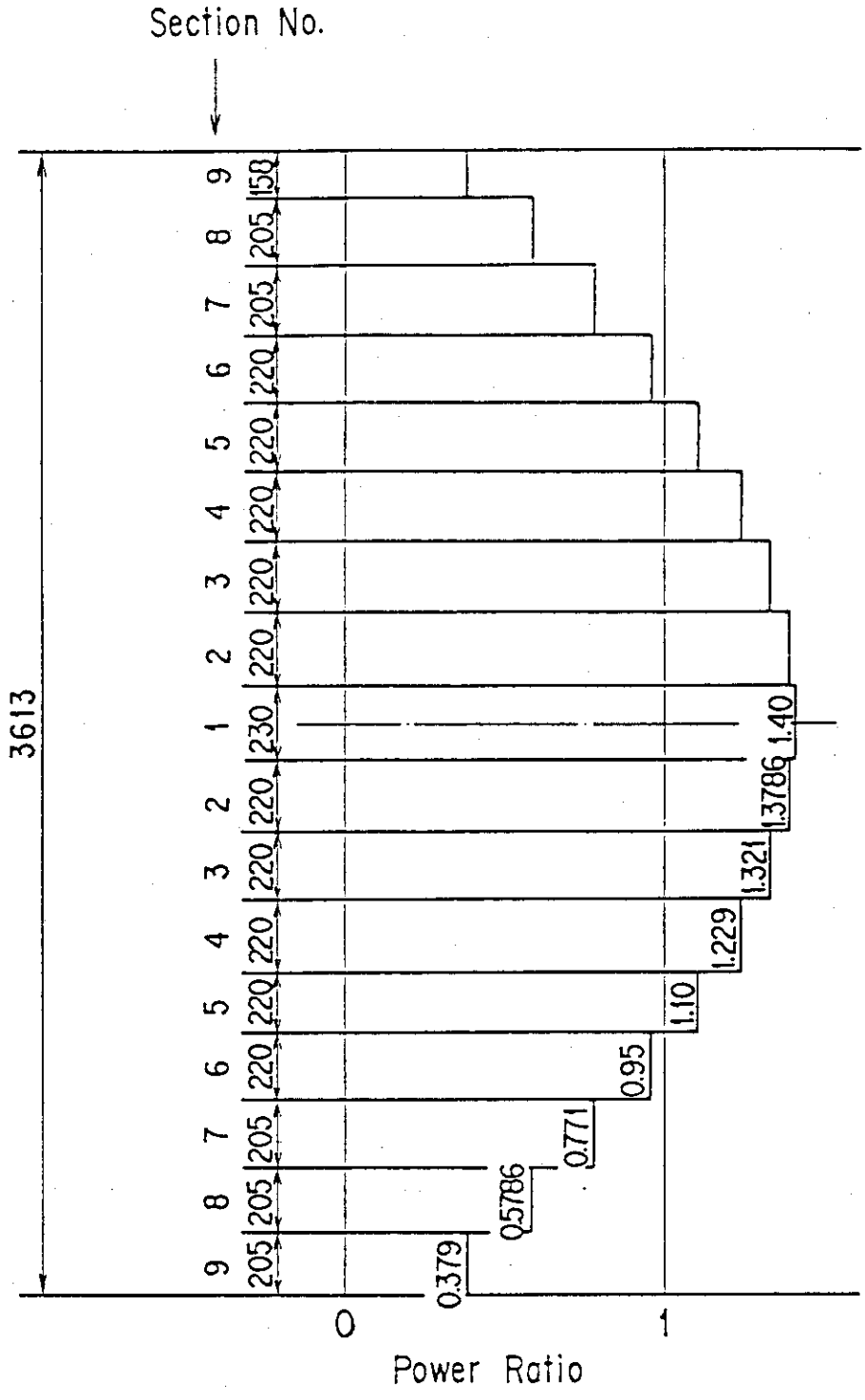

Fig. A-14 Axial Power Distribution of Heater Rods

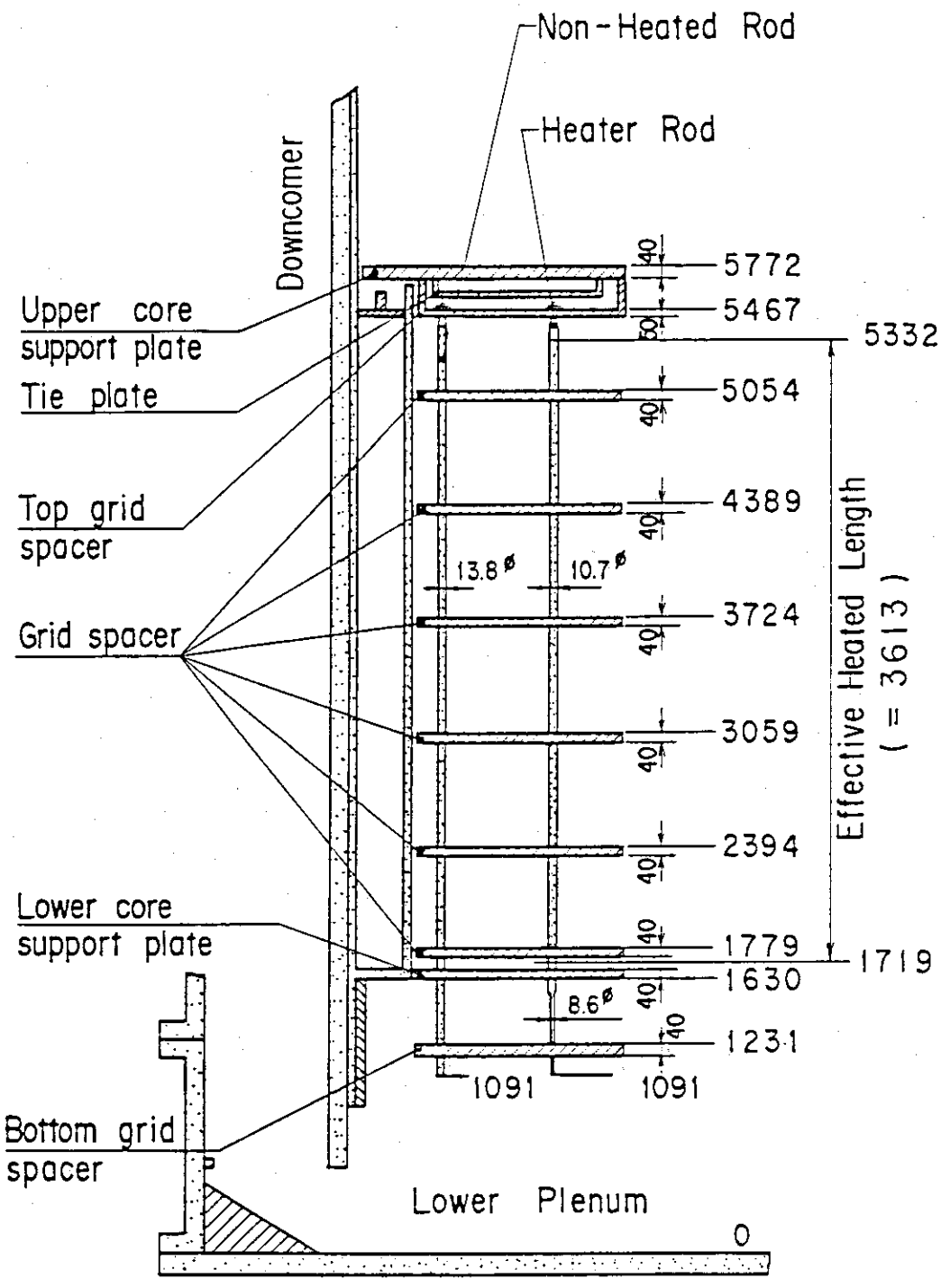

Fig. A-15 Relative Elevation and Dimension of Core

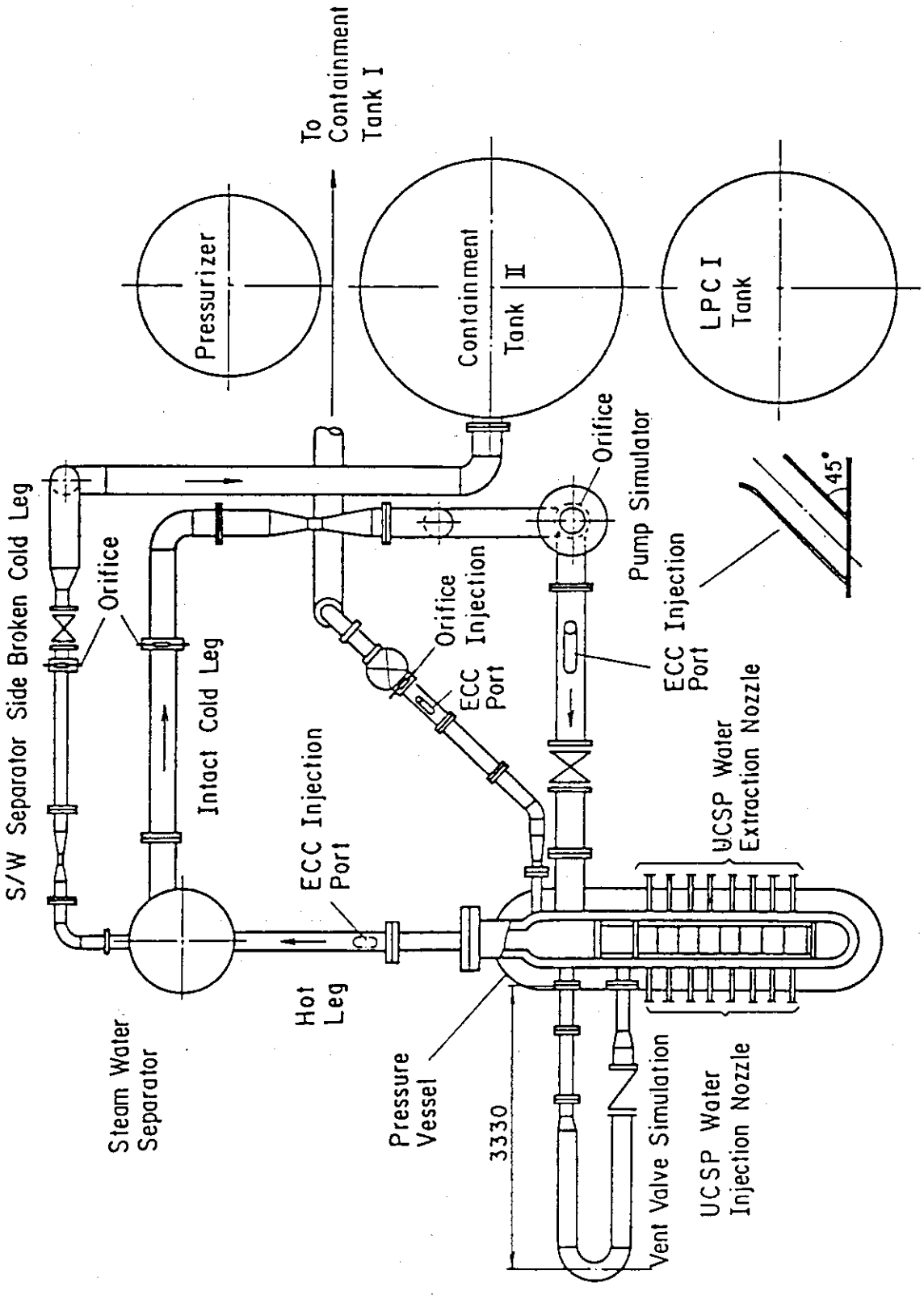

Fig. A-16 Overview of the Arrangements of SCTF

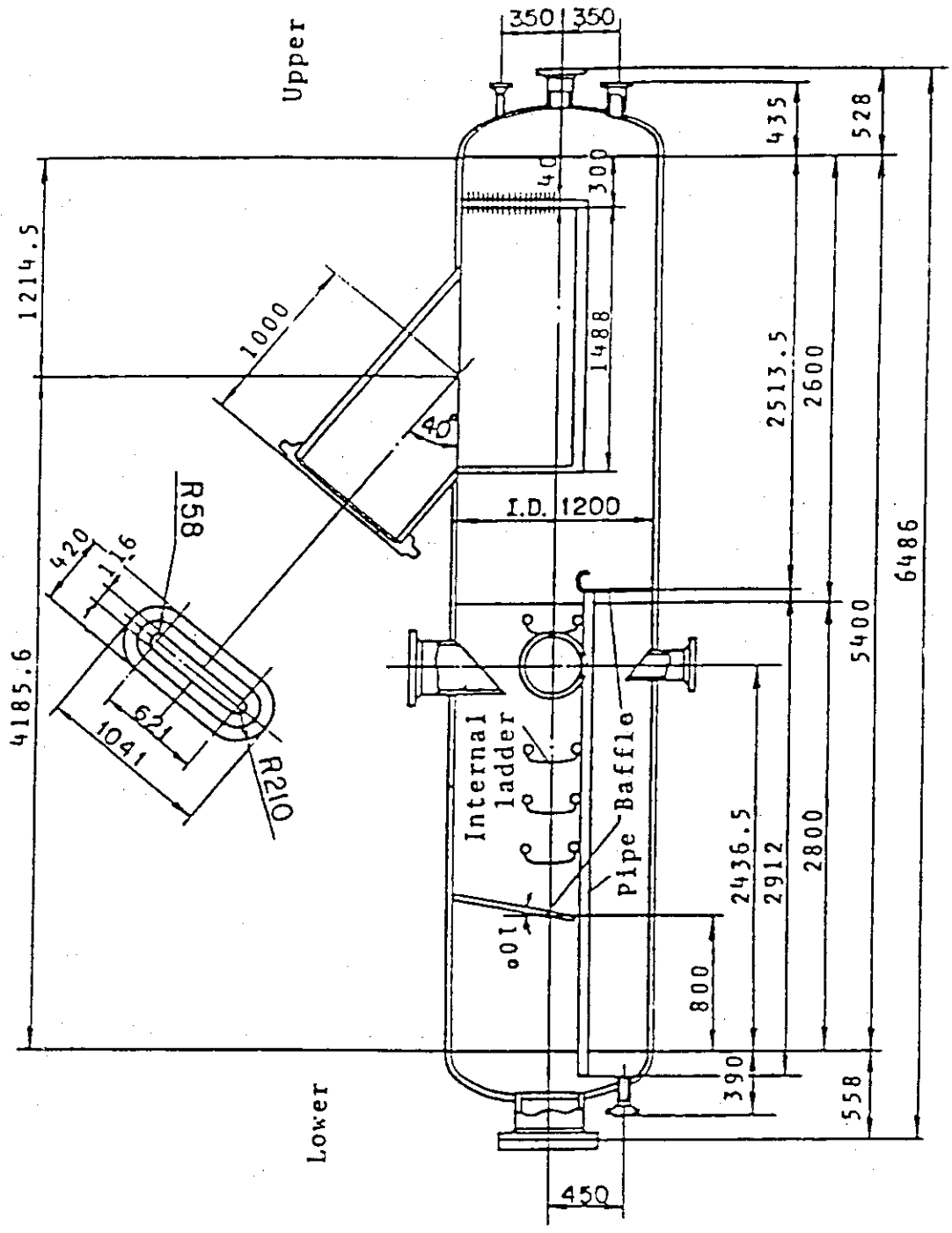

Fig. A-17 Steam/Water Separator

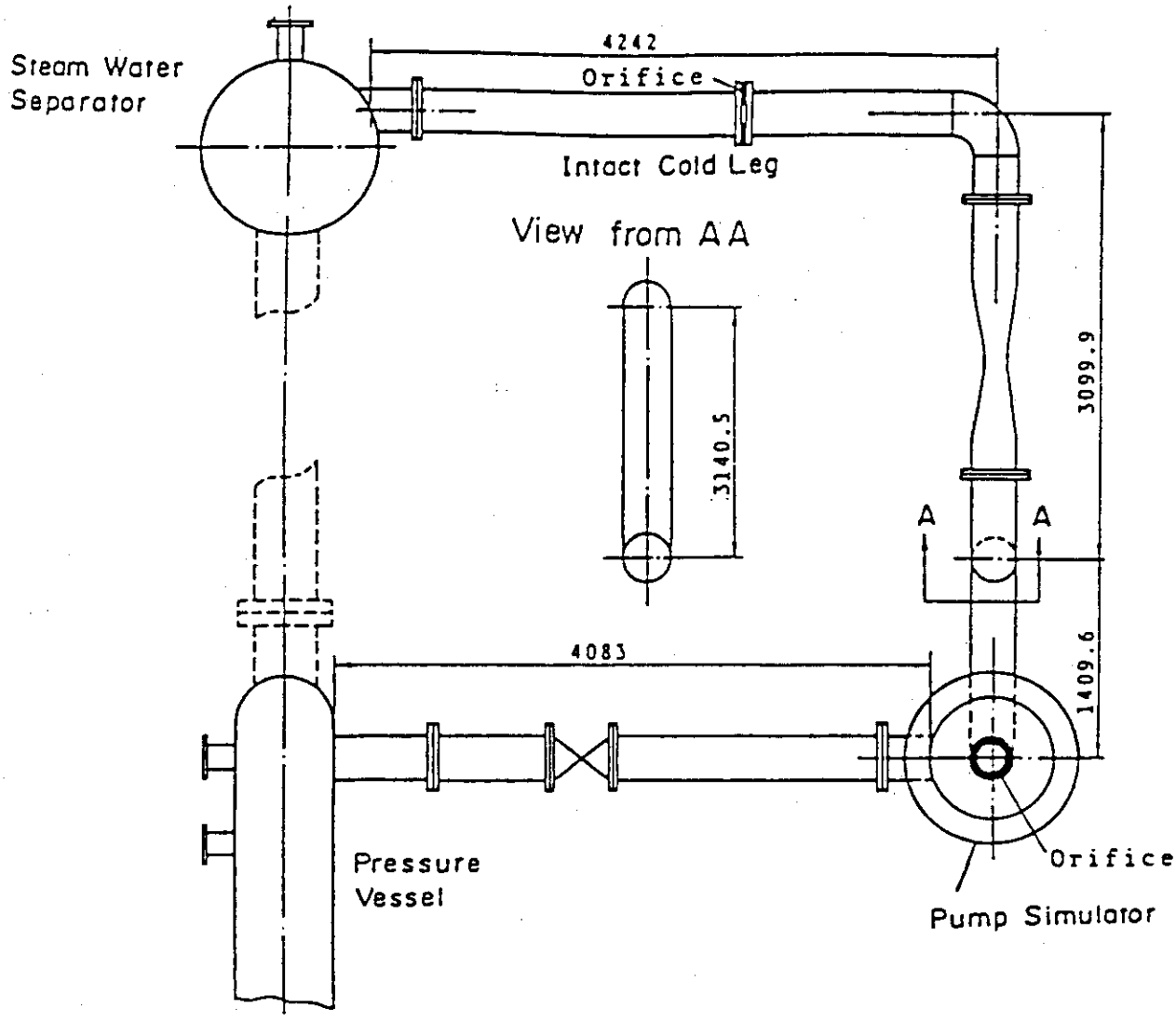

Fig. A-18 Arrangement of Intact Cold Leg

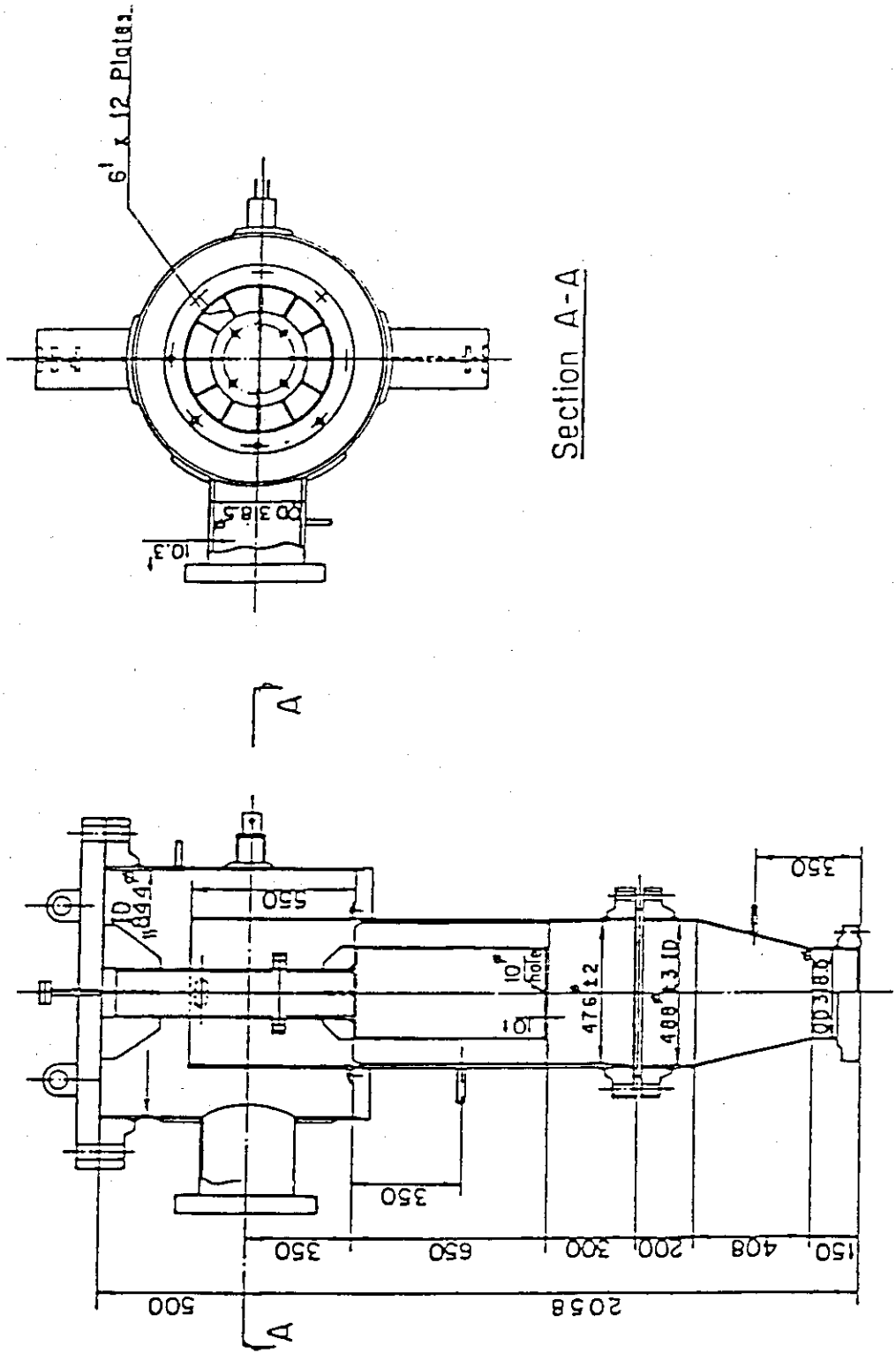

Fig. A-19 Configuration and Dimension of Pump Simulator

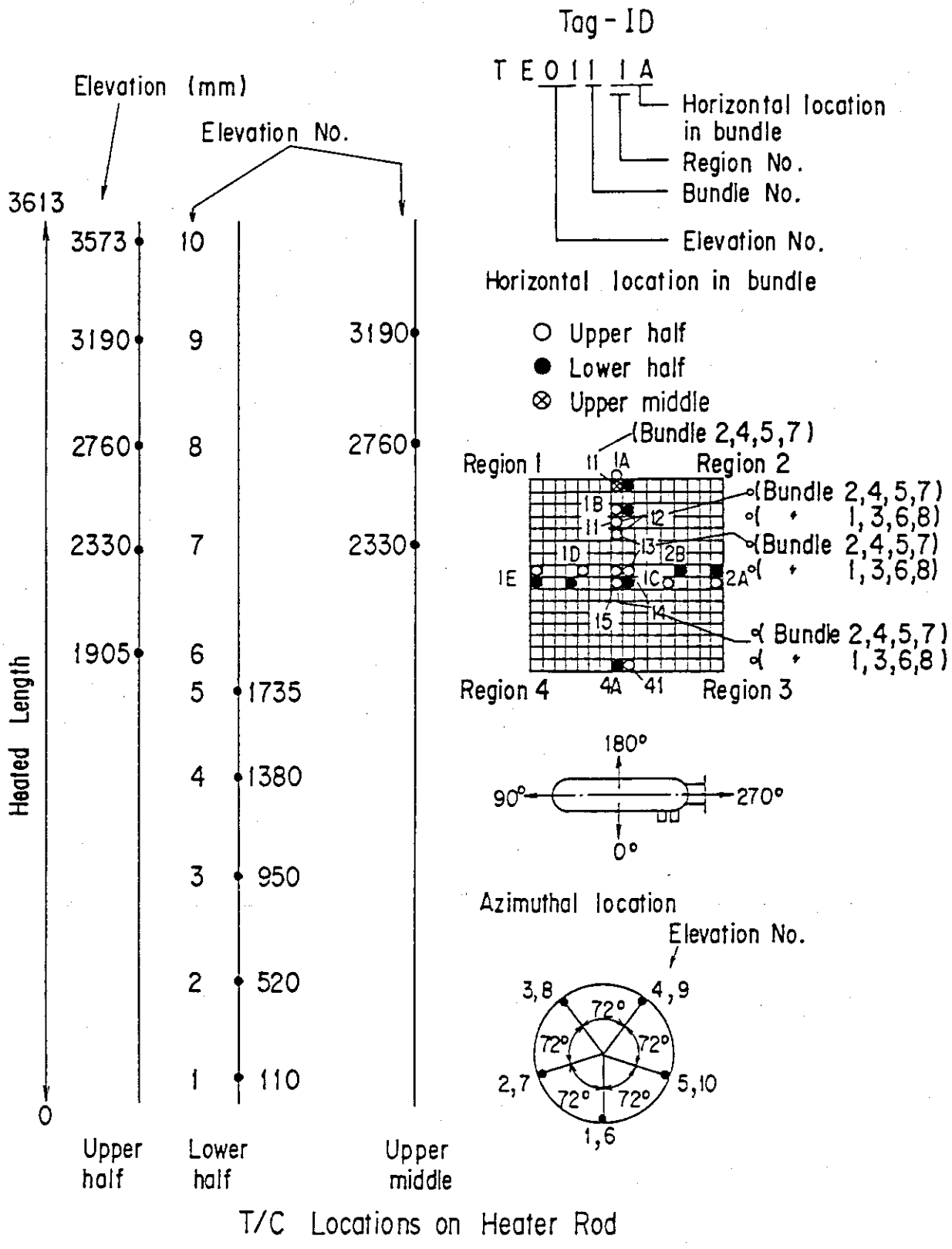

Fig. A-20 Thermocouple Locations of Heater Rod Surface Temperature Measurements

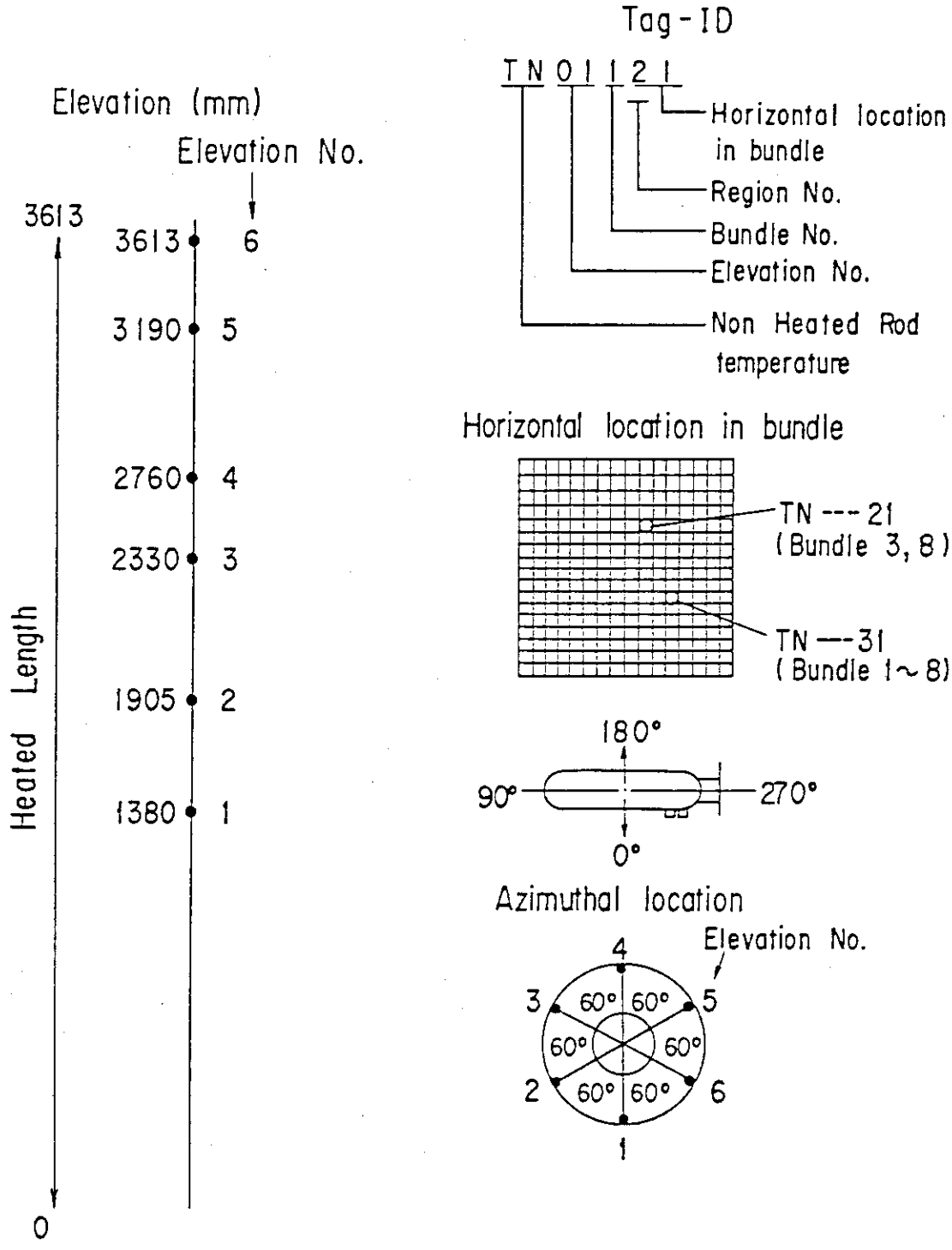

Fig. A-21 Thermocouple Locations of Non-Heated Rod Surface temperature Measurements

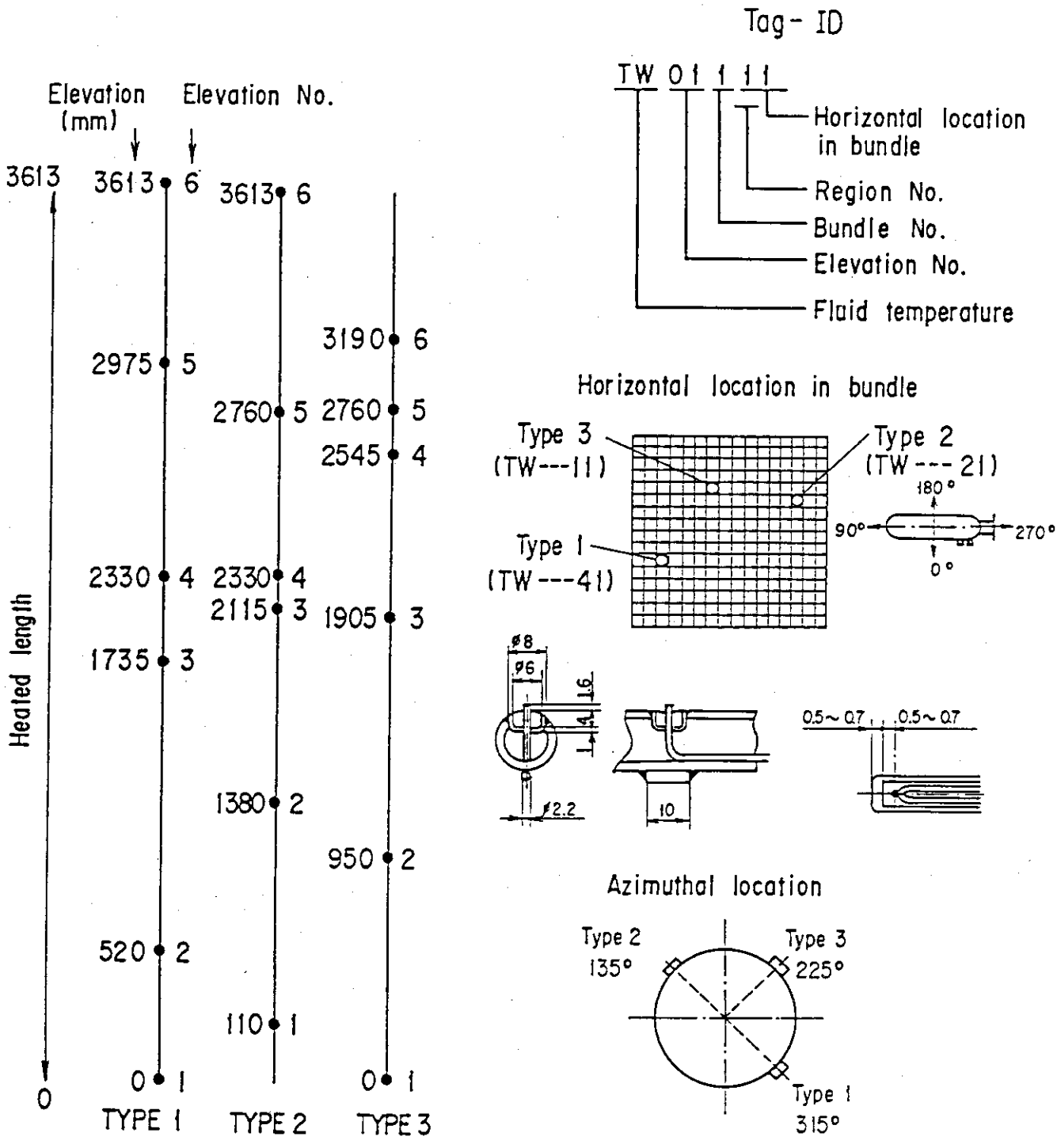

Fig. A-22 Thermocouple Locations of Fluid Temperature Measurements in Core

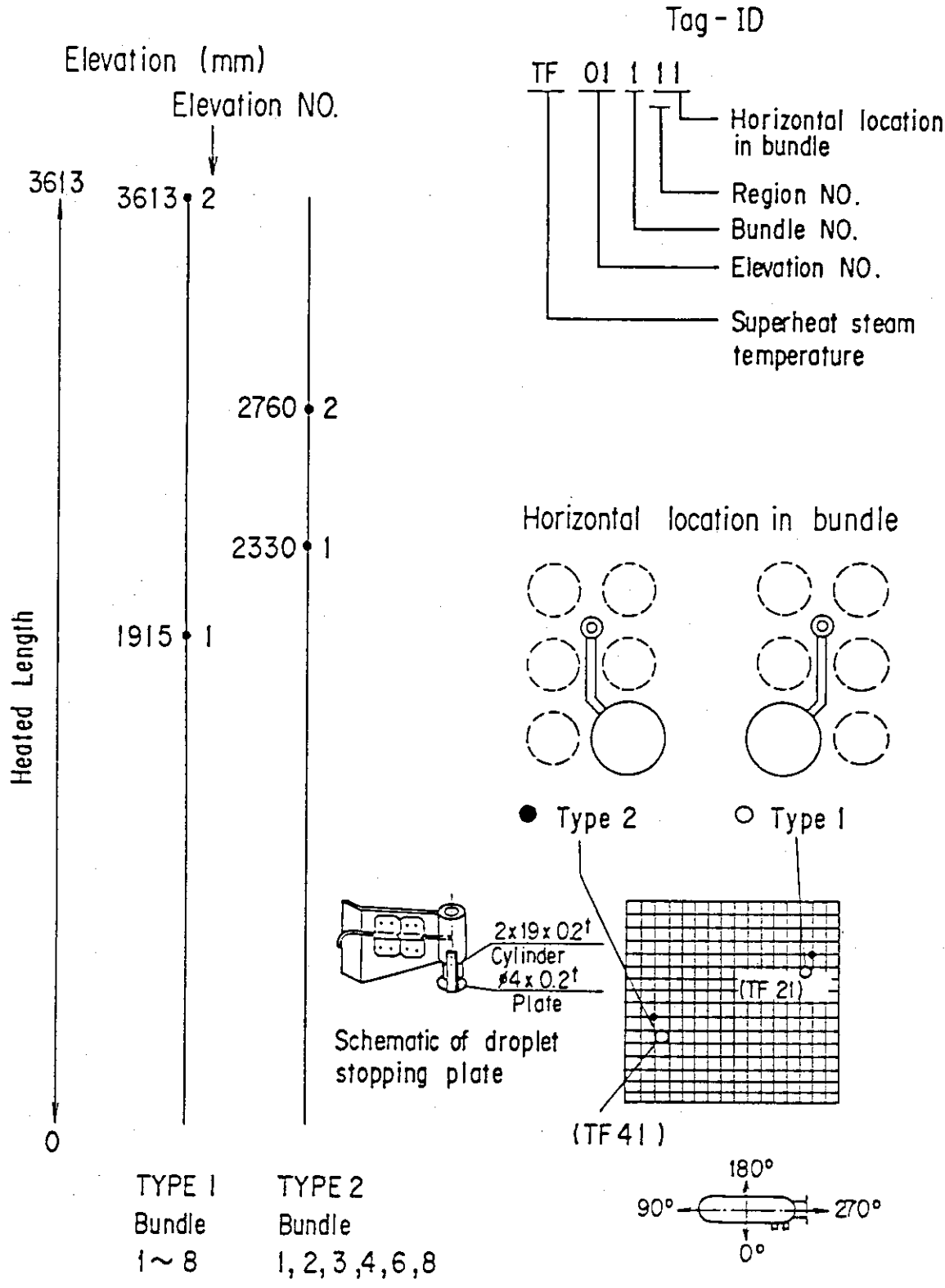

Fig. A-23 Thermocouple Locations of Steam Temperature Measurements in Core

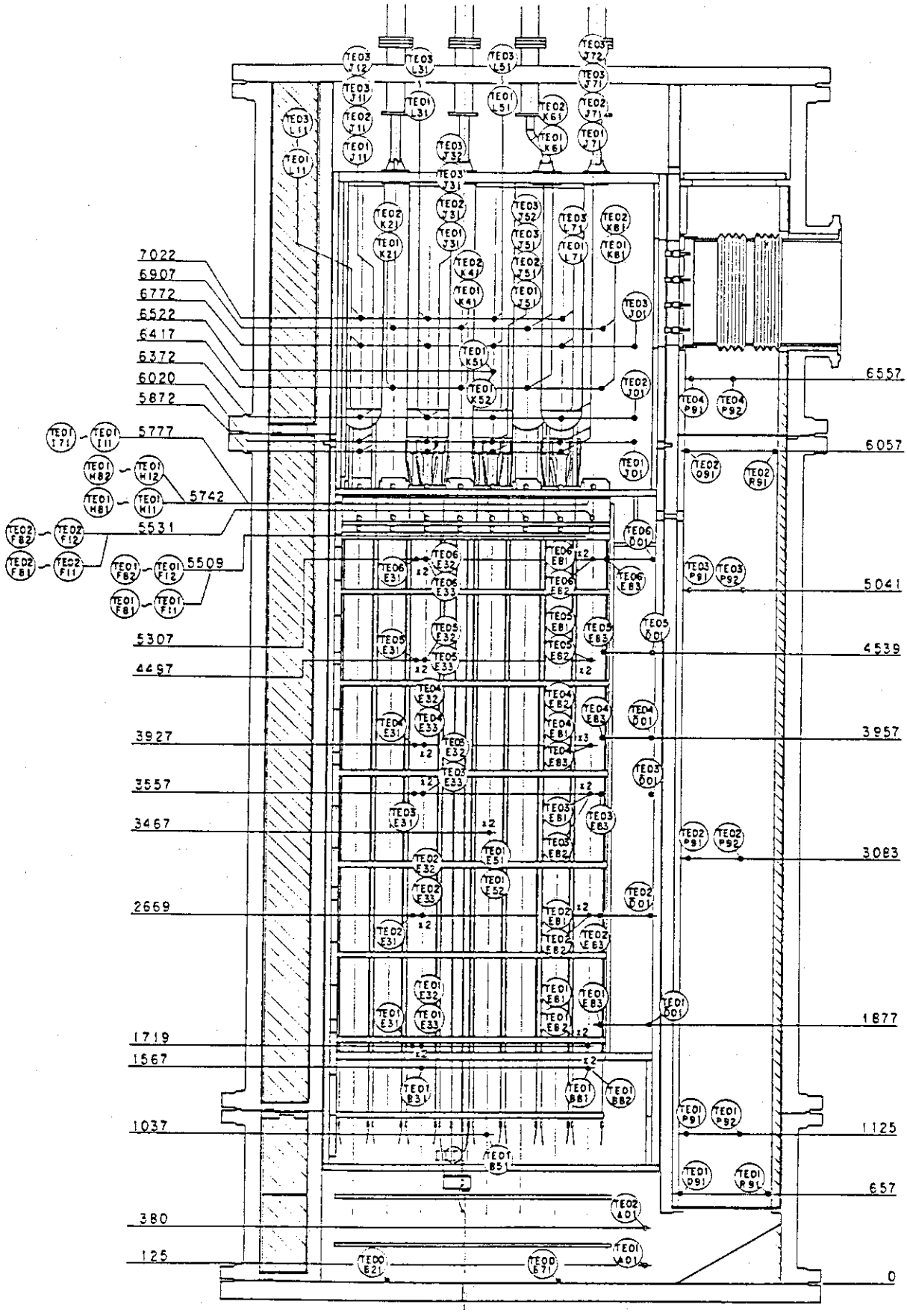

Fig. A-24 Thermocouple Locations of Temperature Measurements in Pressure Vessel except Core Region (Vertical View)

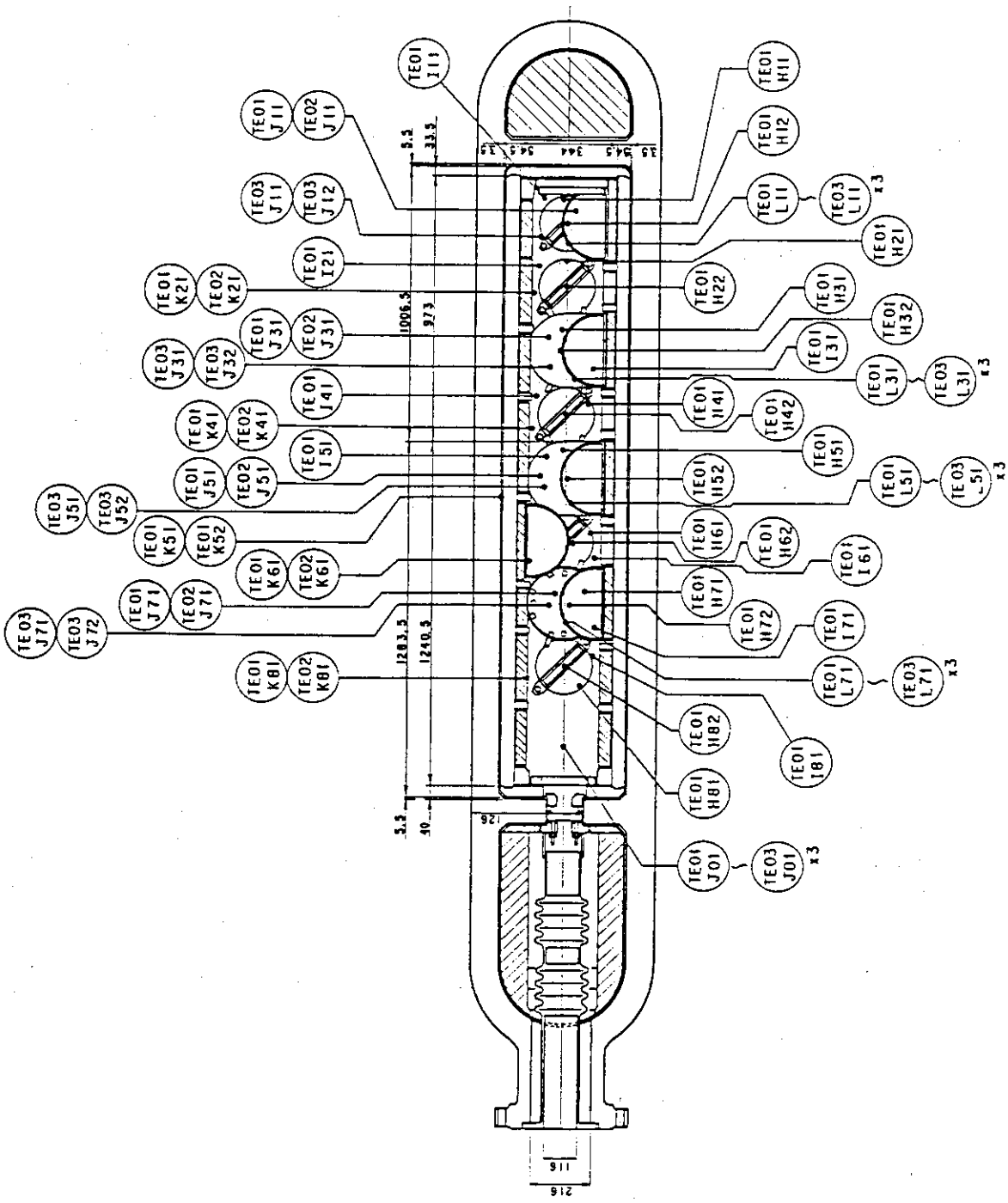

Fig. A-25 Thermocouple Locations of Temperature Measurements in Upper Plenum (Horizontal View)

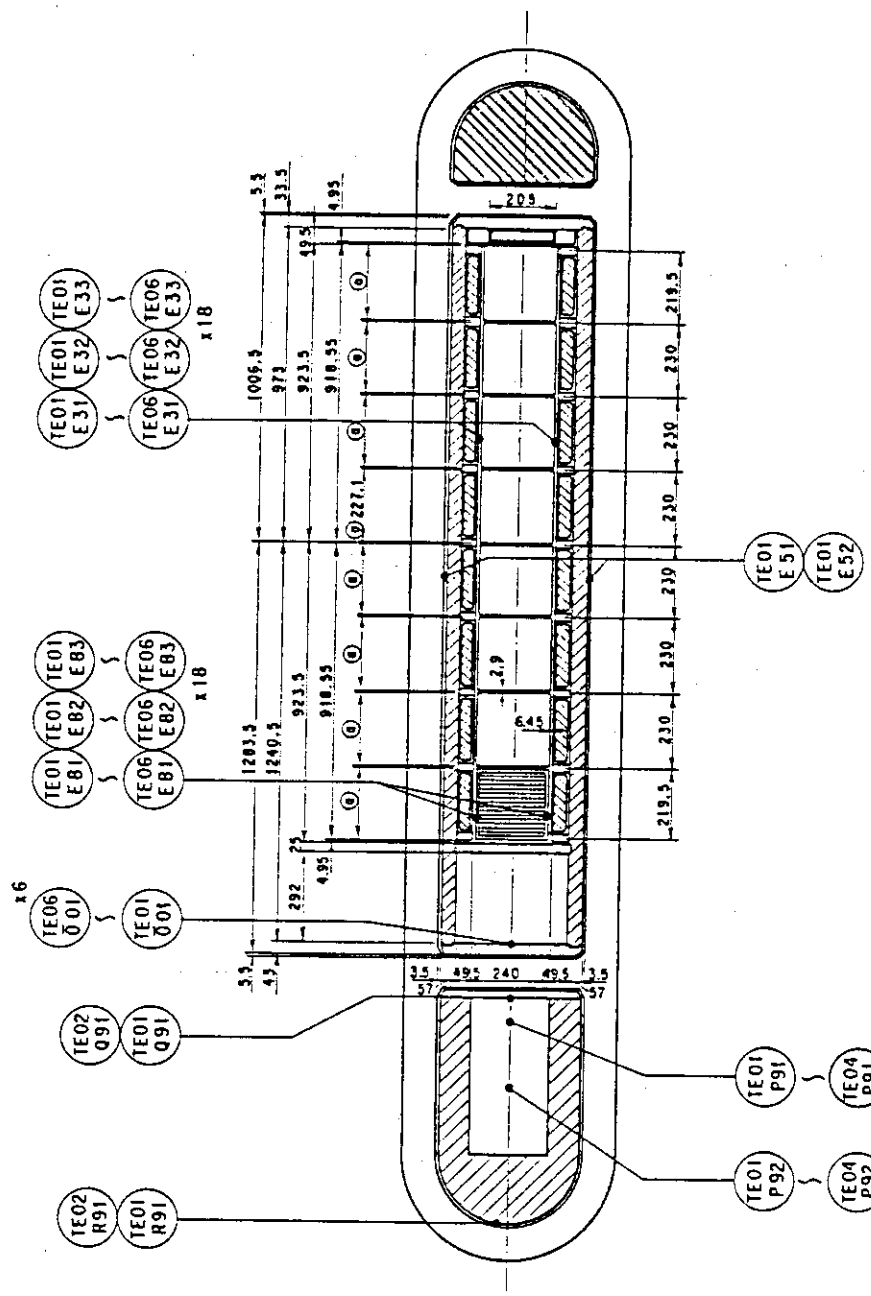

Fig. A-26 Thermocouple Locations of Temperature Measurements in Pressure Vessel except Upper Plenum (Horizontal View)

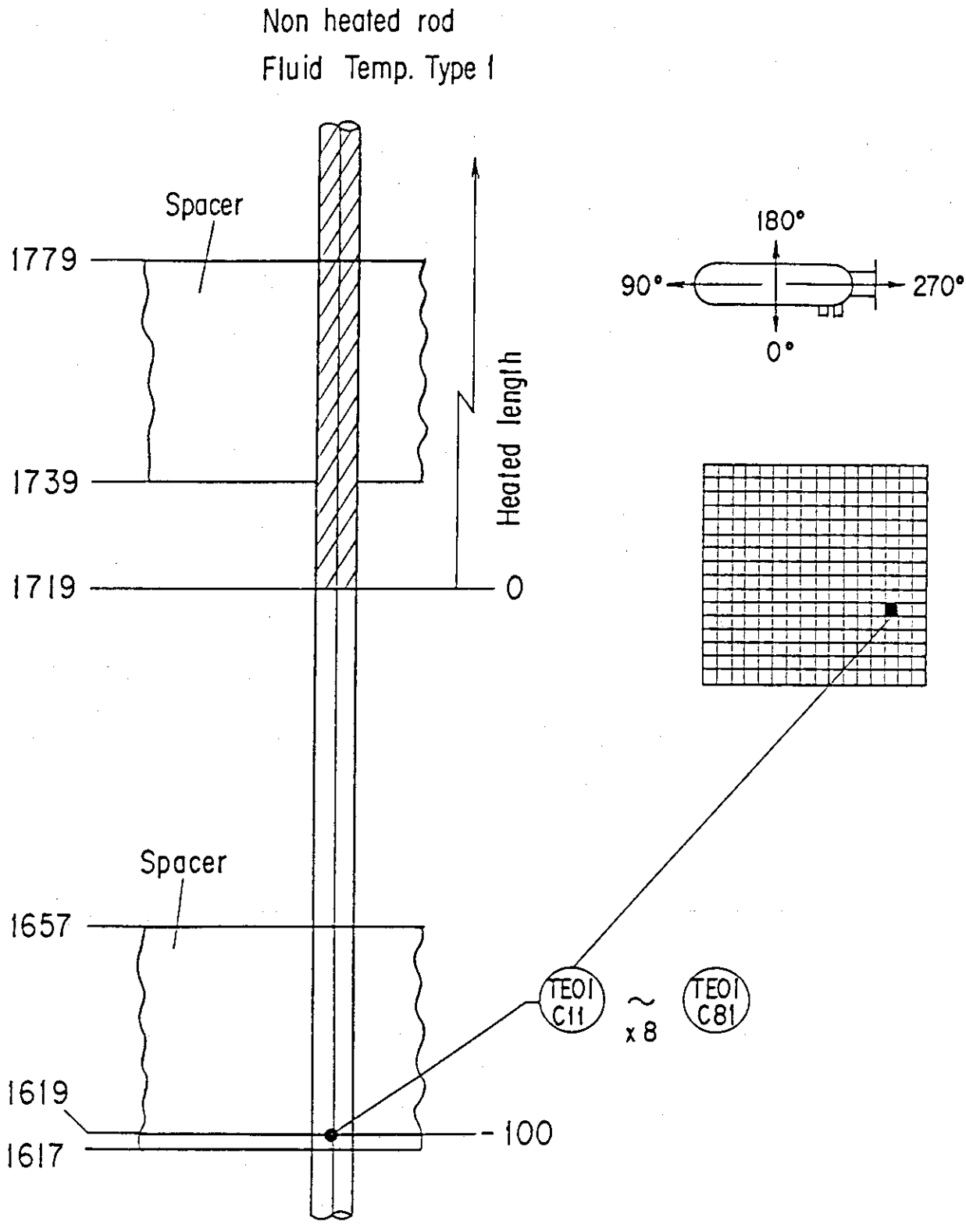

Fig. A-27 Thermocouple Locations of Fluid Temperature Measurements at Core Inlet

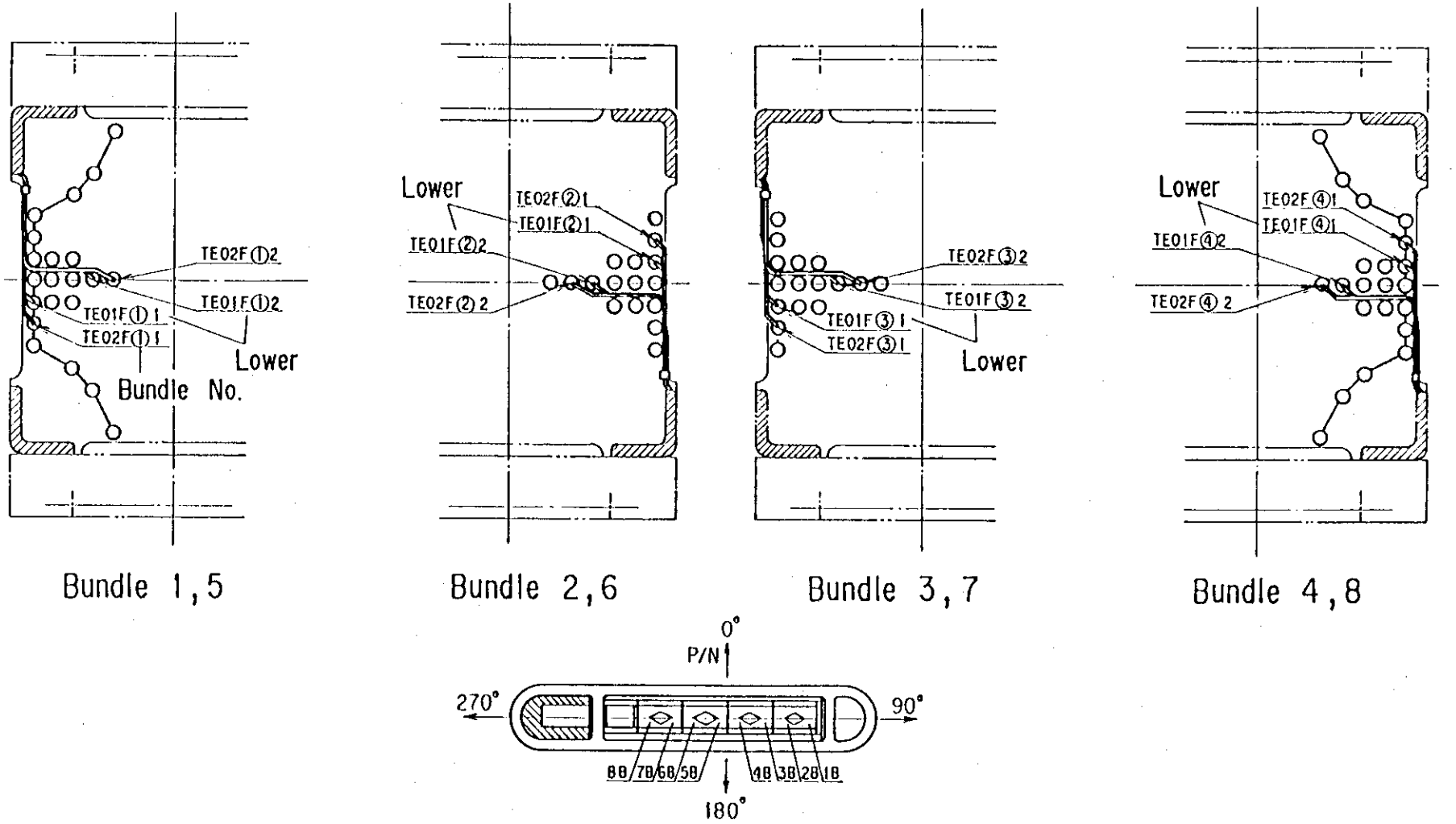

Fig. A-28 Thermocouple Locations of Fluid Temperature Measurements just above and below End Box Tie Plates

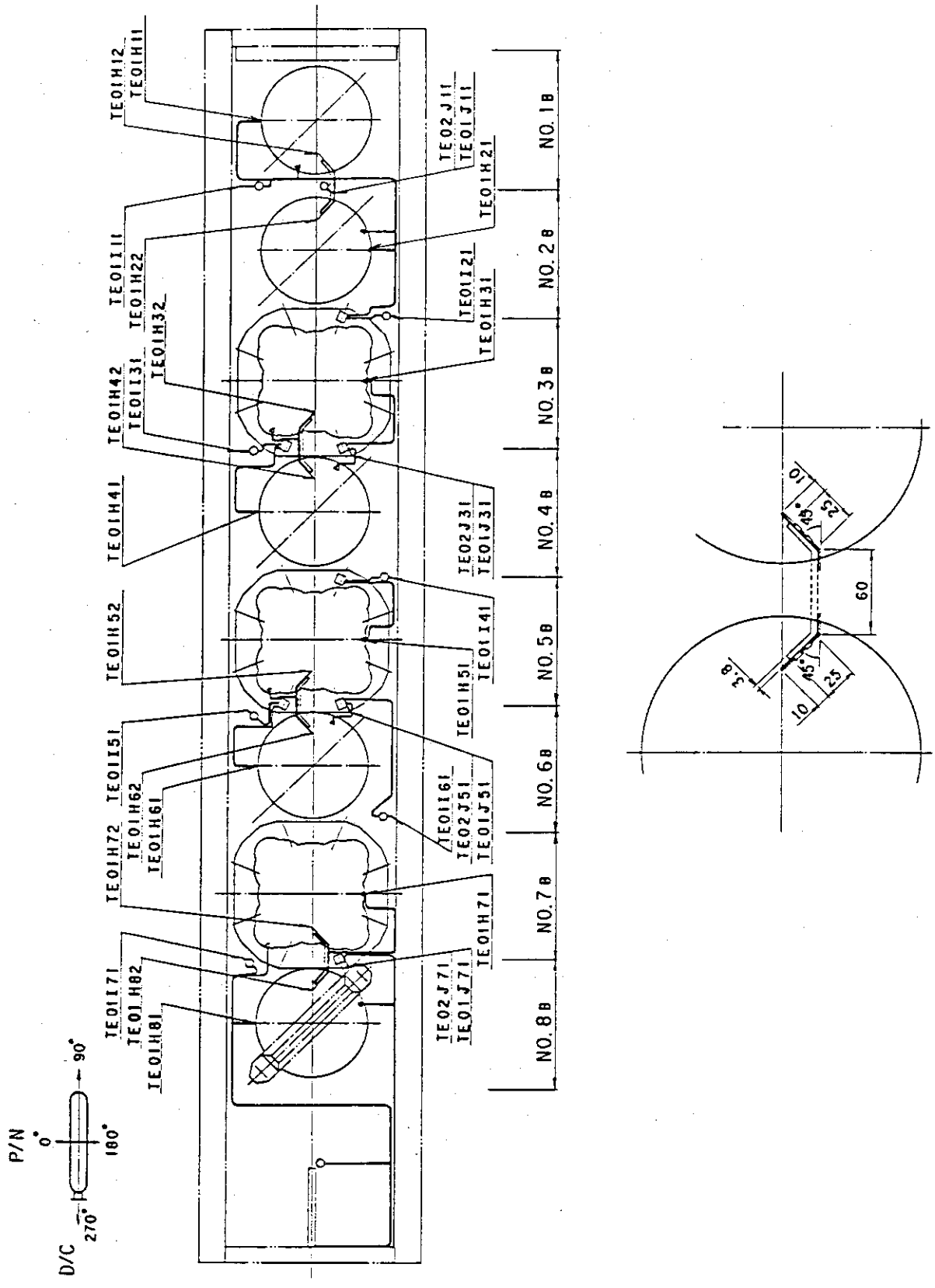

Fig. A-29 Thermocouple Locations of Fluid Temperature Measurements on UCSP and at Inside and Periphery of UCSP Holes

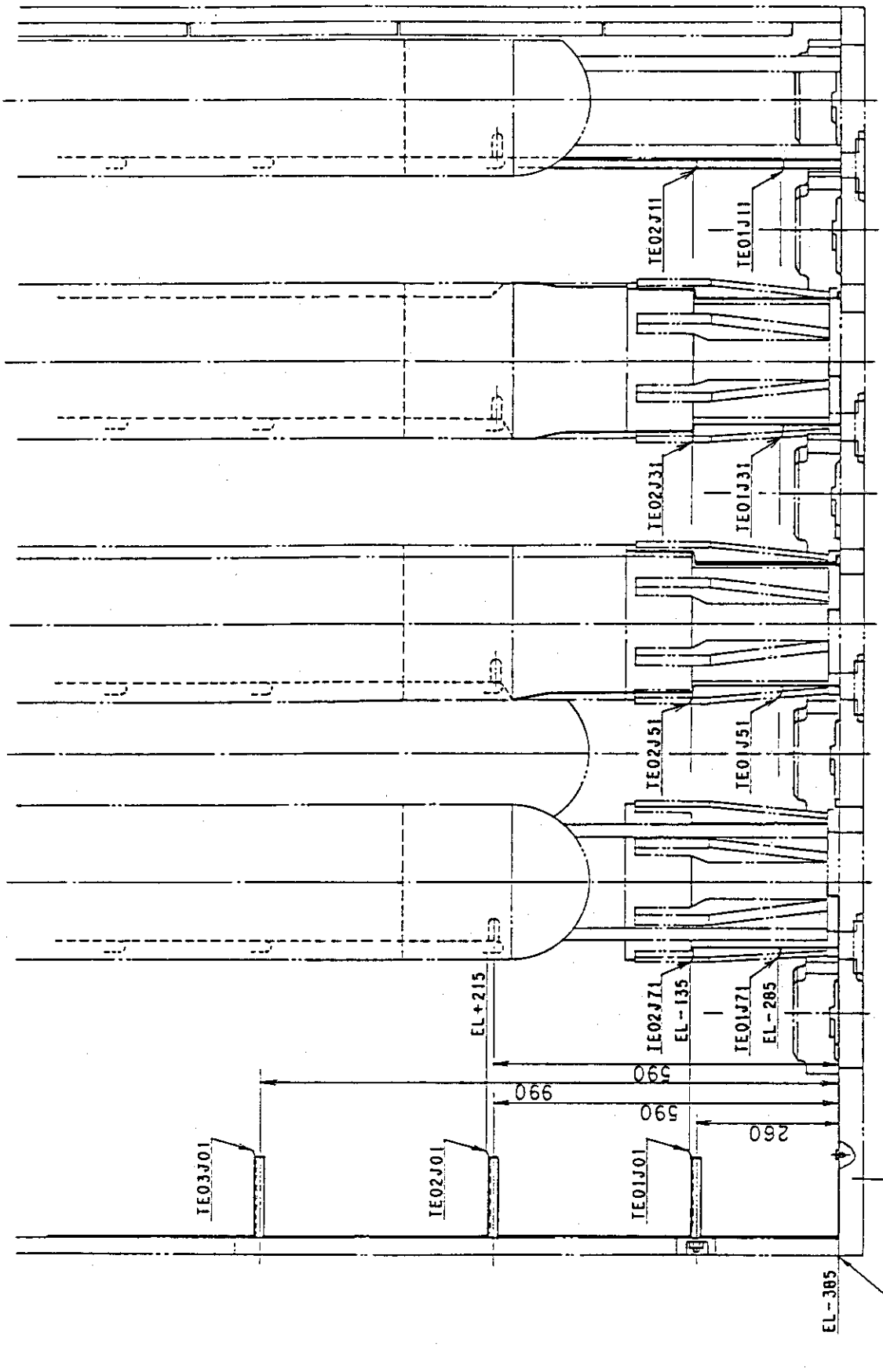

Fig. A-30 Thermocouple Locations of Fluid Temperature Measurements on and above UCSP

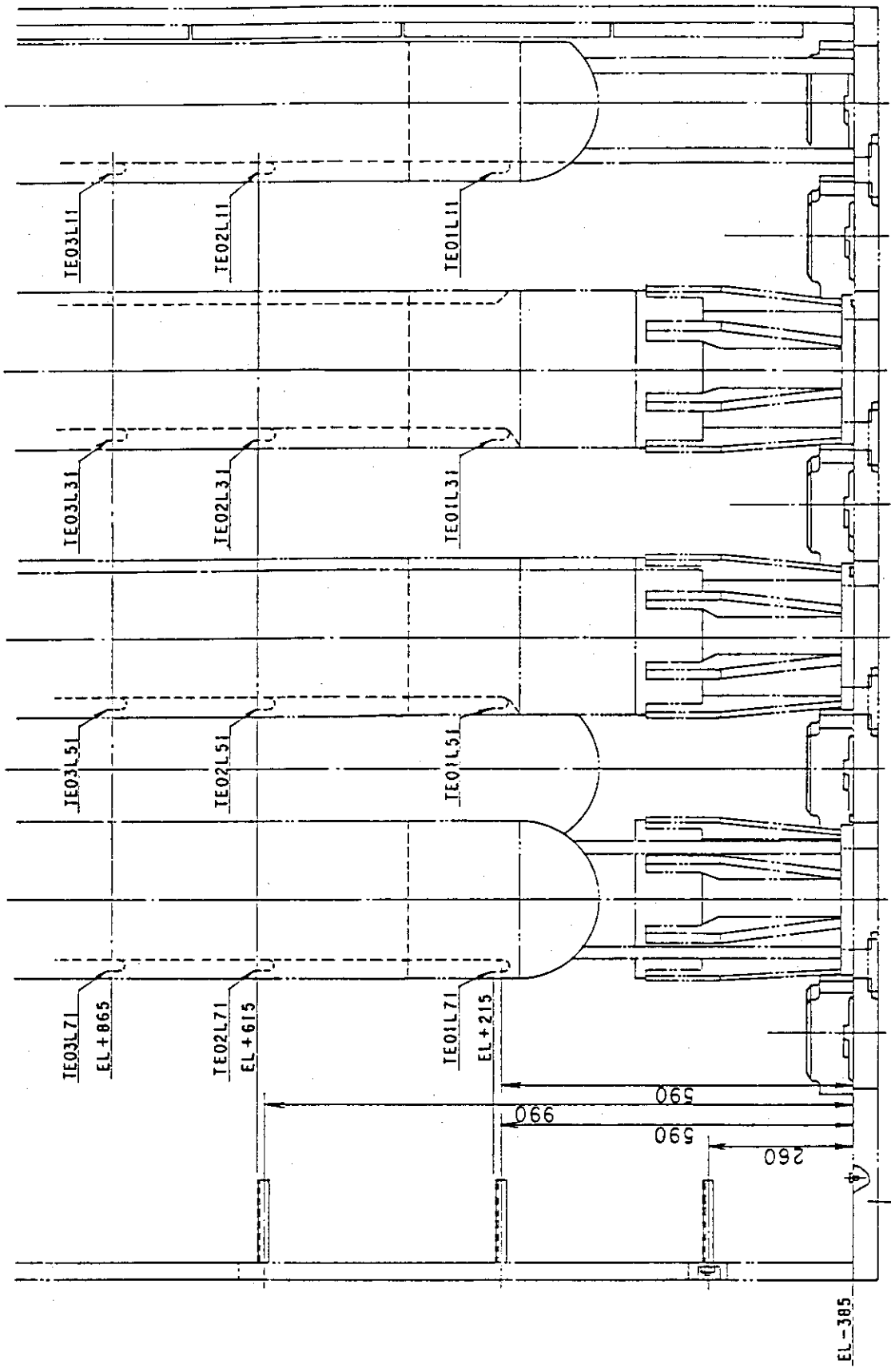

Fig. A-31 Thermocouple Locations of Surface Temperature Measurements of Upper Plenum Structures

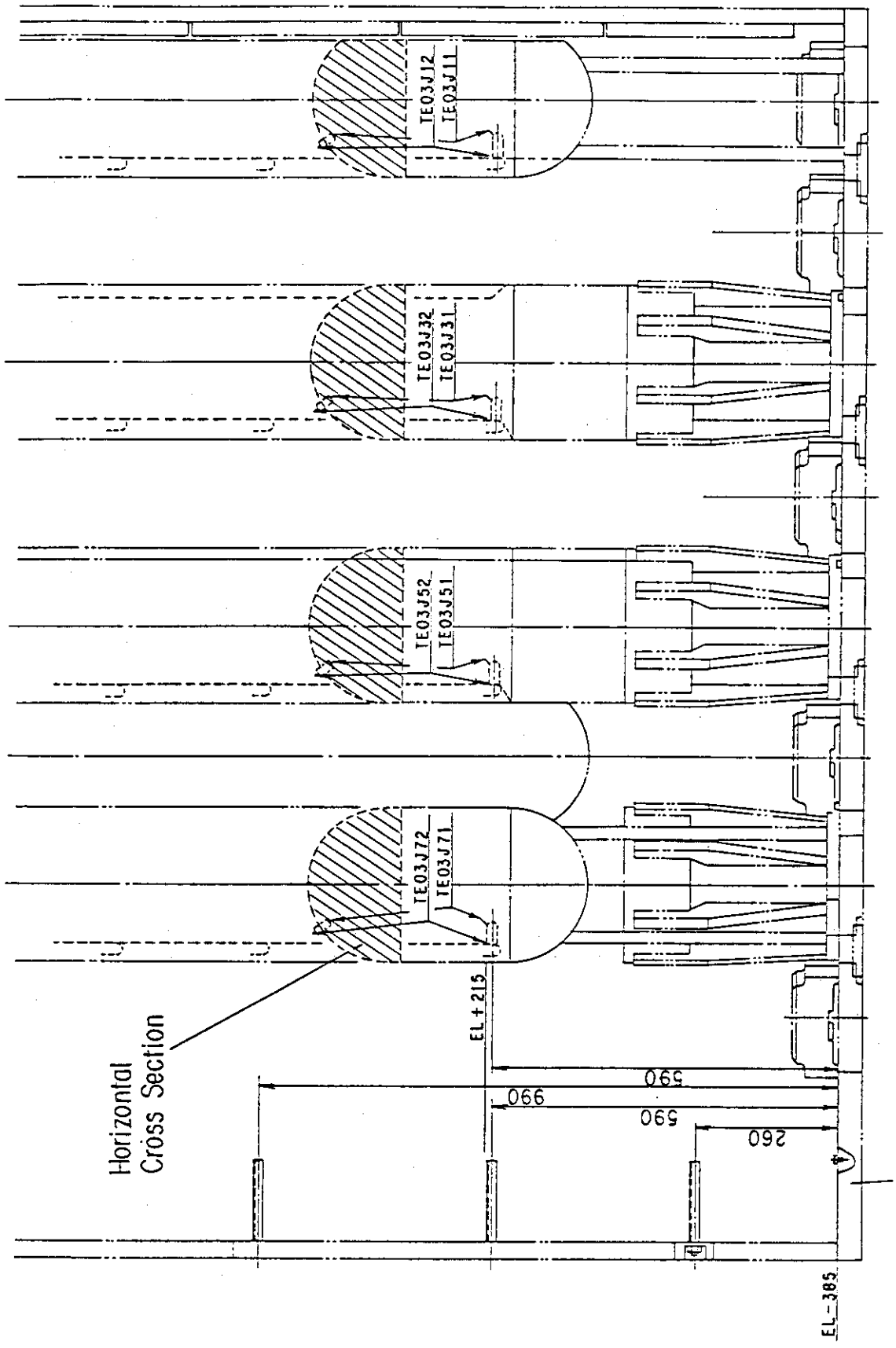

Fig. A-32 Thermocouple Locations of Steam Temperature Measurements above UCSP Holes

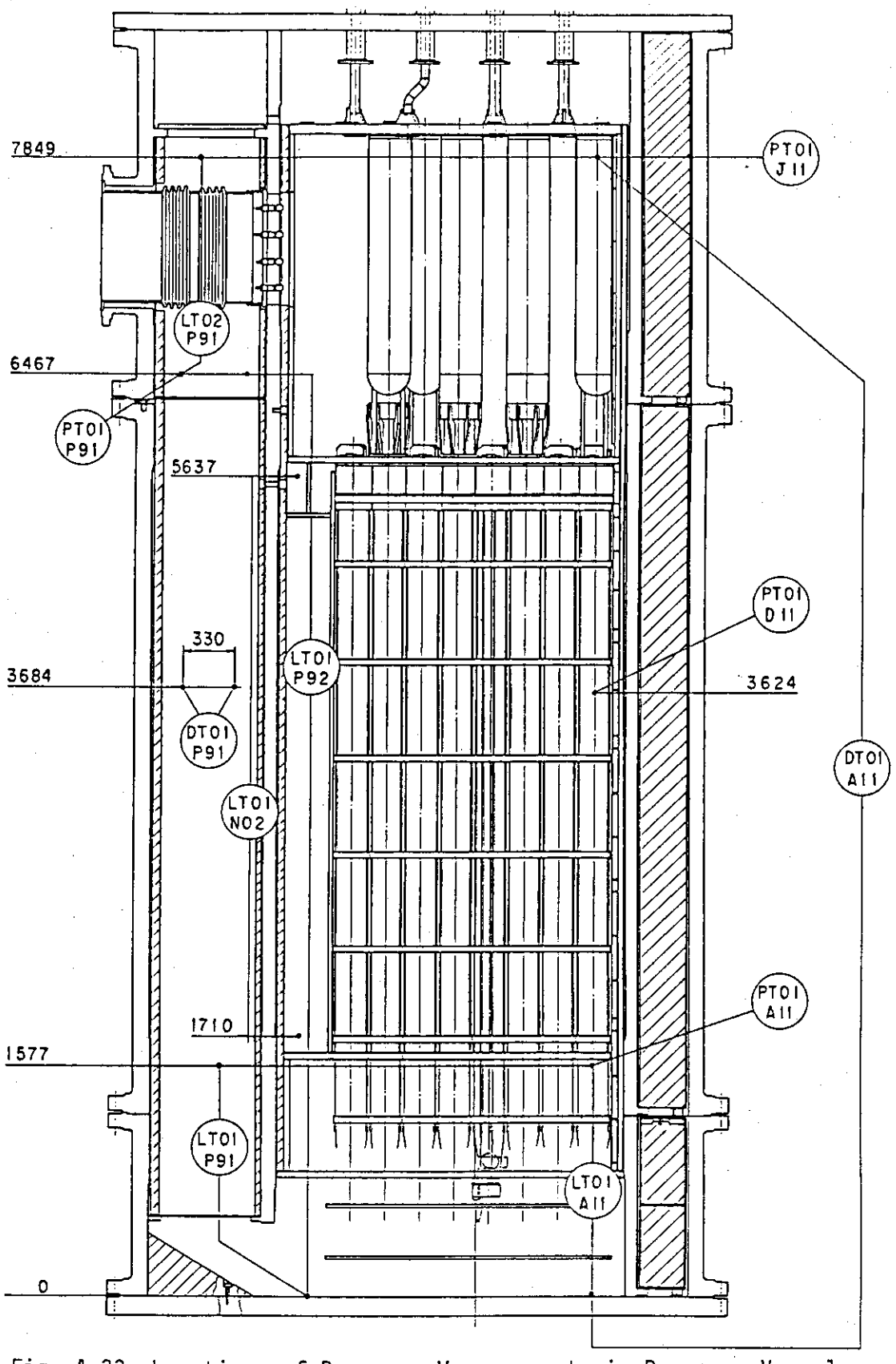

Fig. A-33 Locations of Pressure Measurements in Pressure Vessel, Differential Pressure Measurements between Upper and Lower Plenums and Liquid Level Measurements in Downcomer and Lower Plenums

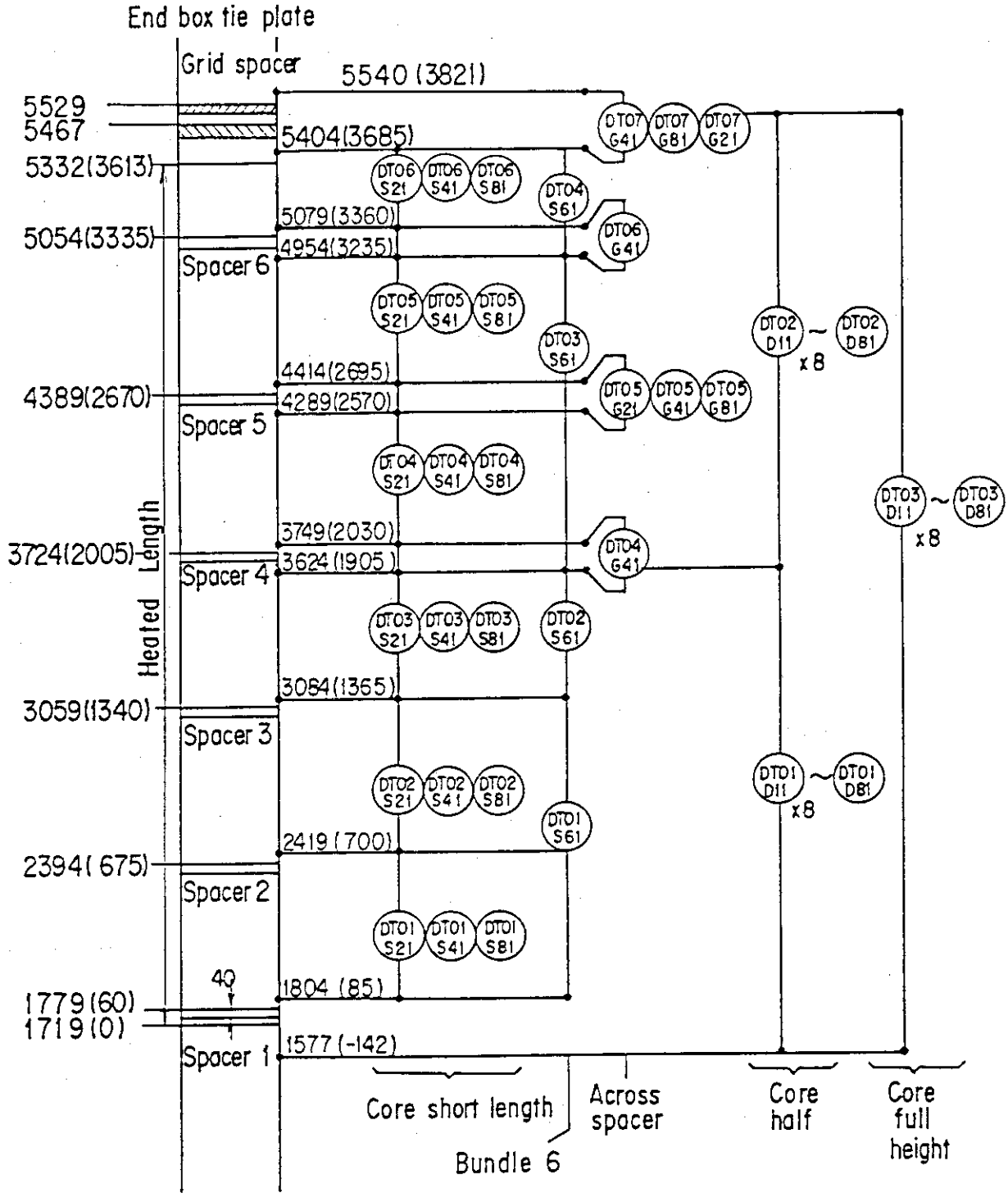

Fig. A-34 Locations of Vertical Differential Pressure Measurements in Core

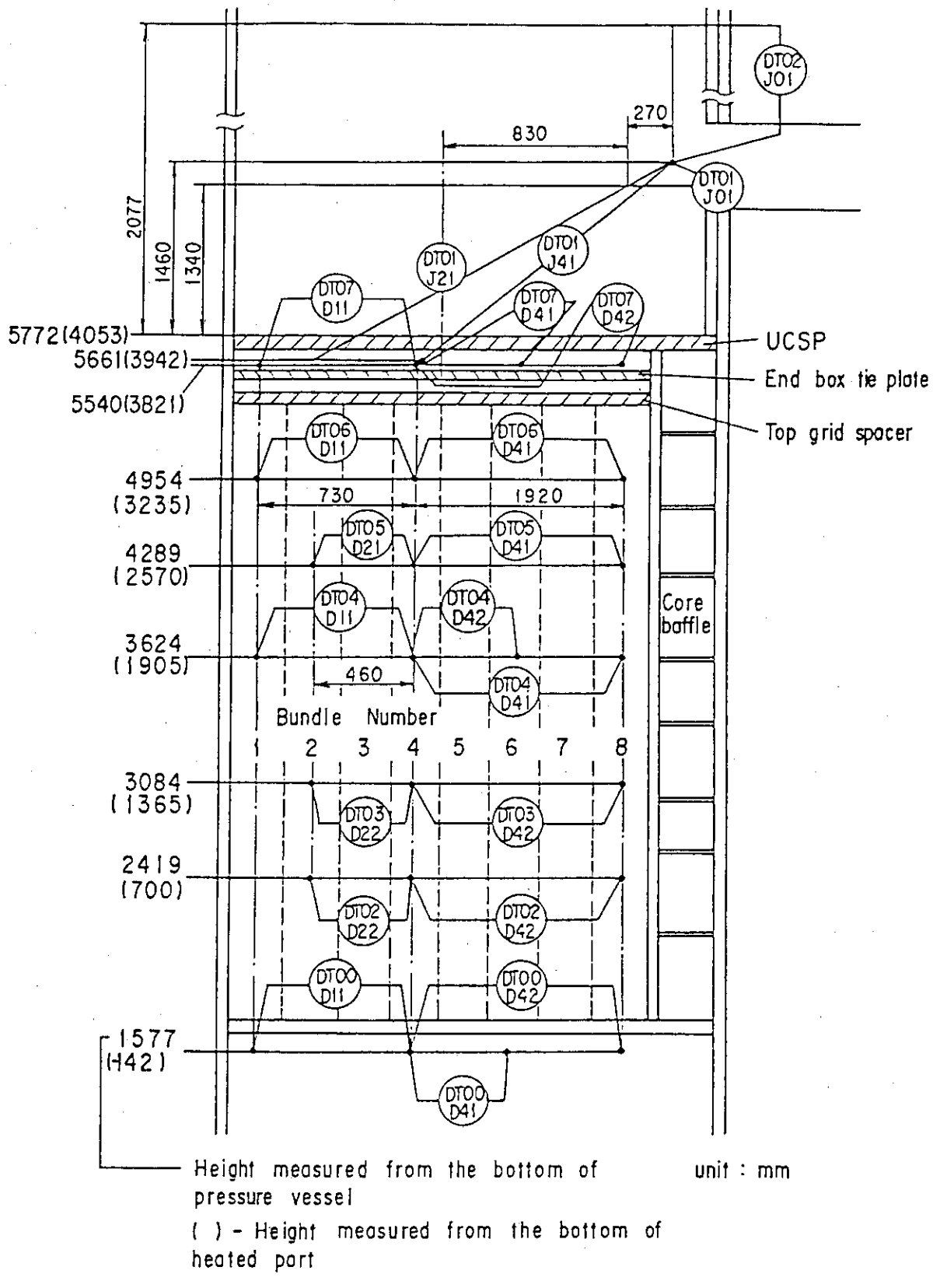

Fig. A-35 Locations of Horizontal Differential Pressure Measurements in Core and Differential Pressure Measurements between End Boxes and Inlet of Hot Leg

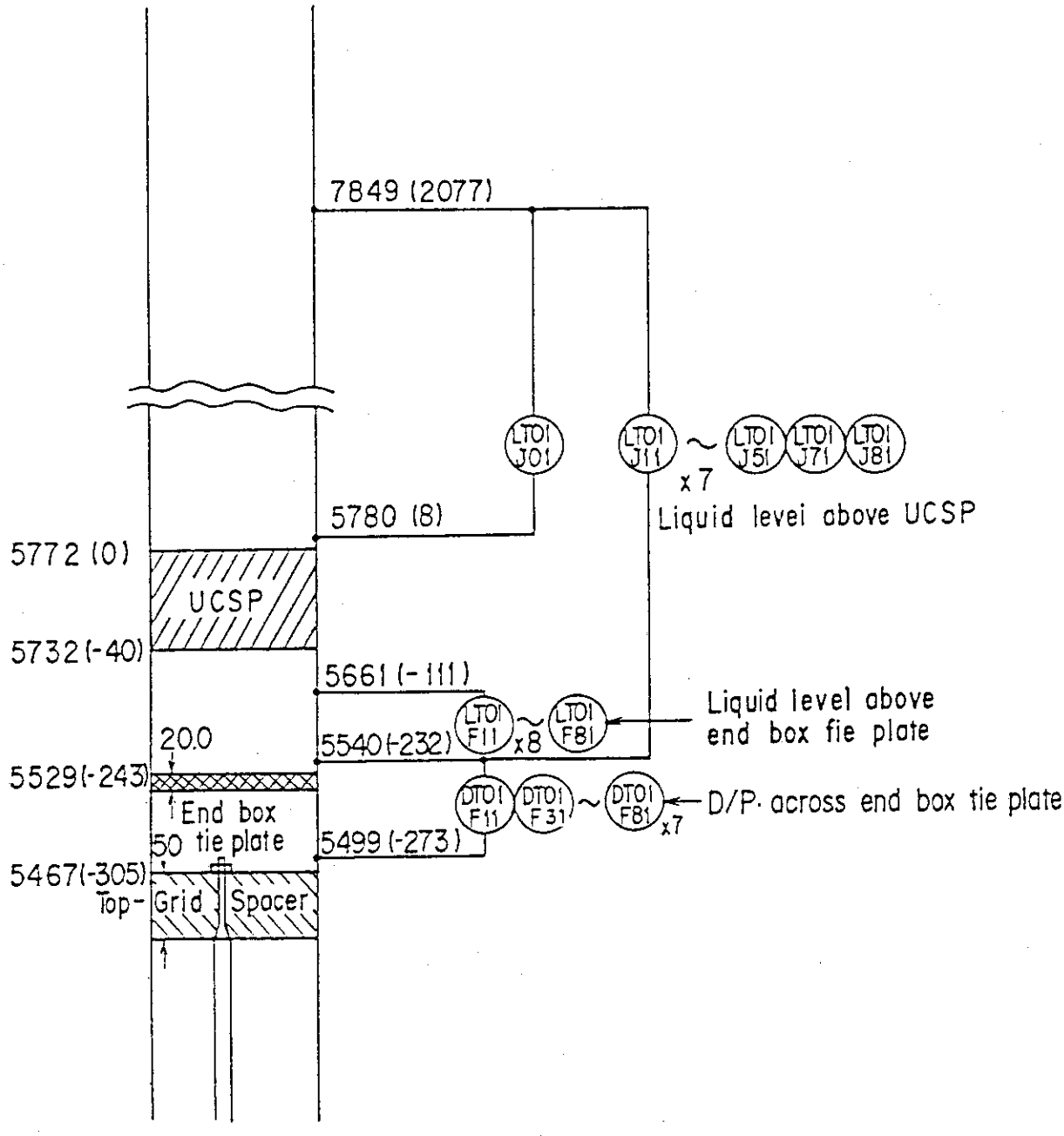

Fig. A-36 Locations of Differential Pressure Measurements across End Box Tie Plate

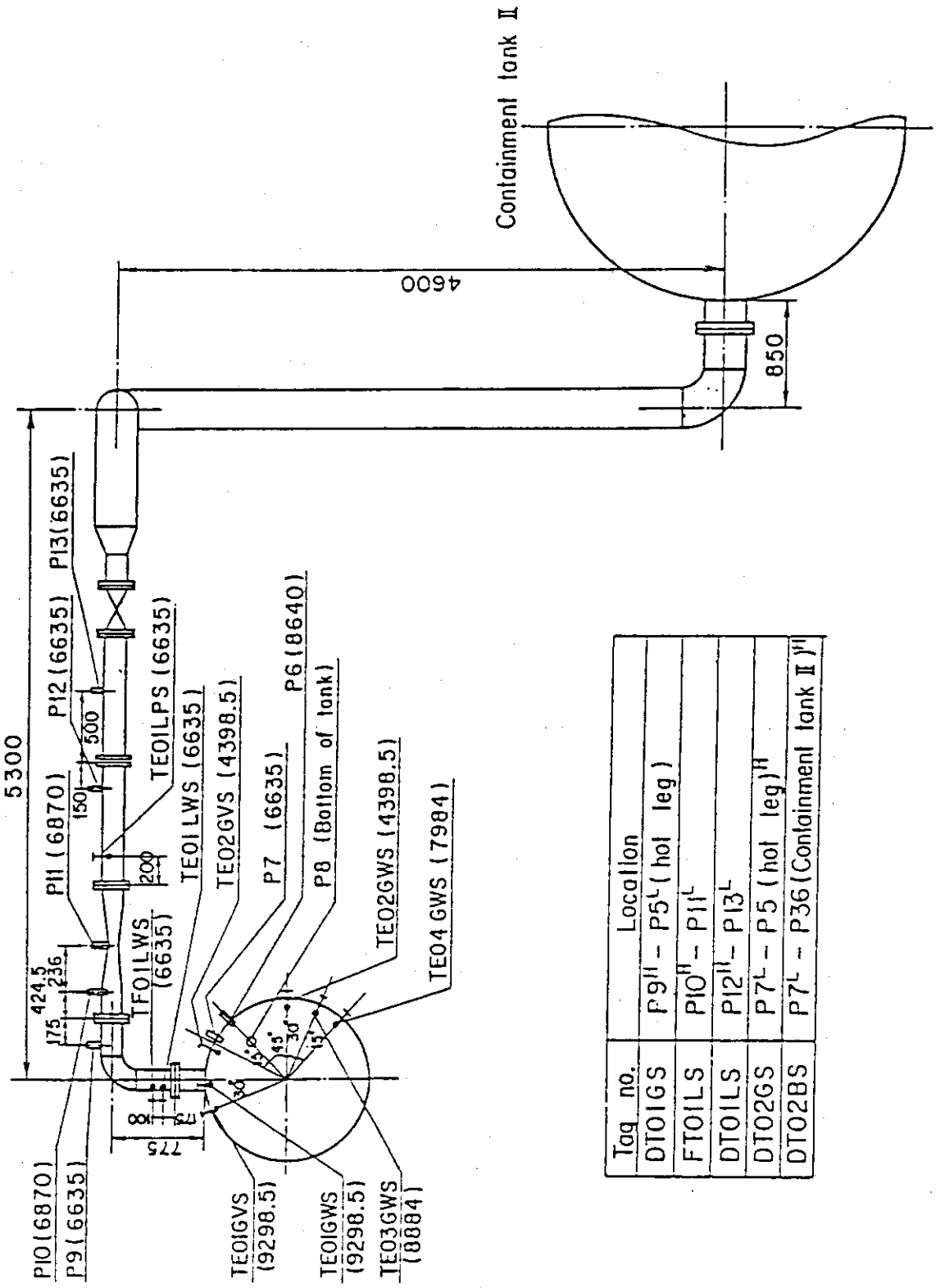

Tag no.	Location
DT01GS	$P9^{H}$ – $P5^{L}$ (hot leg)
FT01LS	$P10^{H}$ – $P11^{L}$
DT01LS	$P12^{H}$ – $P13^{L}$
DT02GS	$P7^{L}$ – P5 (hot leg)^{H}
DT02BS	$P7^{L}$ – P36 (Containment tank II)^{H}

Fig. A-37 Locations of Broken Cold Leg Instruments (Steam-Water Separator Side)

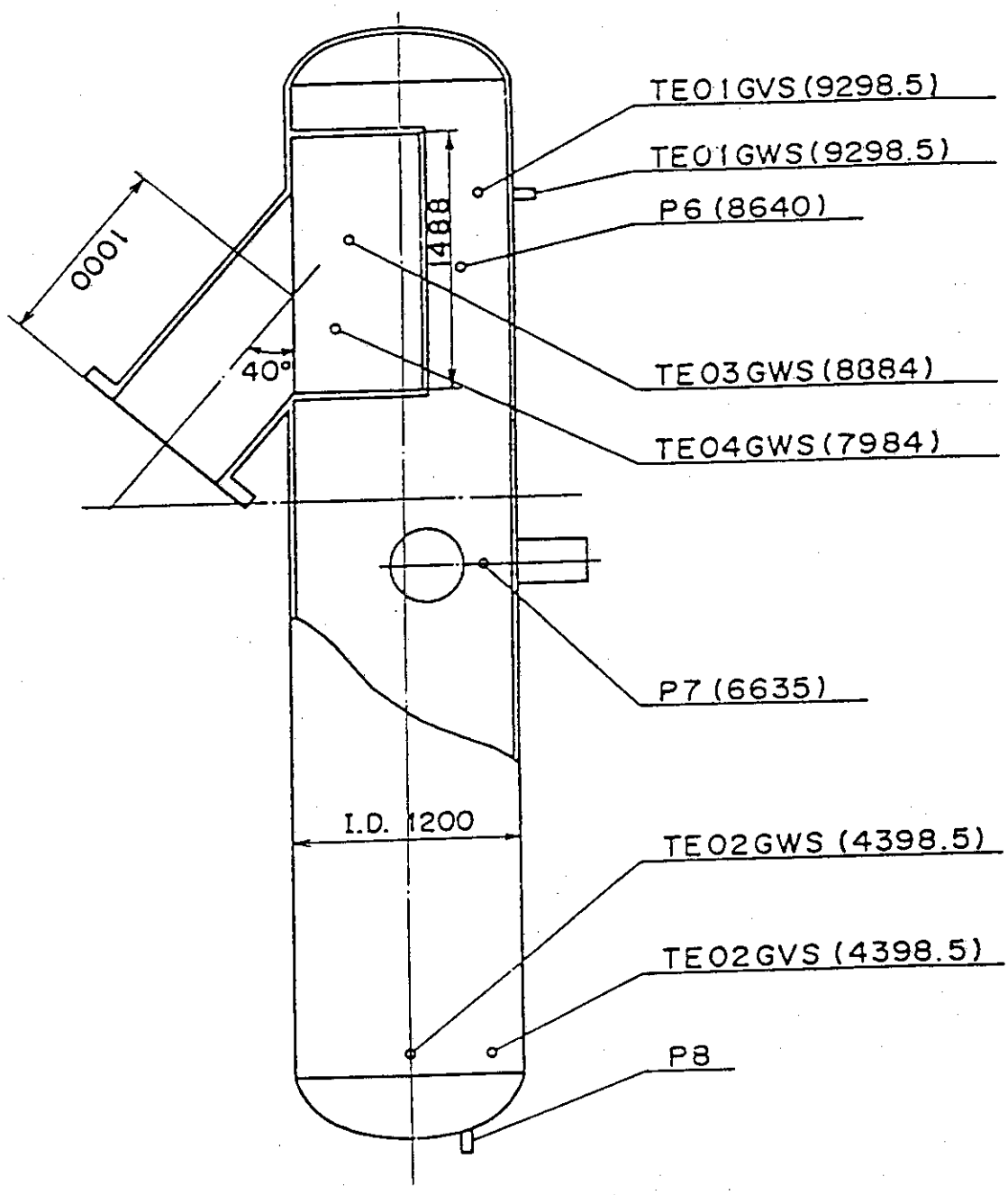

Fig. A-38 Locations of Steam-Water Separator Instruments

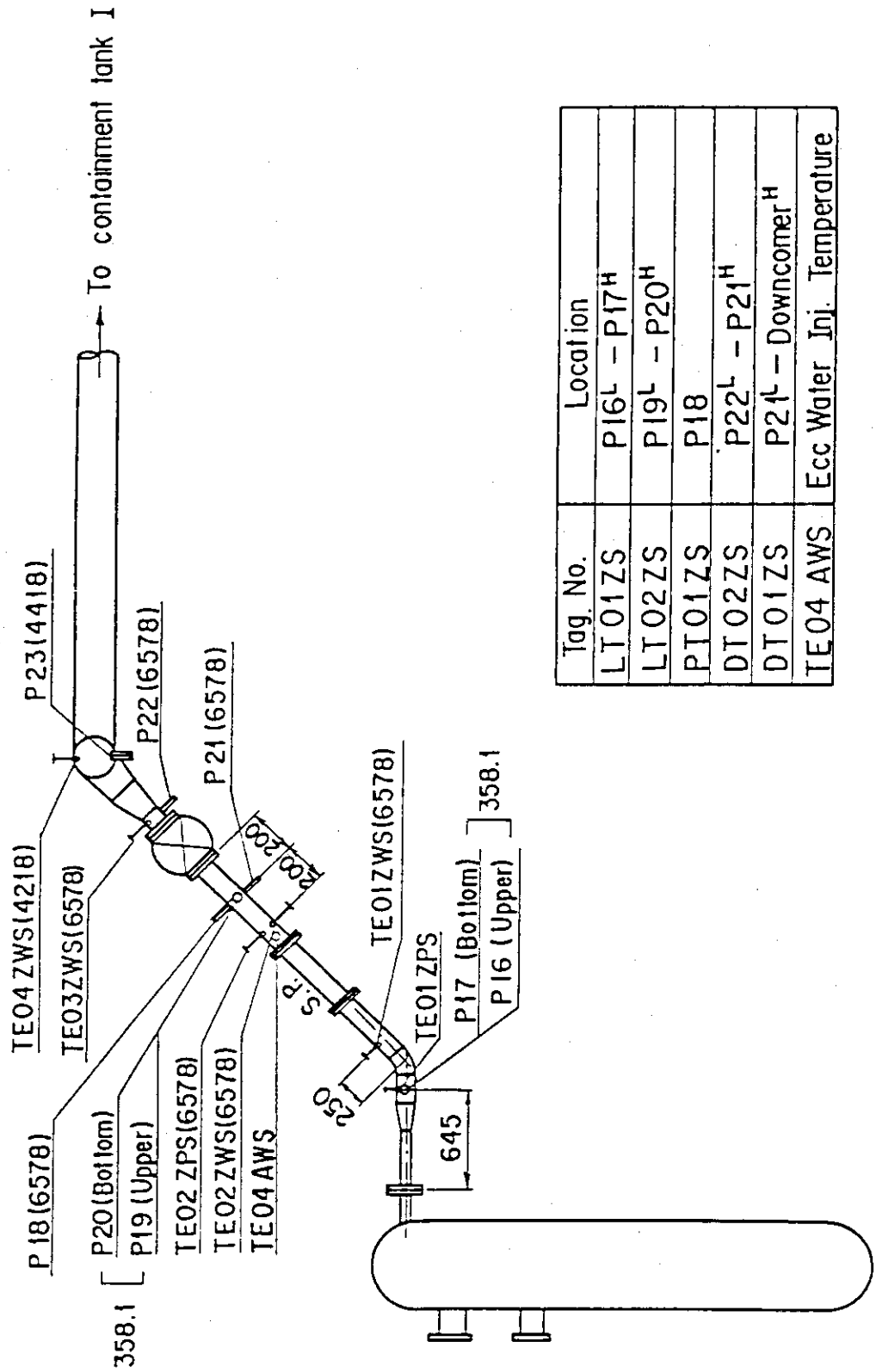

Fig. A-39 Locations of Broken Cold Leg Instruments
(Pressure Vessel Side)

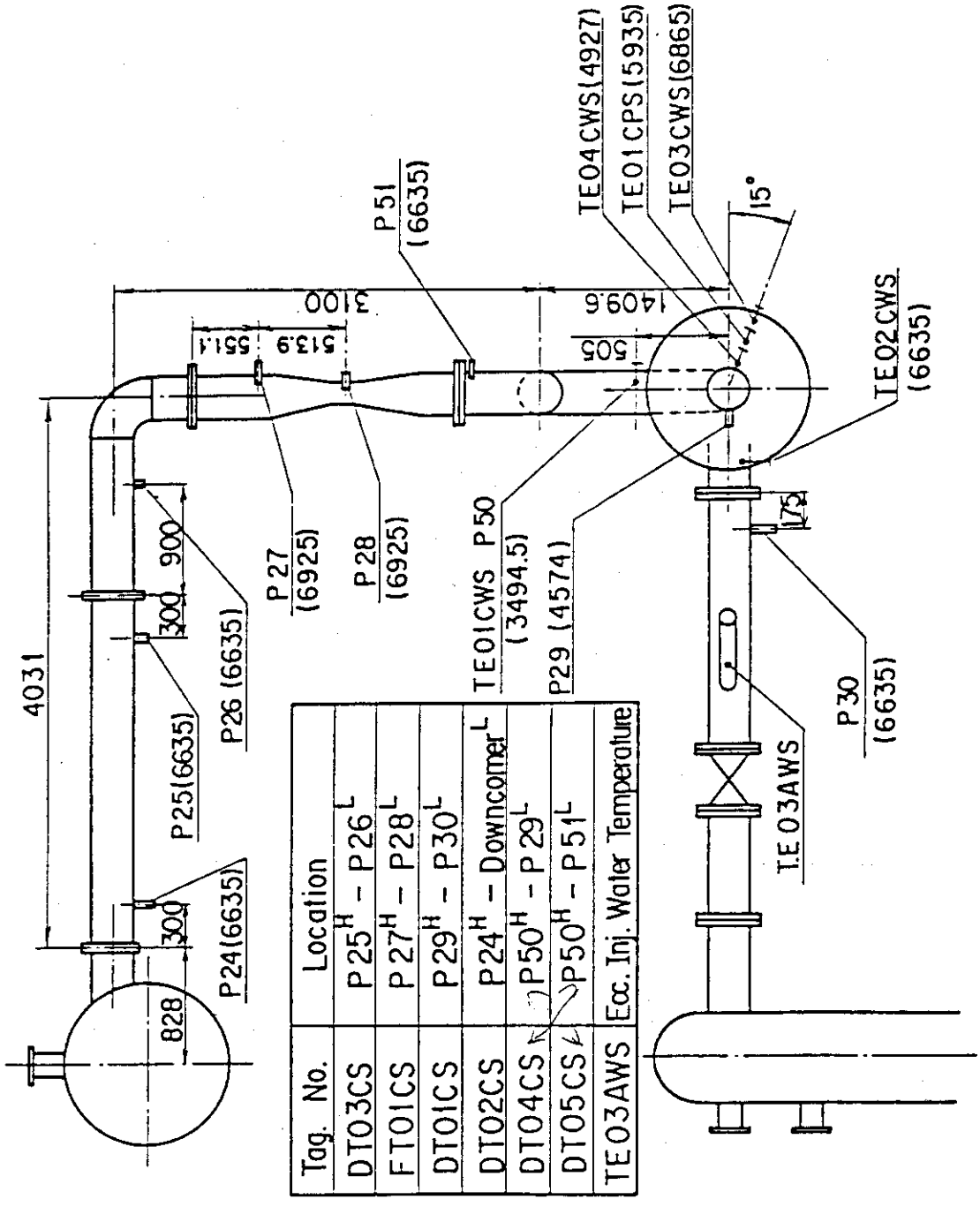

Tag. No.	Location
DT03CS	$P25^{H} - P26^{L}$
FT01CS	$P27^{H} - P28^{L}$
DT01CS	$P29^{H} - P30^{L}$
DT02CS	$P24^{H}$ – Downcomer^{L}
DT04CS	$P50^{H} - P29^{L}$
DT05CS	$P50^{H} - P51^{L}$
TE03AWS	Ecc. Inj. Water Temperature

Fig. A-40 Locations of Intact Cold Leg Instruments

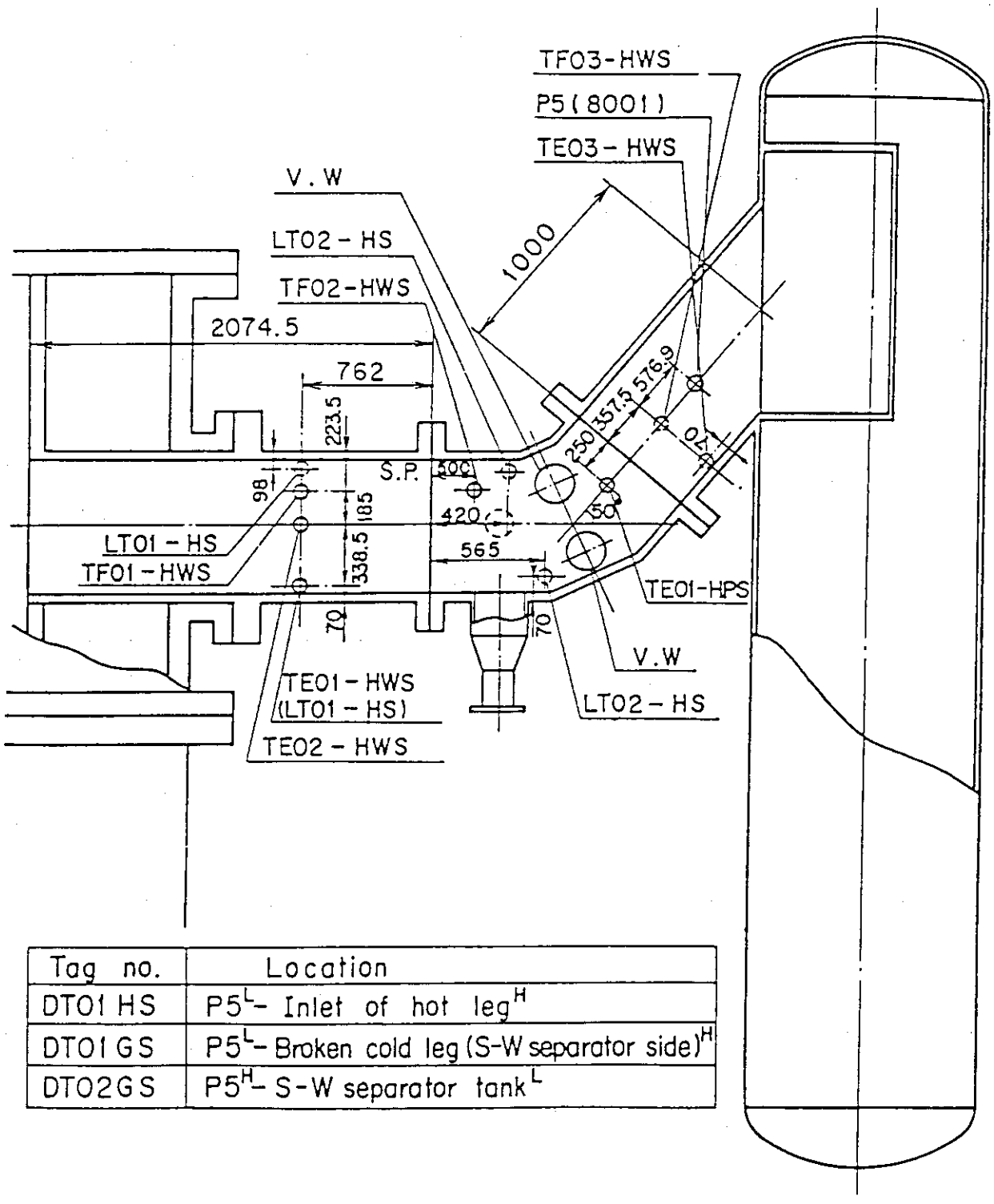

Tag no.	Location
DT01 HS	$P5^{L}$- Inlet of hot leg^{H}
DT01 GS	$P5^{L}$- Broken cold leg (S-W separator side)^{H}
DT02 GS	$P5^{H}$- S-W separator tank^{L}

Fig. A-41 Locations of Hot Leg Instruments

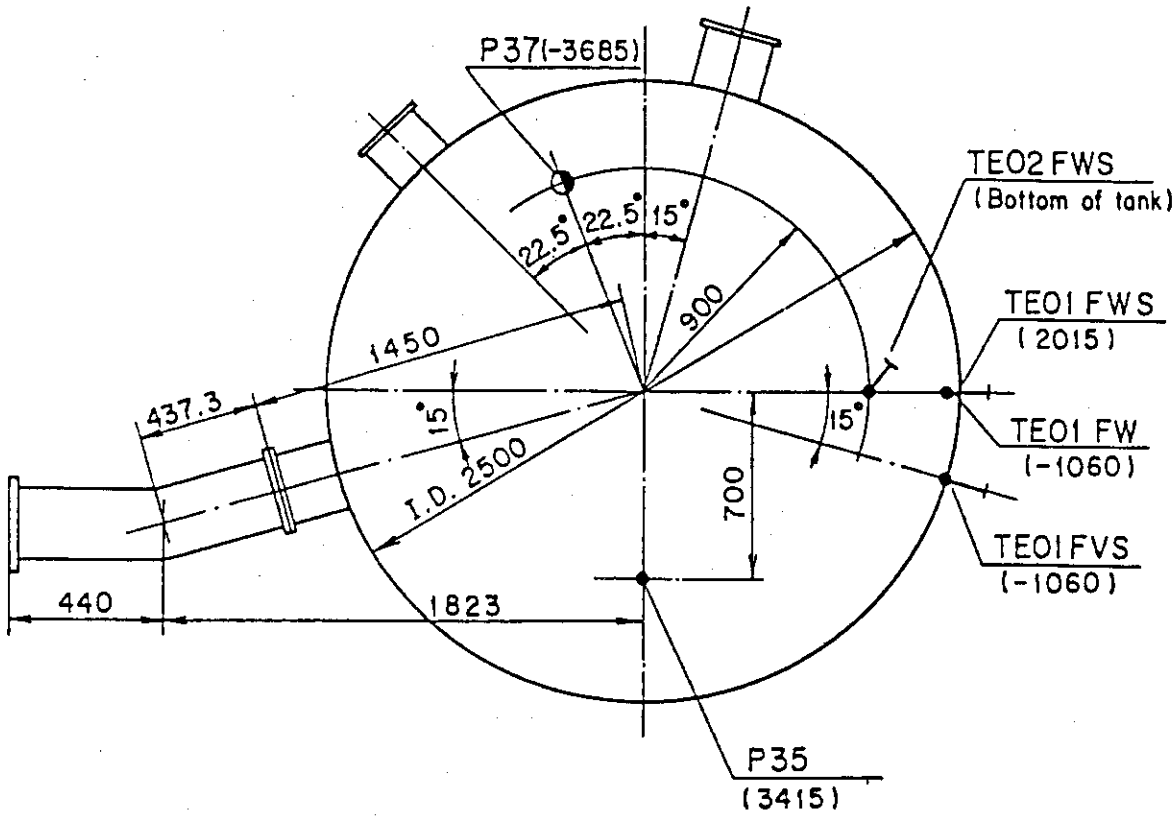

Tag. no.	Location
LT01 FS	$P35^{L}$ – $P37^{H}$
DT01 FS	$P35^{H}$ – $Downcomer^{L}$
DT01 E	$P35^{L}$ – P36(C.T. II)^{H}
PT01 F	P35

Fig. A-42 Locations of Containment Tank-I Instruments

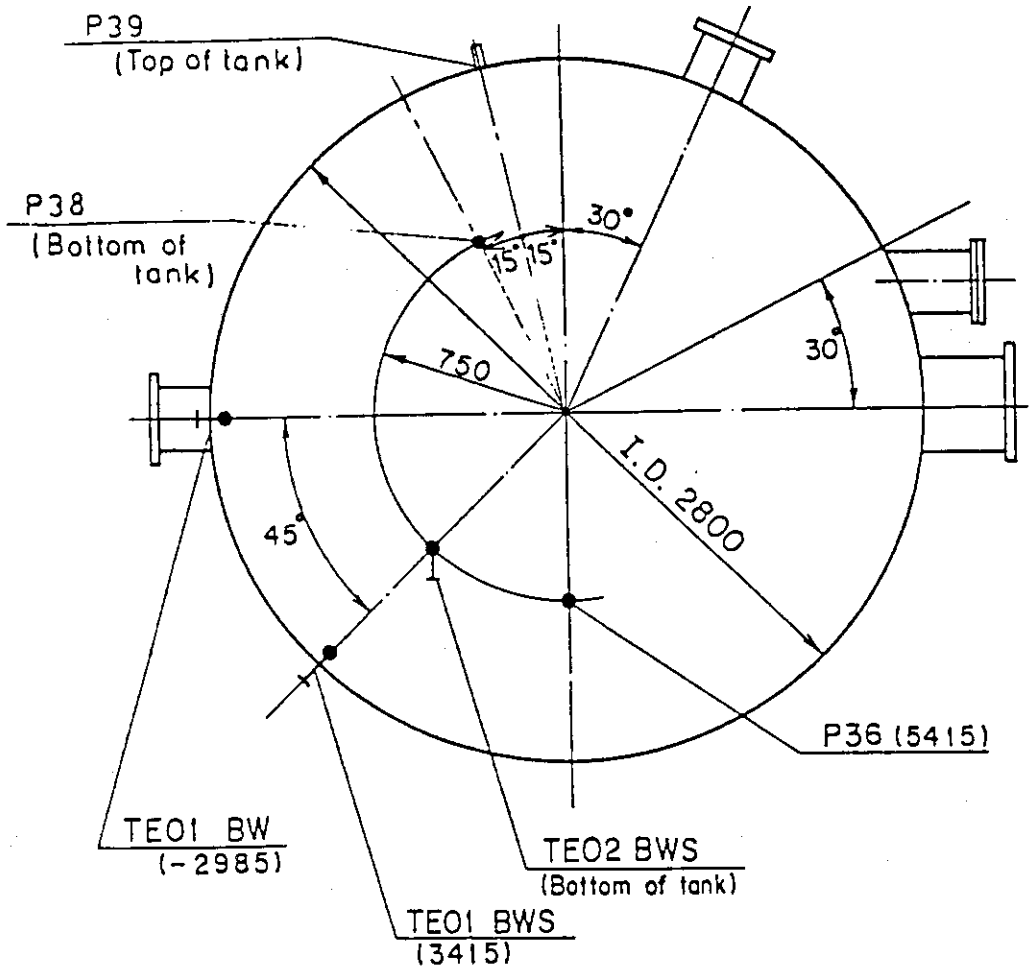

Tag no.	Location
DT01 BS	$P36^{H}$－ Upper plenum^{L}
DT02 BS	$P36^{H}$－ S-W Separator^{L}
DT01 E	$P36^{H}$－ P35 (C.T.I)^{L}
PT01 B	P36
LT01 1B	$P38^{H}$－ $P39^{L}$

Fig. A-43 Locations of Containment Tank-II Instruments

Appendix B Selected Data of Test S3-06

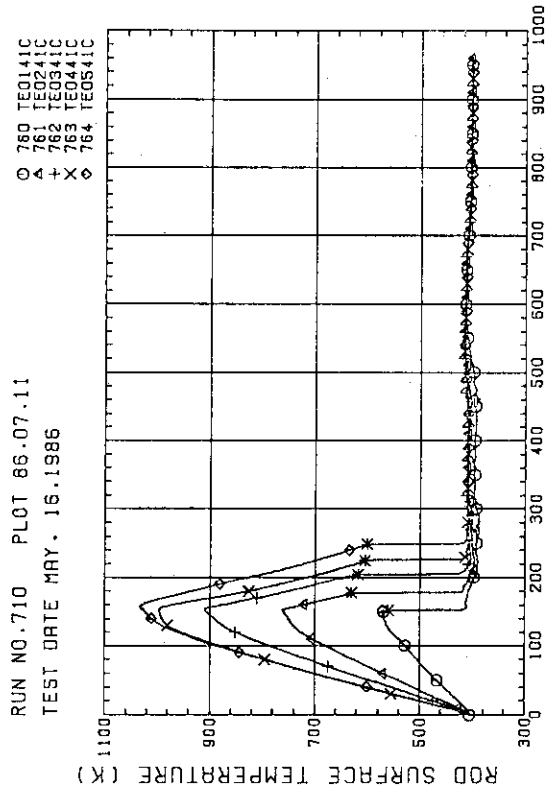

Fig. B-1 HEATER ROD TEMPERATURE (BUNDLE 2-1C, LOWER HALF)

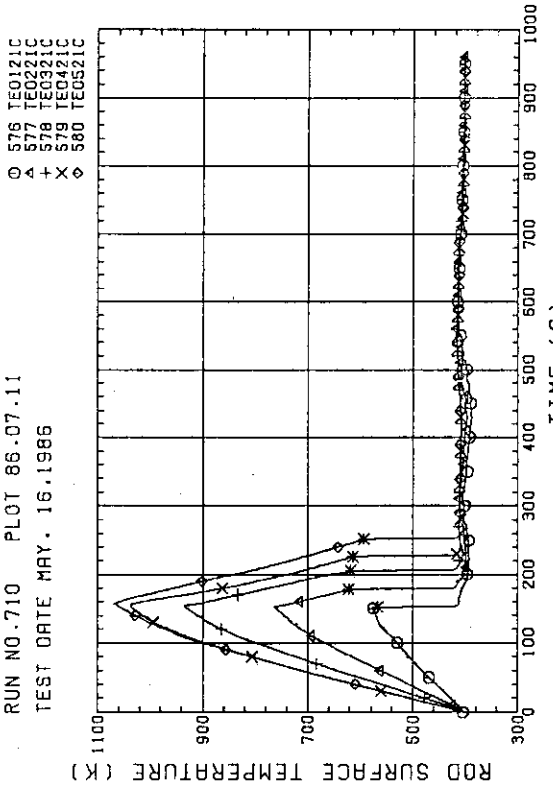

Fig. B-2 HEATER ROD TEMPERATURE (BUNDLE 2-1C, UPPER HALF)

Fig. B-3 HEATER ROD TEMPERATURE (BUNDLE 4-1C, LOWER HALF)

Fig. B-4 HEATER ROD TEMPERATURE (BUNDLE 4-1C, UPPER HALF)

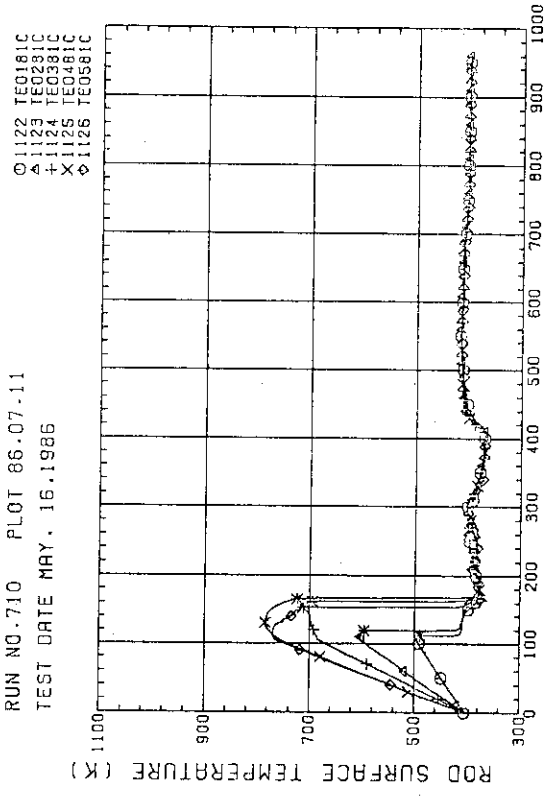

Fig. B-5 HEATER ROD TEMPERATURE (BUNDLE 6-1C, LOWER HALF)

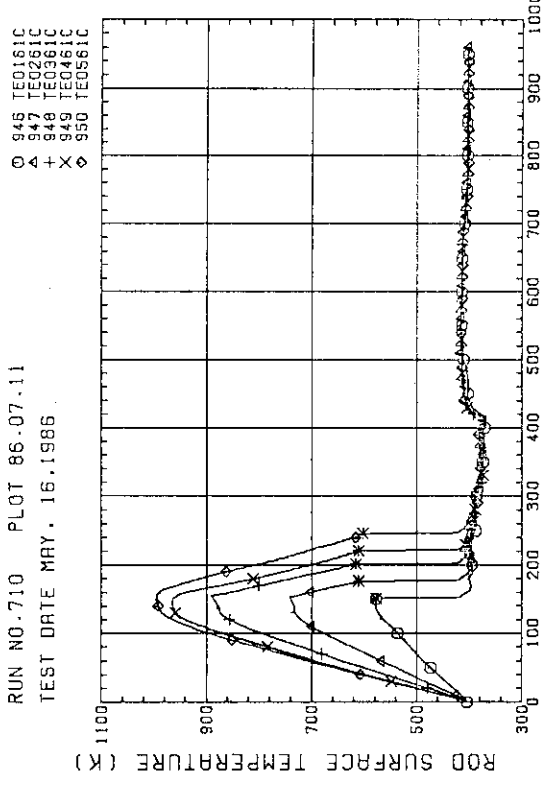

Fig. B-6 HEATER ROD TEMPERATURE (BUNDLE 6-1C, UPPER HALF)

Fig. B-7 HEATER ROD TEMPERATURE (BUNDLE 8-1C, LOWER HALF)

Fig. B-8 HEATER ROD TEMPERATURE (BUNDLE 8-1C, UPPER HALF)

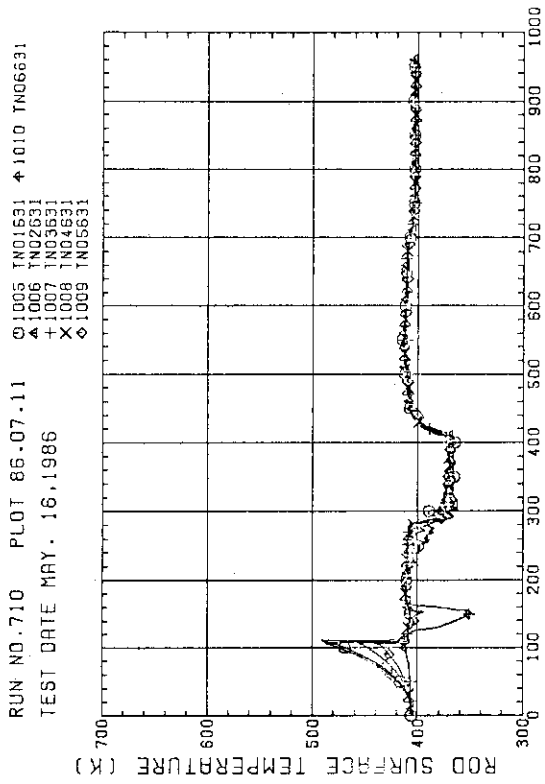

Fig. B-9 NON-HEATED ROD TEMPERATURE (BUNDLE 2-31)

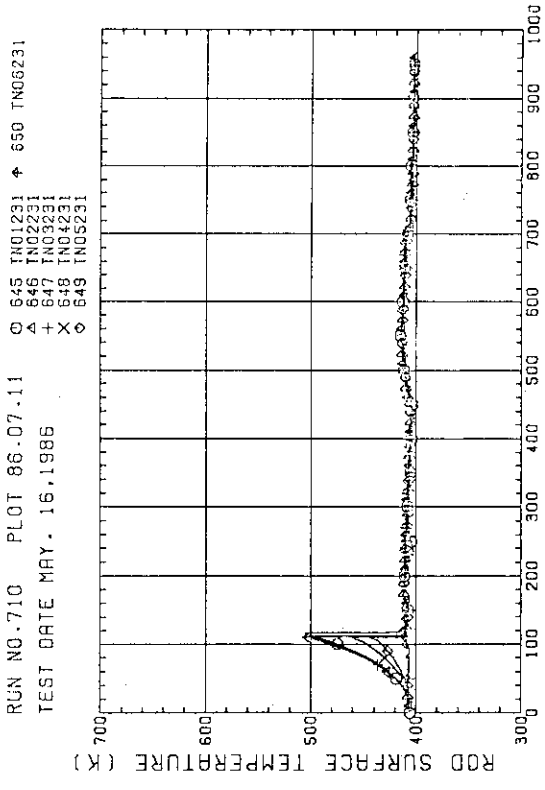

Fig. B-10 NON-HEATED ROD TEMPERATURE (BUNDLE 4-31)

Fig. B-11 NON-HEATED ROD TEMPERATURE (BUNDLE 6-31)

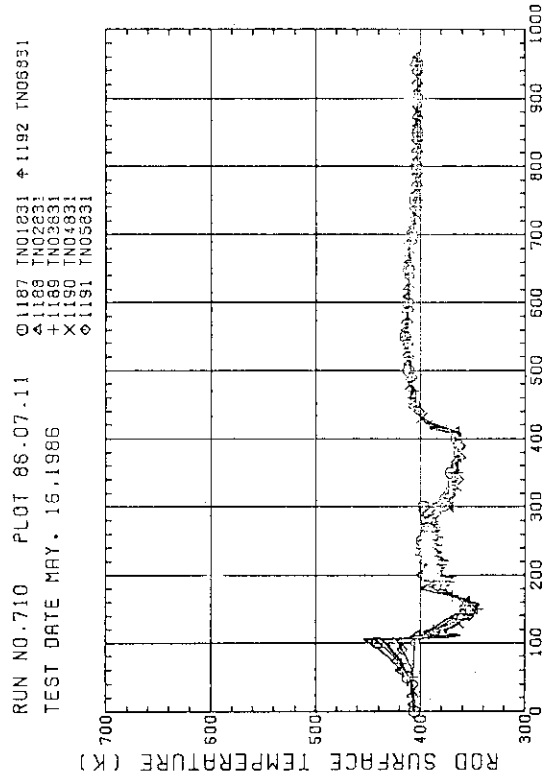

Fig. B-12 NON-HEATED ROD TEMPERATURE (BUNDLE 8-31)

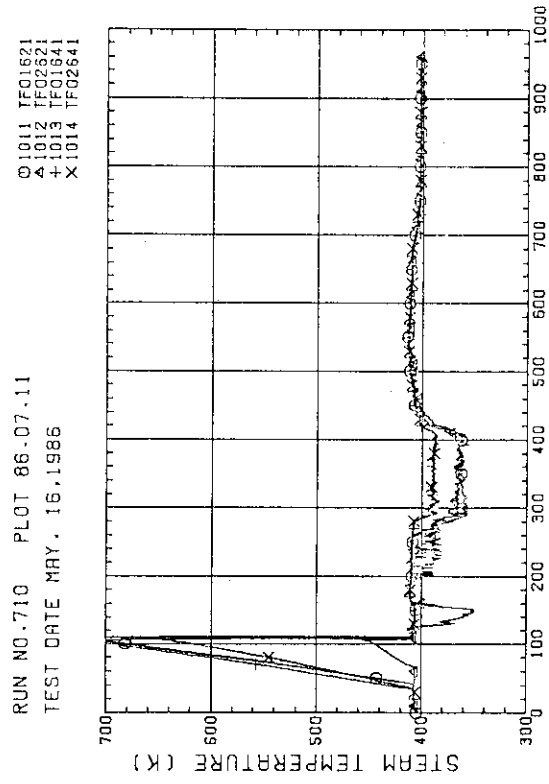

Fig. B-13 STEAM TEMPERATURE IN CORE, BUNDLE 2

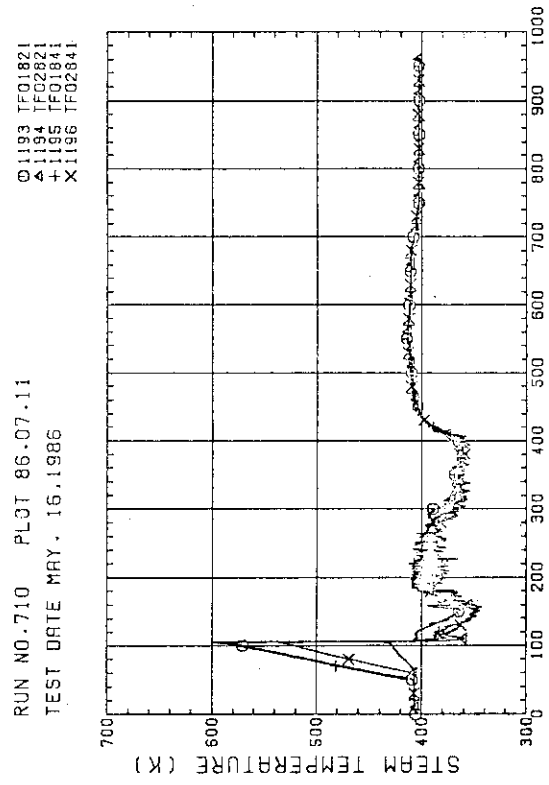

Fig. B-14 STEAM TEMPERATURE IN CORE, BUNDLE 4

Fig. B-15 STEAM TEMPERATURE IN CORE, BUNDLE 6

Fig. B-16 STEAM TEMPERATURE IN CORE, BUNDLE 8

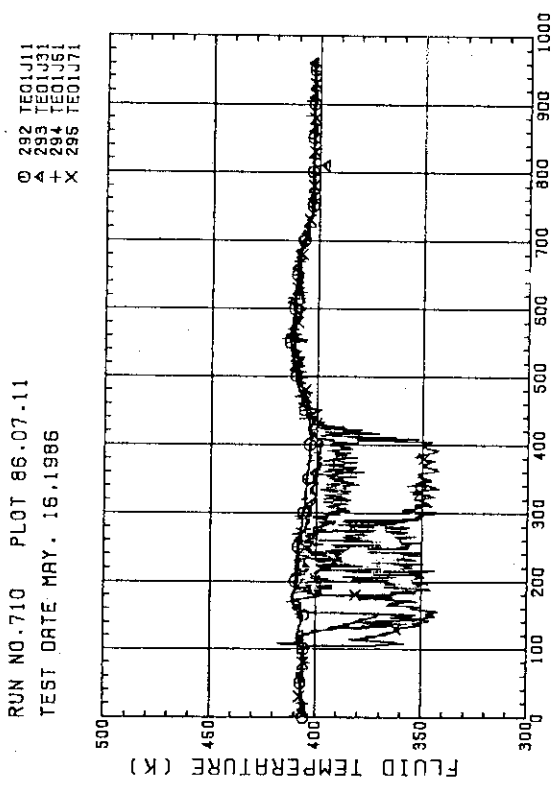

Fig. B-19 FLUID TEMPERATURE ABOVE UCSP (BUNDLE 1,3,5,7, 100MM ABOVE UCSP)

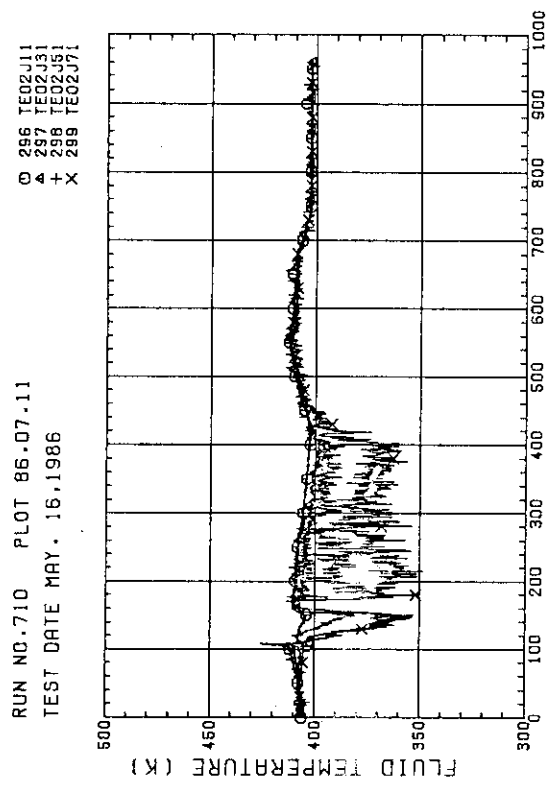

Fig. B-20 FLUID TEMPERATURE ABOVE UCSP (BUNDLE 1,3,5,7, 250MM ABOVE UCSP)

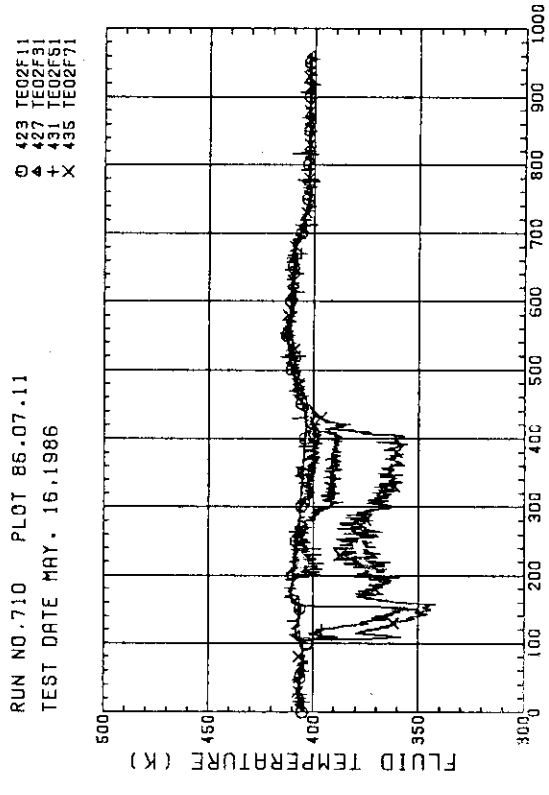

Fig. B-17 FLUID TEMPERATURE JUST ABOVE END BOX TIE PLATE (BUNDLE 1,3,5,7, OPPOSITE SIDE OF COLD LEG, OUTER)

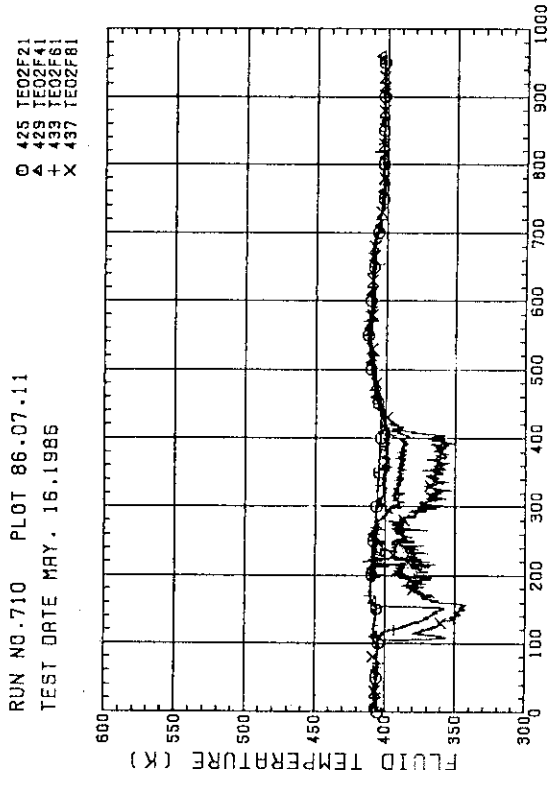

Fig. B-18 FLUID TEMPERATURE JUST ABOVE END BOX TIE PLATE (BUNDLE 2,4,6,8, COLD LEG SIDE, OUTER)

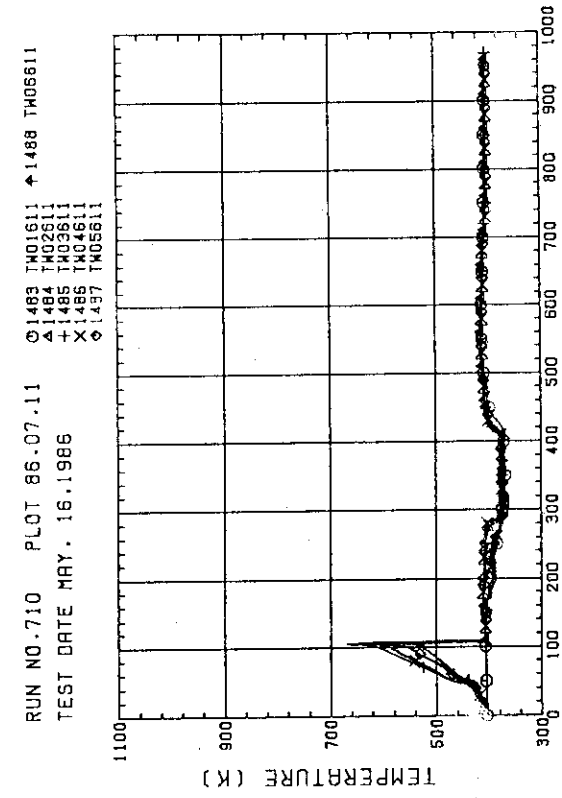

Fig. B-23 TEMPERATURE FOR SPUTTERING DETECTION BUNDLE 6 , REGION 1 , TYPE 1 3

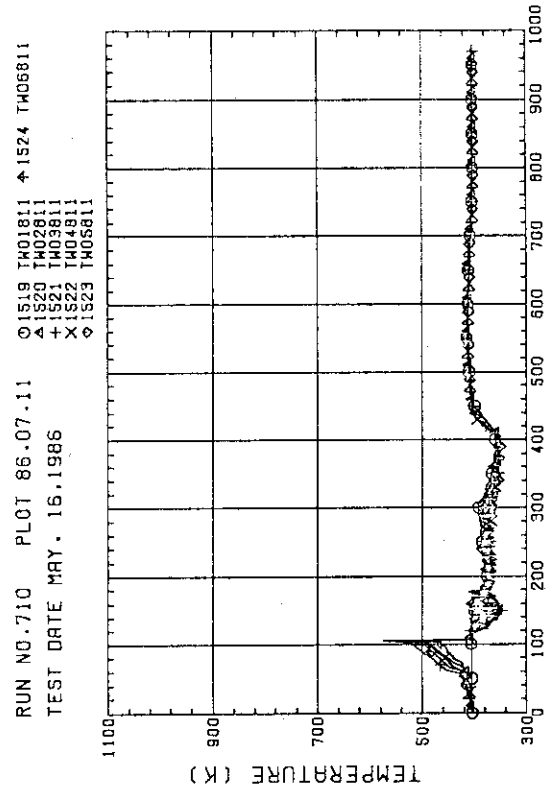

Fig. B-24 TEMPERATURE FOR SPUTTERING DETECTION BUNDLE 8 , REGION 1 , TYPE 3

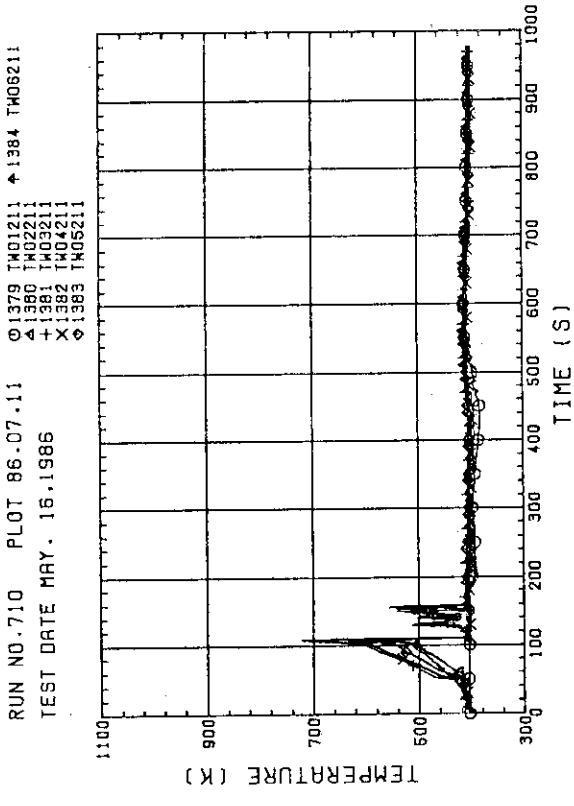

Fig. B-21 TEMPERATURE FOR SPUTTERING DETECTION BUNDLE 2 , REGION 1 , TYPE 3

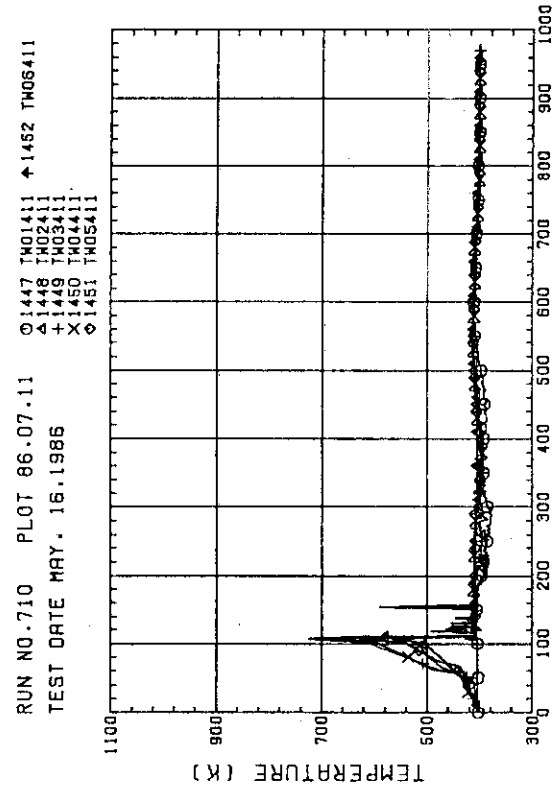

Fig. B-22 TEMPERATURE FOR SPUTTERING DETECTION BUNDLE 4 , REGION 1 , TYPE 3

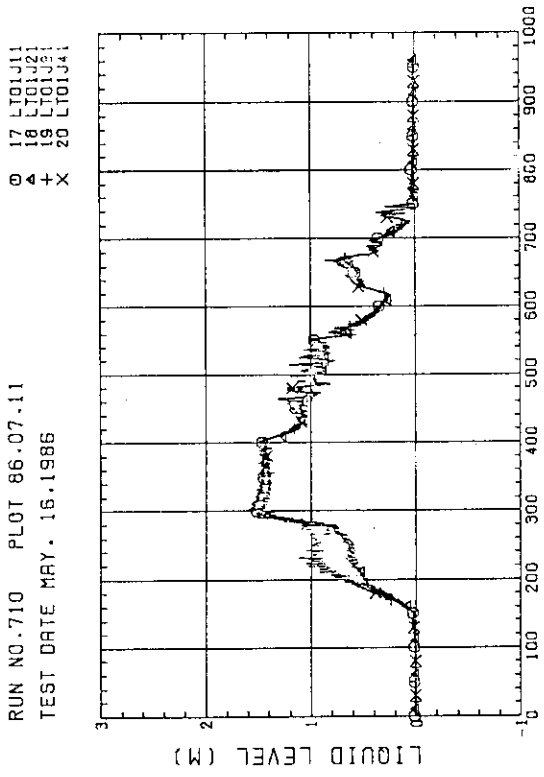

Fig. B-27 LIQUID LEVEL ABOVE UCSP (BUNDLE 1,2,3,4)

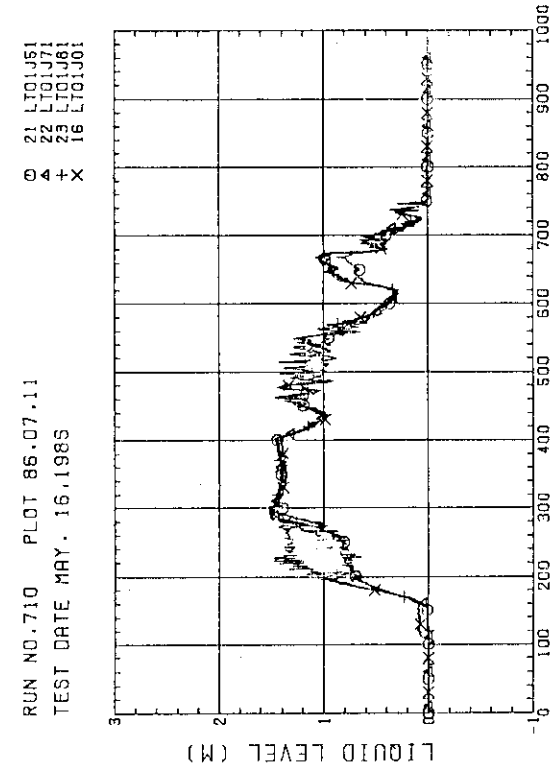

Fig. B-28 LIQUID LEVEL ABOVE UCSP (BUNDLE 5,6,7,8 AND CORE BAFFLE)

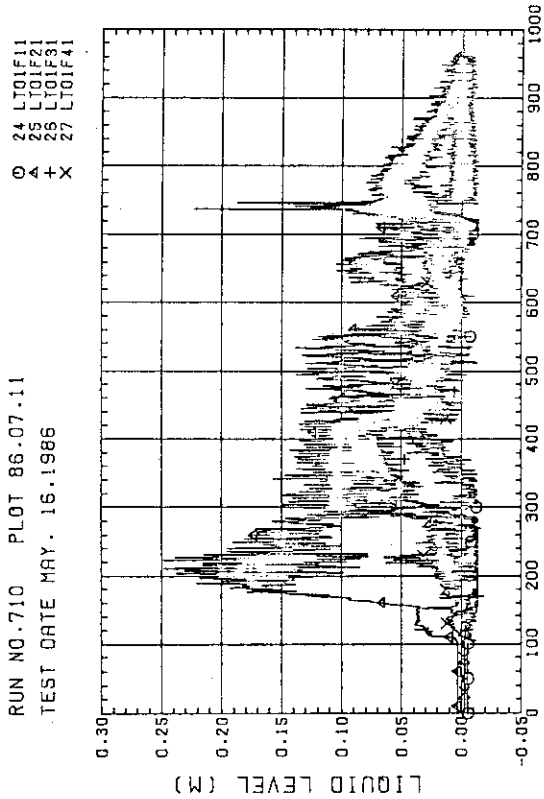

Fig. B-25 LIQUID LEVEL ABOVE END BOX TIE PLATE (BUNDLE 1,2,3,4)

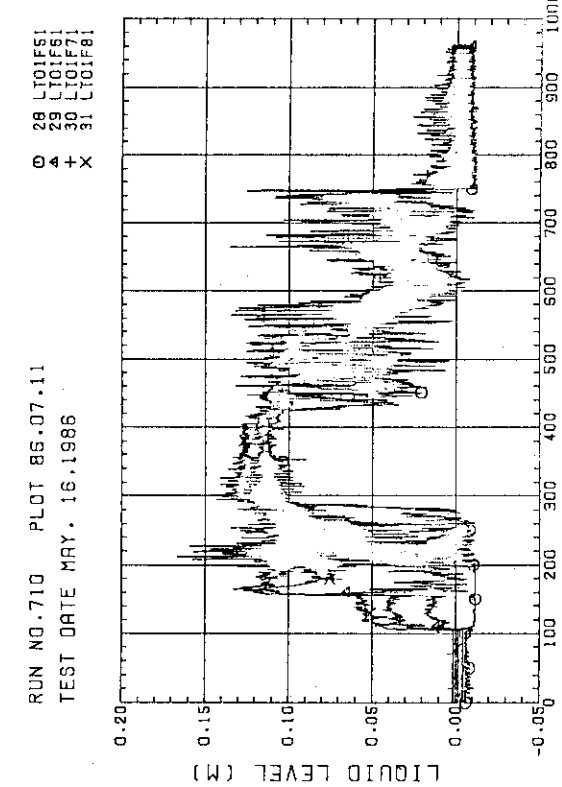

Fig. B-26 LIQUID LEVEL ABOVE END BOX TIE PLATE (BUNDLE 5,6,7,8)

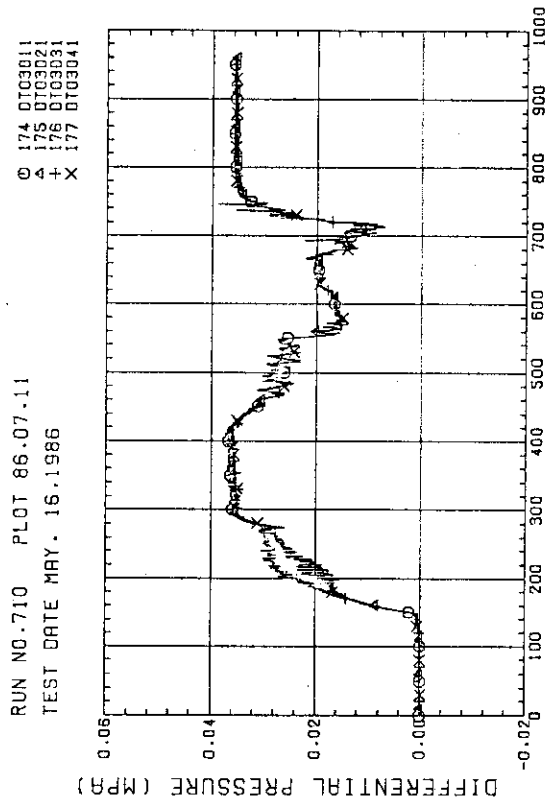

Fig. B-31 DIFFERENTIAL PRESSURE OF CORE FULL HIGHT (BUNDLE 1,2,3,4)

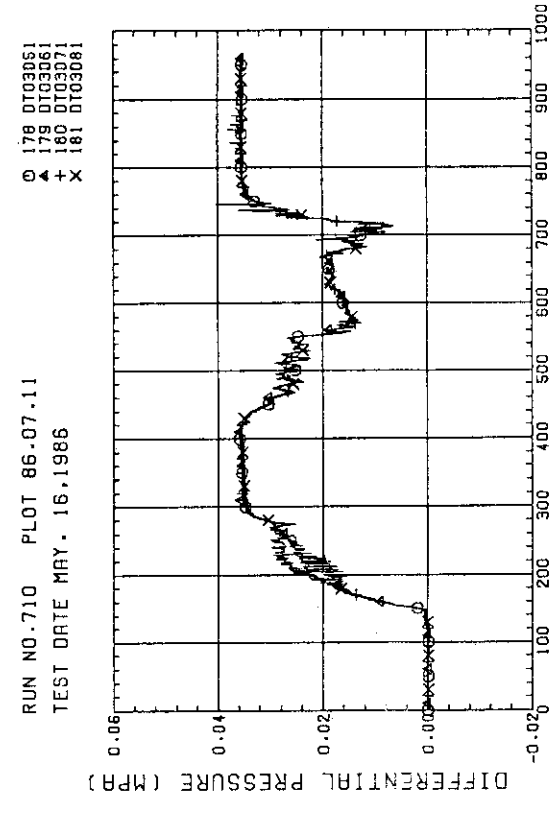

Fig. B-32 DIFFERENTIAL PRESSURE OF CORE FULL HEIGHT (BUNDLE 5,6,7,8)

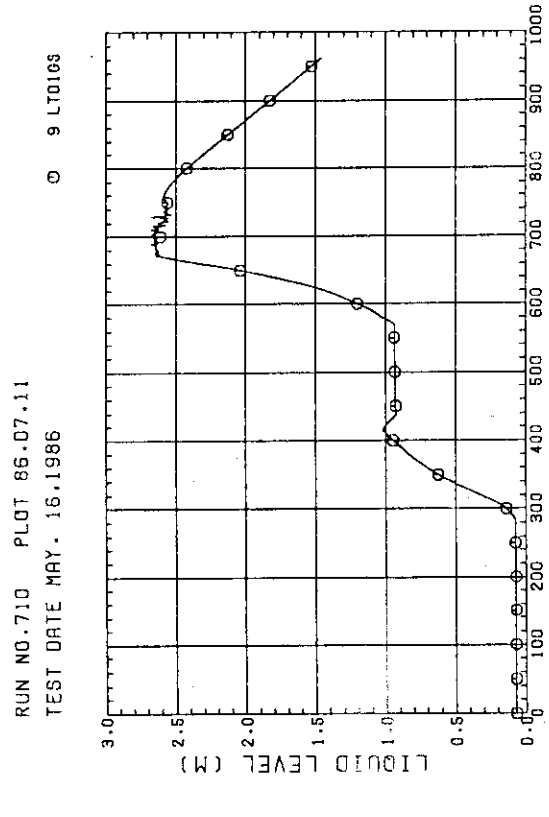

Fig. B-29 LIQUID LEVEL IN STEAM/WATER SEPARATOR

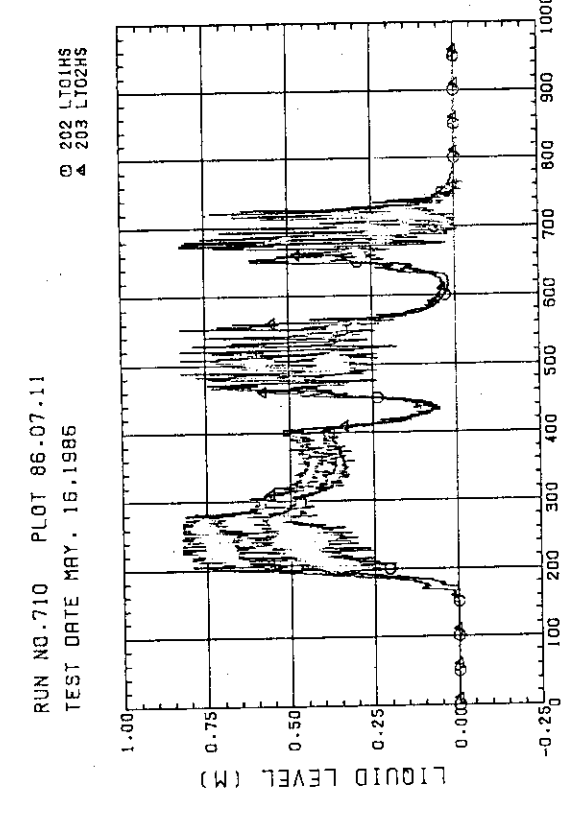

Fig. B-30 LIQUID LEVEL IN HOT LEG (01HS - PV SIDE, 02HS - STEAM/WATER SEPARATOR SIDE)

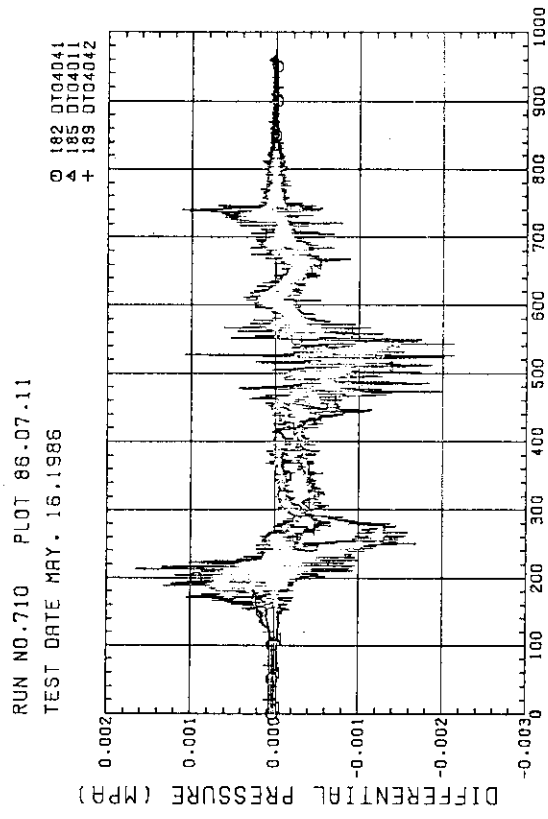

Fig. B-35 DIFFERENTIAL PRESSURE, HORIZONTAL AT 1905 MM (11-BUNDLE 1-4, 41-BUNDLE 4-8, 42-BUNDLE 4-6)

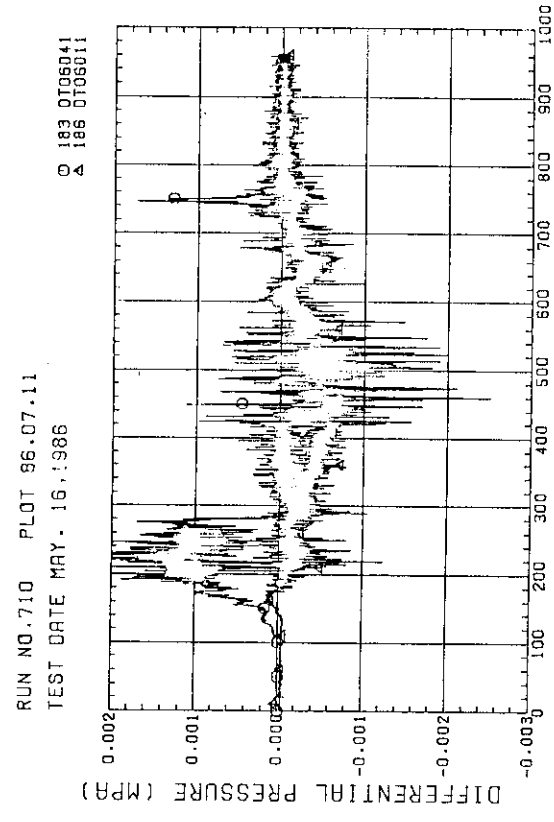

Fig. B-36 DIFFERENTIAL PRESSURE, HORIZONTAL AT 3235 MM (11-BUNDLE 1-4, 41-BUNDLE 4-8)

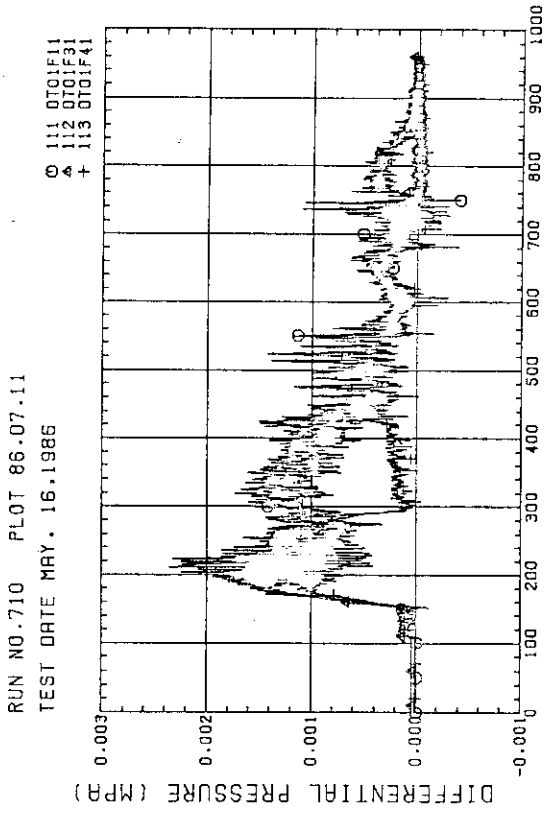

Fig. B-33 DIFFERENTIAL PRESSURE ACROSS END BOX TIE PLATE (BUNDLE 1,3,4)

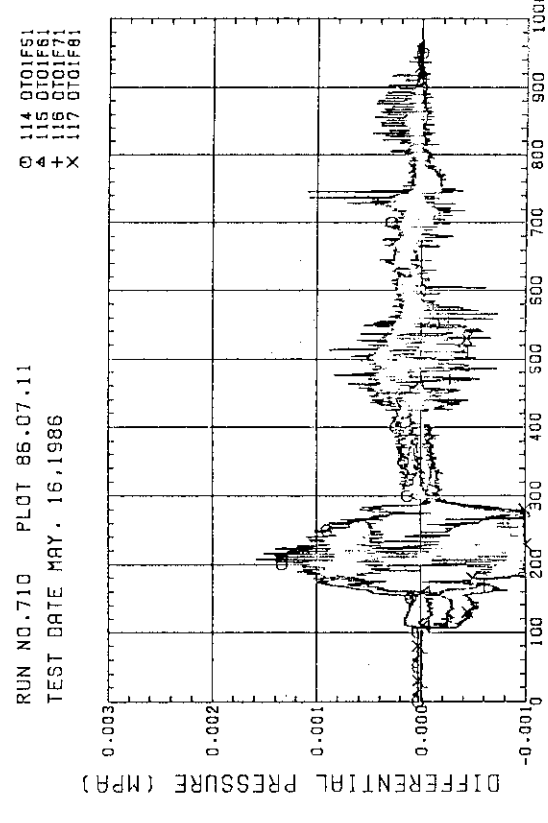

Fig. B-34 DIFFERENTIAL PRESSURE ACROSS END BOX TIE PLATE (BUNDLE 5,6,7,8)

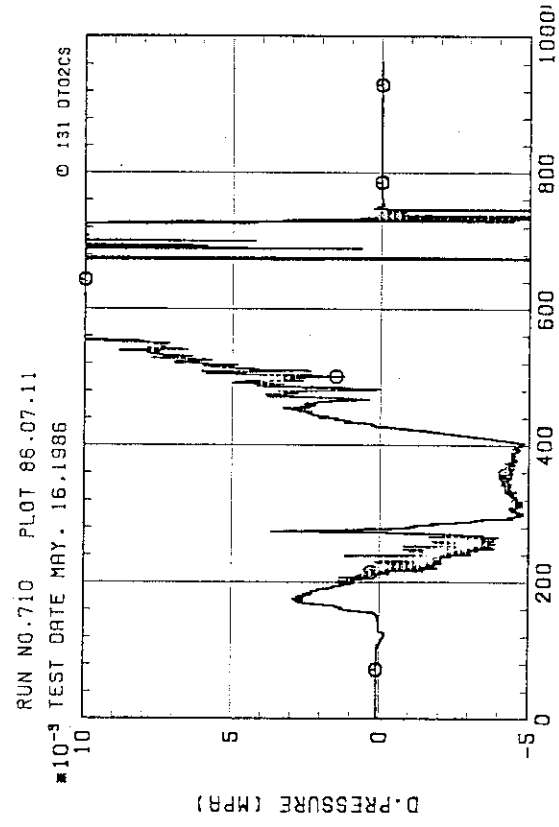

Fig. B-39 DIFFERENTIAL PRESSURE OF INTACT COLD LEG

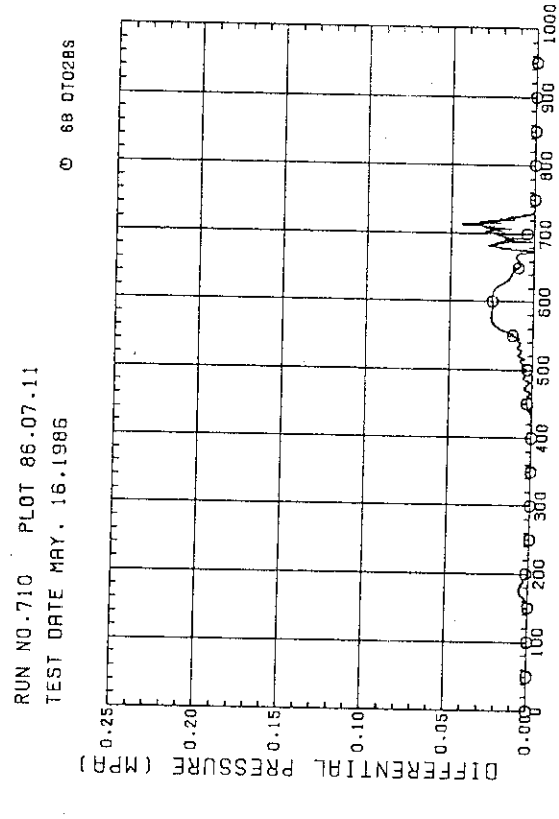

Fig. B-40 DIFFERENTIAL PRESSURE, STEAM/WATER SEPARATOR - CONTAINMENT TANK-II

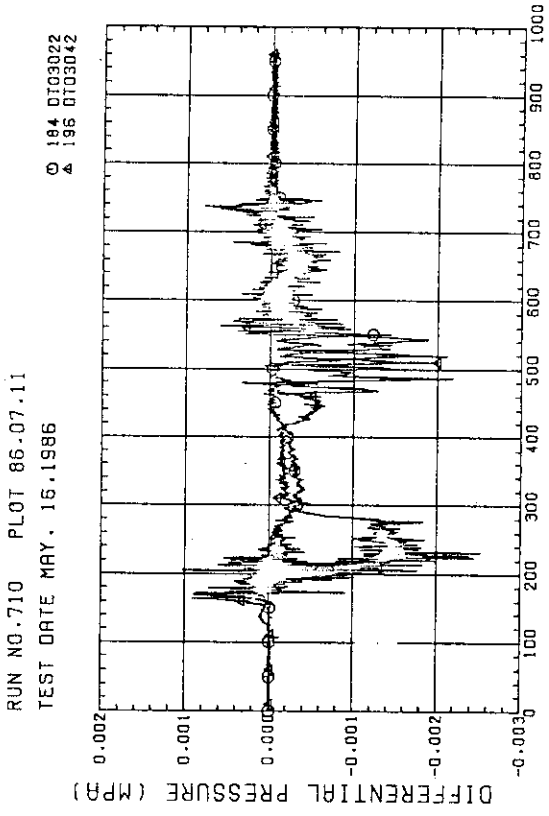

Fig. B-37 DIFFERENTIAL PREESURE, HORIZONTAL AT 1365 MM (22-BUNDLE 2-4, 42-BUNDLE 4-8)

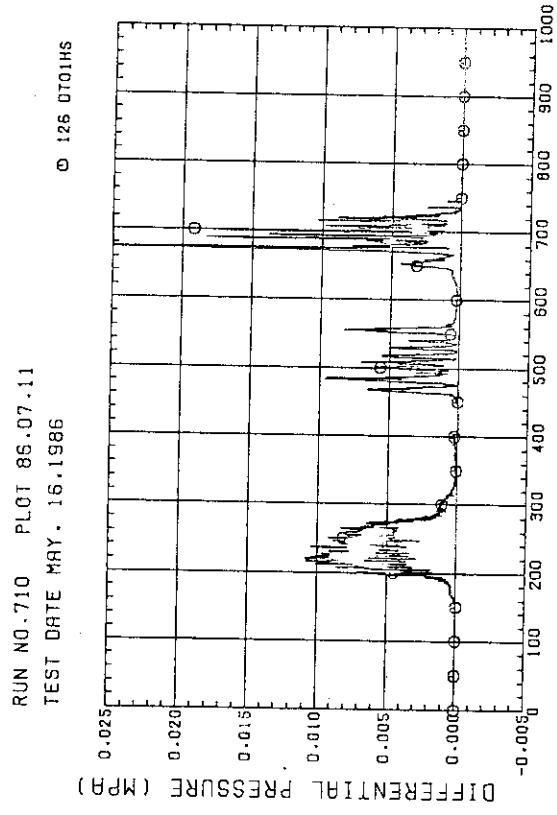

Fig. B-38 DIFFERENTIAL PRESSURE OF HOT LEG, HOT LEG INLET - STEAM/WATER SEPARATOR INLET

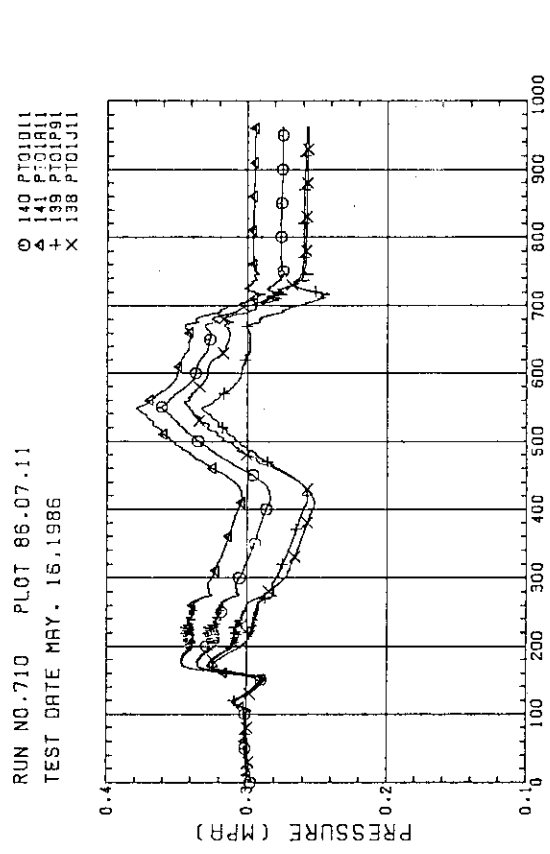

Fig. B-43 PRESSURE IN PV (J - TOP OF PV, D - CORE CENTER, A - CORE INLET, P - BELOW COLD LEG NOZZLE IN DOWNCOMER)

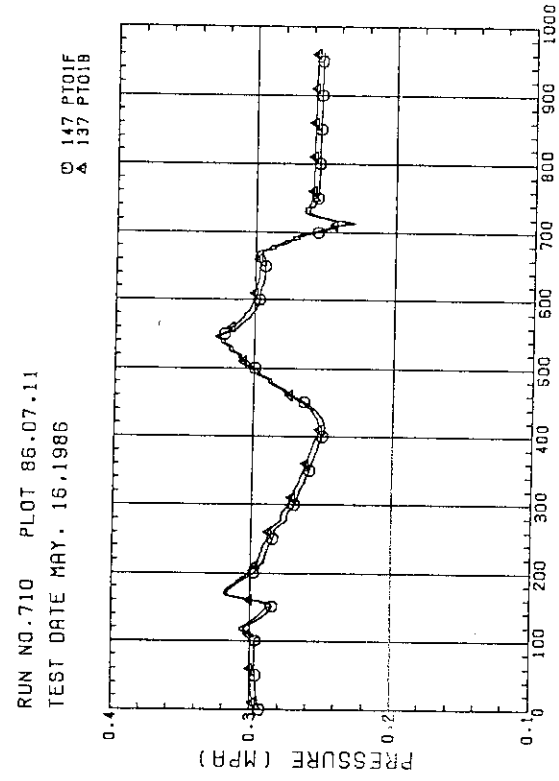

Fig. B-44 PRESSURE AT TOP OF CONTAINMENT TANK-I AND CONTAINMENT TANK-II (F-CONTAINMENT TANK-I, B-CONTAINMENT TANK-II)

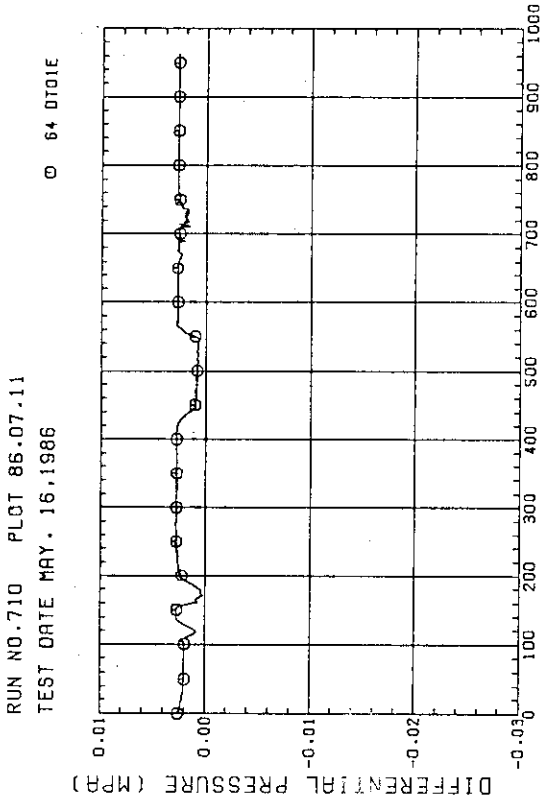

Fig. B-41 DIFFERENTIAL PRESSURE, CONTAINMENT TANK-II - CONTAINMENT TANK-I

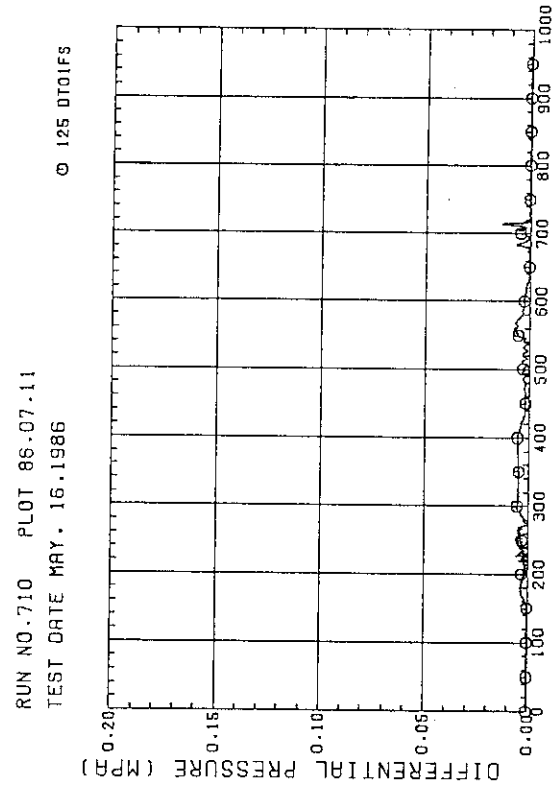

Fig. B-42 DIFFERENTIAL PRESSURE OF BROKEN COLD LEG - PV SIDE, DOWNCOMER - CONTAINMENT TANK-I

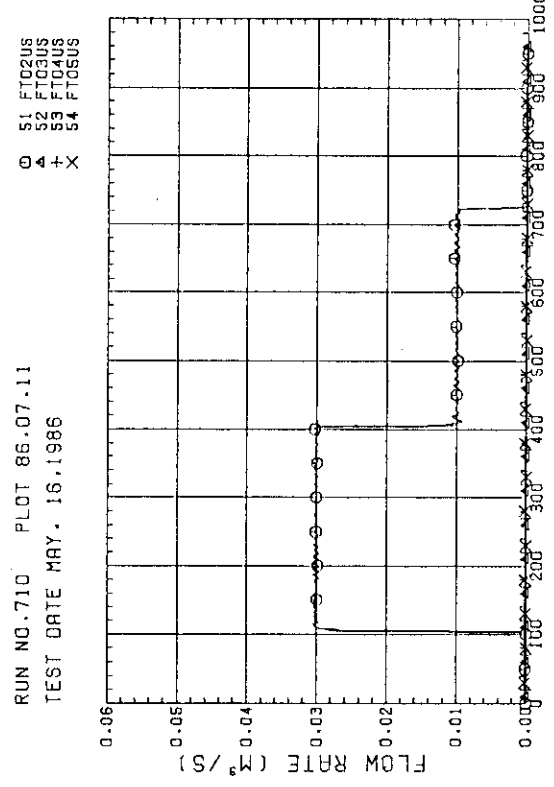

Fig. B-47 FLOW RATE OF UCSP INJECTION
LINE-1(BUNDLE7,8),LINE-2(5,6),LINE-3(3,4),LINE-4(1,2)

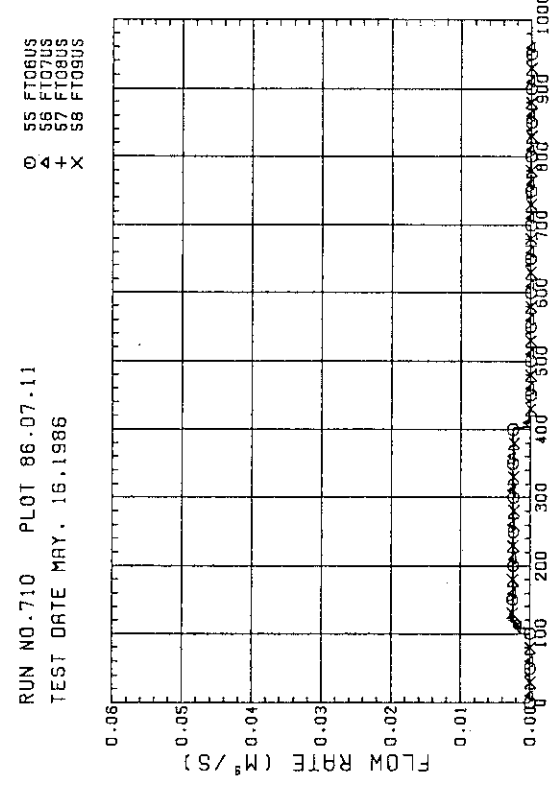

Fig. B-48 FLOW RATE OF UPPER HEAD INJECTION
LINE-4(BUNDLE1,2),LINE-3(3,4),LINE-2(5,6),LINE-1(7,8)

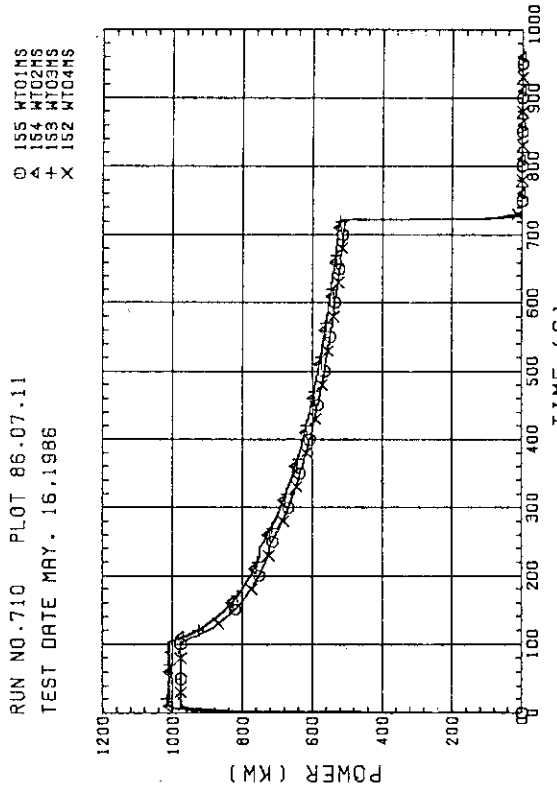

Fig. B-45 BUNDLE POWER
(BUNDLE 1,2,3,4)

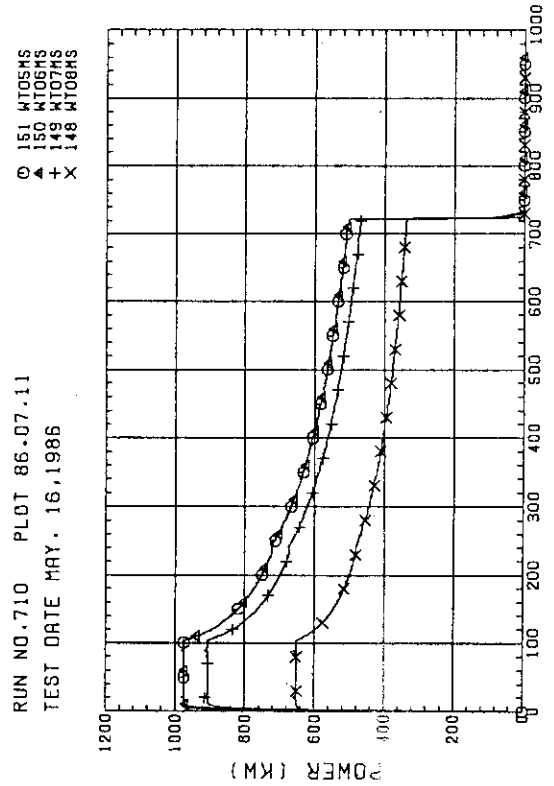

Fig. B-46 BUNDLE POWER
(BUNDLE 5,6,7,8)